

The FAST Galactic Plane Pulsar Snapshot Survey: II. Discovery of 76 Galactic rotating radio transients and their enigma

D. J. Zhou^{1,2}, J. L. Han^{1,2}, Jun Xu¹, Chen Wang¹, P. F. Wang¹, Tao Wang^{1,2}, Wei-Cong Jing^{1,2}, Xue Chen^{1,2}, Yi Yan^{1,2}, Wei-Qi. Su^{1,2}, Heng-Qian Gan^{1,2}, Peng Jiang^{1,2}, Jing-Hai Sun^{1,2}, Hong-Guang Wang^{3,4}, Na Wang^{5,6}, Shuang-Qiang Wang⁵, Ren-Xin Xu⁷, and Xiao-Peng You⁸

¹ National Astronomical Observatories, Chinese Academy of Sciences, 20A Datun Road, Chaoyang District, Beijing 100101, China; hjl@nao.cas.cn

² School of Astronomy, University of Chinese Academy of Sciences, Beijing 100049, China;

³ Department of Astronomy, School of Physics and Materials Science, Guangzhou University, Guangzhou 510006, Guangdong Province, China

⁴ National Astronomical Data Center, Great Bay Area, Guangzhou 510006, Guangdong Province, China

⁵ Xinjiang Astronomical Observatory, Chinese Academy of Sciences, 150 Science 1-street, Urumqi 830011, China;

⁶ Key Laboratory of Radio Astronomy, Chinese Academy of Sciences, Nanjing 210008, China;

⁷ Department of Astronomy, Peking University, Beijing 100871, China;

⁸ School of Physical Science and Technology, Southwest University, Chongqing 400715, China

Received 2023 January 4; revised 2023 March 27; accepted 2023 March 30; published 2023 September 29

Abstract We are carrying out the Galactic Plane Pulsar Snapshot (GPPS) survey by using the Five-hundred-meter Aperture Spherical radio Telescope (FAST), the most sensitive systematic pulsar survey in the Galactic plane. In addition to about 500 pulsars already discovered through normal periodical search, we report here the discovery of 76 new transient radio sources with sporadic strong pulses, detected by using the newly developed module for a sensitive single pulse search. Their small DM values suggest that they all are the Galactic rotating radio transients (RRATs). They show different properties in the following-up observations. More radio pulses have been detected from 26 transient radio sources but no periods can be found due to a limited small number of pulses from all FAST observations. The following-up observations show that 16 transient sources are newly identified as being the prototypes of RRATs with a period already determined from more detected sporadic pulses, and 10 sources are extremely nulling pulsars, and 24 sources are weak pulsars with sparse strong pulses. On the other hand, 48 previously known RRATs have been detected by the FAST either during verification observations for the GPPS survey or through targeted observations of applied normal FAST projects. Except for 1 RRAT with four pulses detected in a session of five minute observation and 4 RRATs with only one pulse detected in a session, sensitive FAST observations reveal that 43 RRATs are just generally weak pulsars with sporadic strong pulses or simply very nulling pulsars, so that the previously known RRATs always have an extreme emission state together with a normal hardly detectable weak emission state. This is echoed by the two normal pulsars J1938+2213 and J1946+1449 with occasional brightening pulses. Though strong pulses of RRATs are very outstanding in the energy distribution, their polarization angle variations follow the polarization angle curve of the averaged normal pulse profile, suggesting that the predominant sparse pulses of RRATs are emitted in the same region with the same geometry as normal weak pulsars.

Key words: pulsars: general

1 INTRODUCTION

Time-domain astronomical observations reveal more and more the Galactic or extragalactic transients in many elec-

tromagnetic wave bands, rested on the new development of high sensitivity detectors which can outline the light curves of sources. Most successful were the detection of the Gamma-Ray bursts (see review by [Fishman & Meegan](#)

1995), Fast Radio Bursts (FRB, Lorimer et al. 2007) and extrasolar planets (e.g. Mayor & Queloz 1995; Butler & Marcy 1996). Radio pulsar detection, even in the first discovery (Hewish et al. 1968), has been working in the time domain. It started with a high time resolution of seconds, later milliseconds (e.g. Burke-Spolaor & Bailes 2010), and nowadays microseconds or even to nanoseconds (e.g. Hankins et al. 2003). For a bright pulsar, each individual pulse from every pulsar period can be directly observed if a radio telescope is sensitive enough. For a weak pulsar, signals have to be integrated over many periods, so that a mean pulse profile is obtained. Because of the interstellar medium, the pulses must be dedispersed to diminish the delay between frequency channels in an observational radio band.

Most known pulsars were discovered through searching in the Fourier domain by using the packages such as PRESTO¹ (Ransom 2011) and SIGPROC² (Lorimer 2011), or using the fast-folding algorithm (FFA, Staelin 1969; Kondratiev et al. 2009; Cameron et al. 2017; Parent et al. 2018) in the time domain. The enhanced red noise from the observation system caused by the fluctuations of the receiver gain, system temperature and radio frequency interference (RFI) affects the detection of long-period pulsars in the Fourier domain. Cordes & McLaughlin (2003) developed a new single pulse search technology, finding enhance points in dedispersed data series. When the signal to noise ratio (S/N) is much larger than a given threshold, then a radio transients can be found as an isolated distribution in the image of dispersion measurement (DM) versus time. By using this technology, McLaughlin et al. (2006) discovered the first rotating radio transients (RRATs), and Lorimer et al. (2007) discovered the first FRB. This technology is effective for the searching of bright radio transients, and has been used in many pulsar surveys (Cordes et al. 2006; Hessels et al. 2008; Deneva et al. 2009; Burke-Spolaor & Bailes 2010; Keane et al. 2010; Burke-Spolaor et al. 2011; Keane et al. 2011; Coenen et al. 2014; Stovall et al. 2014; Karako-Argaman et al. 2015; Deneva et al. 2016; Keane et al. 2018).

As defined by Burke-Spolaor & Bailes (2010), RRATs are often considered as a special group of pulsars that emit bright pulses sporadically, making them difficult to be found in a normal periodic search method. They are usually discovered by a single-pulse search method. Up to now, more than 160 RRATs have been discovered, see the list in the RRATalog³ and also a recent summary by Abhishek et al. (2022), plus more new RRATs recently discovered (Patel et al. 2018; Tyul'bashev et al. 2018b,a;

Good et al. 2021; Han et al. 2021; Bezuidenhout et al. 2022; Dong et al. 2022; Tyul'bashev et al. 2022). The number of known RRATs claimed in literature (Abhishek et al. 2022) is about or more than five percent of the known pulsars. It is quite possible that many RRATs or long period pulsars are missed in some pulsar surveys, if the single-pulse search has not properly been carried out for surveys (see Keane et al. 2010). Discovery of more RRATs can help to understand the neutron star population in the Galaxy.

To understand why the pulses radiate very occasionally, sensitive observations and detailed statistics of long term observations are desired (Bhattacharyya et al. 2018). However, only a small fraction of RRATs have been well studied. The energy distribution or peak flux distribution of single pulses from a very sensitive observation could give the answer to how an RRAT behaves. For a generally very weak pulsar, it could appear as an RRAT if only a few bright pulses are detectable for a given sensitivity. The energy of normal pulses of a pulsar always follows a log-normal distribution, while abnormal bright pulses should show an extra component at the high energy end as if they are giant pulses. This has been verified by some RRATs, such as PSR J1846–0257 (Mickaliger et al. 2018). For other RRATs, Cui et al. (2017) and Mickaliger et al. (2018) did not find the tail beyond the log-normal distribution, indicating that the pulses are normal but just very nulling (Burke-Spolaor & Bailes 2010), so that they radiate pulses by the same emission mechanism as pulsars. Then, the concerns are turned to why RRATs are very nulling. Some RRATs, e.g. PSR J0941–39 (Burke-Spolaor & Bailes 2010) and PSR J1752+2359 (Sun et al. 2021), can have two emission states, one with occasional bright pulses and one with a very nulling state or normal pulsar state. Lu et al. (2019) observed three RRATs by using the Five-hundred-meter Aperture Spherical radio Telescope (FAST, Nan et al. 2011), and they detected many bursts for PSRs J1538+2345 and J1854+0306, while PSR J1913+1330 radiates pulses continuously but clearly shows nulling nature. Based on the FAST observation of PSR J0628+0909, Hsu et al. (2023) concluded that this known RRAT has weak single pulses as a normal pulsar with transient-like strong pulses, similar to PSR J0659+1414 (B0656+14, Weltevrede et al. 2006).

To understand the sporadic behavior of RRATs and the switching of different emission states, the polarization observations are desired not only for bright single pulses but also for weaker normal pulses. Previously available measurements were made for single pulses of PSR J1819–1458 by Karastergiou et al. (2009), of 17 RRATs by Caleb et al. (2019), of PSR J1752+2359 by Sun et al. (2021) and of PSR J1905+0849g by Han et al. (2021).

¹ <https://www.cv.nrao.edu/~sransom/presto>

² <http://sigproc.sourceforge.net>

³ <http://astro.phys.wvu.edu/rratalog/>

Mean polarization profiles of only a few RRATs have been measured (Karastergiou et al. 2009), which in fact is the key to understand the radiation mechanism and radiation geometry.

Timing is fundamental for a rotating neutron star to get the period derivative measured, and hence the characteristic age and magnetic field derived. For RRATs, it is challenging to do timing, because only a small number of strong pulses can be detected in a limited observation time. The initial discovery position of detection is often poorly given. Single pulses probably emerge randomly in the averaged pulse emission window. A mean pulse profile can therefore rarely be obtained because of the sparseness of pulses, and the timing residual by using these individual pulses could be as large as hundred milliseconds (Bhattacharyya et al. 2018). The available timing results for several RRATs in the P-Pdot diagram (McLaughlin et al. 2009; Keane et al. 2011; Cui et al. 2017; Bhattacharyya et al. 2018) show that long-period RRATs look like either magnetars if they have a large period derivative, or simply aged pulsars near the death line if they have small period derivatives. Statistical analysis of populations of known RRATs by Abhishek et al. (2022) shows no correlation with nulling pulsars, nor tending to be older and closer to the death line. Very surprising is a glitch detected from PSR J1819-1458⁴ (Lyne et al. 2009), which indicates that some RRATs may be just young pulsars with merely bright single pulses ever detectable.

The FAST (Nan et al. 2011) has a larger collecting area with an aperture diameter of 300 m. Mounted with a 19-beam L-band receiver with a system temperature of 22 K (Jiang et al. 2020), it has a great sensitivity to study the universe in radio waves, such as the discovery of weak pulsars (Han et al. 2021; Pan et al. 2021; Wang et al. 2021b), and the discovery of new FRBs (Zhu et al. 2020; Niu et al. 2021, 2022) or study the details of known pulsars (Wang et al. 2022) and FRBs (Luo et al. 2020; Xu et al. 2022b). At present, the FAST Galactic Plane Pulsar Snapshot (GPPS) survey⁵ (Han et al. 2021) is hunting pulsars in the Galactic plane, and has discovered more than 500 pulsars already. In the first paper by Han et al. (2021), the GPPS survey strategy is introduced and the discoveries of 201 pulsars and 1 RRAT have been presented, together with parameter improvements for 64 previously known pulsars. In this second paper, we report the discoveries of 76 Galactic transient sources from our single-pulse search, and also present FAST observations of previously known RRATs. In Section 2, we briefly summarize the GPPS survey ob-

servations, and introduce our single pulse search module and the data processing. All the newly discovered results are presented in Section 3. During the GPPS surveys, the covers with known pulsars have been observed for system verification in every observation session. With these data, together with targeted observations of some RRATs in several normal applied FAST projects (see details below), 59 previously known RRATs have been observed by FAST as presented in Section 4, which can tell the RRAT enigma. A summary and discussions are given in Section 5.

2 OBSERVATIONS AND DATA PROCESSING

2.1 The GPPS survey and other observations

The FAST GPPS survey (see details in Han et al. 2021) plans to hunt for pulsars in the Galactic plane within $\pm 10^\circ$ visible in the zenith angle of 28.5° , by using the L-band 19-beam receiver covering the frequency range of 1000 – 1500 MHz. Up to now, about 10% of the planned survey regions have been observed⁵. The observations have been carried out with *the snapshot mode* specially designed for the survey, in which four pointings of 19 beams fully cover a hexagonal sky area of 0.1575 square degrees aligned with the Galactic plane. Each pointing tracks for 5 minutes, and a quick beam switching costs less than 20 seconds, so that a *cover* can be observed by 4×19 beams in 21 minutes. A *cover* is named with the Galactic coordinates, such as G31.91+0.42. The beams are then named in the format as being G31.91+0.42-MxxPn. Here, Mxx represents the beam number for one of 19 beams of the receiver, i.e. M01 to M19, and Pn is for one of 4 pointings, i.e. P1 to P4.

During the survey, signals of the two polarization channels of XX and YY from each of the 19 beam receiver are channelized to 2048 channels for the total band of 500 MHz. The data are recorded in PSRFITS format with a sampling time of $49.152\mu\text{s}$. In verification observations for a *cover* having a known pulsar located in the sky area, data of four polarization channels of XX, X*Y, XY* and YY are recorded in the PSRFITS file. During FAST observations, data streams are continuously recorded in a series of PSRFITS files, each lasting for about 12.885 s (if for four polarization channels) or 25.770 s (for two polarization channels). All the GPPS survey data are searched for radio transients.

Signals of newly discovered transients are often too weak to be detected by other telescopes, so we have to use the FAST for following-up observations. After a pulsar candidate or a transient source is found in a beam, a following-up observation is carried out with a *tracking mode* for generally 15 minutes, occasionally for a longer time, with the central beam of the L-band 19-beam receiver pointing to the position. Very often we record data

⁴ As we believe that RRATs are a sub-class of pulsars, therefore we name an RRAT in the general format of pulsars, such as PSR J1234+3456 or simply J1234+3456.

⁵ <http://zmtt.bao.ac.cn/GPPS/>

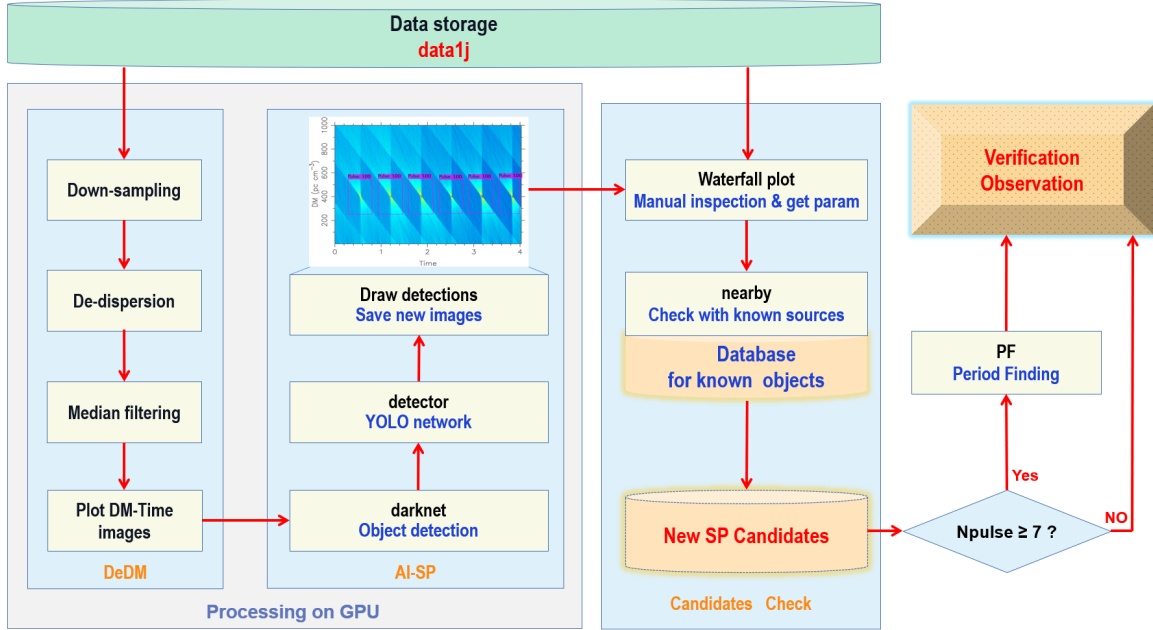


Fig. 1 The flowchart for the single pulse search module for the GPPS survey.

for all 19 beams, all of which are used for slightly deeper pulsar searches. We often name the beam with the source name and the beam number, such as J1849+0001-M09 is for data from the beam M09 of tracking observations for the source J1849+0001. The data of 4 polarization channels are recorded for the studies of polarization characteristics of a pulsar or a transient source. For some sources, we have also applied normal FAST project (PT2020_0155 and PT2022_0177, PI: D.J. Zhou) to track even for one hour.

For known RRATs in the sky area of the GPPS survey, the verification observations take the data for 4 polarization channels on the cover with a high priority. For known RRATs outside the survey region, we take data from the tracking observations of other normal applied FAST projects, such as PT2021_0051 (PI: Jun Xu) or PT2021_0151 (PI: D.J. Zhou). For some objects with only a coarse position, we take data of 4×19 beams observed at the suggested position with a modified snapshot mode, called the *snapshotdec mode*, which covers a sky area with beams aligned along the equator plane.

2.2 Data analysis

In principle, single pulse search simply has three steps: 1) dedisperse data, 2) pick out pulses above a threshold of significance over the system noise, 3) sift candidates. For example, in the single pulse search pipeline on PRESTO (Ransom 2011), the first step is to use the `prepsubband` to dedisperse data, and then the second step is to find the outstanding data points in each dedisperse data based on the software `single_pulse_search.py`. Finally, the

classifier `RRATtrap`⁶ is used for candidates sifting, which is a single pulse sifting algorithm used in the Green Bank North Celestial Cap (GBNCC) survey and Low Frequency Array (LOFAR) survey, developed by Karako-Argaman et al. (2015) and updated by Patel et al. (2018).

After a huge number of outstanding data points are found in dedispersed data, a skillful job is the step for candidates sifting. Many software packages have been developed for ‘classifier’. In the package `Clusterrank`⁷ used in Arecibo 327 MHz Drift Pulsar Survey (AO327), Devine et al. (2016) developed a machine-learning classifier for identifying and classifying dedispersed pulse groups in single pulse search output. Agarwal et al. (2020) developed a new classifier to recognize the original achromatic waterfall image and the diagram of the occurrence DM-time of candidates. Other similar packages have been developed by Men et al. (2019) and Zhang et al. (2021) as well. Michilli et al. (2018) introduce the machine-learning classifier L-SPS⁸ (based on SPS⁹, Michilli & Hessels 2018) to discriminate astrophysical signals and RFI for the LOTAAS. All these classifiers are basically working on the bright points in the DM-time image, which is output by `single_pulse_search.py` or other similar codes. The parameters for such a single pulse search must be set differently for different projects by different telescopes, and they affect directly on candidate classification, otherwise narrow, weak or scattered pulses could be mis-

⁶ <http://github.com/ckarako/rratrap>

⁷ <http://github.com/juliadeneva/clusterrank>

⁸ <http://github.com/danielemichilli/LSPS>

⁹ <http://github.com/danielemichilli/SPS>

eliminated. In general, these classifiers are hard to work in real time.

With the developments of the Graphics Processing Unit (GPU) and Artificial Intelligence (AI), the single pulse search has adopted these technologies to improve the computation efficiency. For example, [Petroff et al. \(2014\)](#) searched for fast radio transients by using HEIMDALL¹⁰ based on GPU devices for dedispersion and candidates clustering, which can process data in real-time and directly produces a list of candidates for multi-beam surveys. [Magro et al. \(2011\)](#) developed a GPU-based real time transient search machine.

2.2.1 Single pulse search in the GPPS survey

The single pulse search module has been developed (see Fig. 1) and applied to the GPPS survey data.

The original data of 2048 channels cover the frequency range of 1000 – 1500 MHz. The channels within 31.25 MHz from each edge of the band are discarded due to their low gain. The original data of other channels for polarization channels XX and YY are scaled according to their root mean square (RMS) and added together for the total power, and then deposited into the *data1j* repository for pulsar searching. The details for data preparation are described in the first paper ([Han et al. 2021](#)). The single pulse search module is taking these fits files from the *data1j* repository.

We have developed a source code to do quick dedispersion and generate DM-time images in GPU. The process includes three steps: loading data, dedispersion in the range from 3 pc cm⁻³ to 1000 pc cm⁻³ with a step of 1.0 pc cm⁻³, and plotting DM-time images for every 4 seconds of data. This process consumes only about 0.25 s of computation time in one node of the FAST computing cluster. In addition to recognize the pulse signal with a high DM, mostly for searching FRBs, images for three DM ranges are plotted and searched for radio transients independently: 900 – 1900 pc cm⁻³, 1800 – 2800 pc cm⁻³ and 2700 – 3700 pc cm⁻³. Because single pulses also rarely have a width less than one millisecond, after loading data, we down-sample the data from 49.152 μ s to $4 \times 49.152 = 196.608$ μ s and also combine every 4 frequency channels together. This not only improves the detection efficiency of single pulses, but also makes the subsequent data processing fast. After the data are dedispersed, in order to suppress the noise level and preserve the pulse features, the ‘fifth-order median filter’ is applied to the dedispersed data, in which the median of in a sliding window of 5×5 data points in the two-dimensional Time-DM image is taken to replace the original point value. This filtering process can

effectively smooth out strong RFI emerging in only one or two data bins and preserve the original features of the image. Because some transient pulses have a steep spectrum or an inverse spectrum, we also make two more DM-time images for data in the upper half and lower half of the band, i.e. channels below and above 1250 MHz, and plot an image every 1.5 s. This operation ensures an effective detection of narrow and weak pulses with a steep spectrum, especially for the repeating FRBs ([Zhou et al. 2022](#)).

After the above-mentioned DM-time images are generated for a beam or even a cover, we used the YOLO object detection technology to recognize the outstanding points, which is developed in the Darknet¹¹ neural network framework for searching the distinctive features in the DM-time images. At the beginning of this single pulse search for the GPPS survey, the `yolov3.cfg` network file of YOLOv3¹² ([Redmon & Farhadi 2018](#)) version was used. In 2021, we switched to YOLOv4 ([Bochkovskiy et al. 2020](#)) and the new `yolov4_csp.cfg`¹³ network file ([Wang et al. 2021a](#)). After the huge number of images sifted by this AI technology, the left images of single pulse candidates are manually examined, and the final burst candidates are listed with the DM and time of arrival (TOA, in MJD) for further verification observations and period-finding (see below).

Most of our single pulse searches of the GPPS survey have been carried out by using the GPU node of the computing cluster in the FAST data center. For data of 76 beams from one cover of the GPPS snapshot observation of 21 minutes, we organize the multitask parallel computing in the GeForce RTX 2080Ti GPU*4 with the program of GNU Parallel ([Tange 2018](#)). The processing costs about 9 minutes for single pulse search in the DM range from 3 to 1000 pc cm⁻³.

2.2.2 Sensitivity and pulse parameters

For any pulse detected from the single pulse searches of the GPPS survey data, some parameters must be determined.

The first is the DM value estimated by using the method given by [Zhu et al. \(2020\)](#), in which the most refined pulse structure is preserved when turning DM values, and the uncertainty is given as being the half-width of the Gaussian function fitted for the curve of $\sum (\frac{d}{dt})^2$ over DMs. If a number of pulses are detected with the almost the same DM, they probably come from the same source. The final DM is determined by the brightest pulses.

Second is the time of arrival (TOA) of a pulse. We dedispersed all the candidates and get the time of arrival

¹⁰ <http://sourceforge.net/projects/heimdall-astro>

¹¹ <https://pjreddie.com/darknet/>

¹² <https://pjreddie.com/darknet/yolo/>

¹³ <https://github.com/WongKinYiu/ScaledYOLOv4>

(TOA, in MJD) at the pulse peak. This TOA must be converted to the time at the Solar barycentric center using the DE438 ephemeris.

For a single detected pulse, we have to get other necessary parameters, such as the observed pulse width (W_{obs}) and the signal-to-noise ratio ($R = S/N$). Supposing the pulse in n bins has an equivalent width of W_{obs} (or simply written as W in units of ms in tables or figures), the $R = S/N$ of the pulse detection can be estimated from the total energy of n on-pulse bins ($\sum S_i$) divided by the standard deviation (σ) of a nearby off-pulse range in the dedispersed data series, as

$$R = S/N = \frac{\sum S_i}{\sigma \cdot \sqrt{n}}. \quad (1)$$

Note that the observed pulse width is a combination of the intrinsic pulse width with other factors. In addition to the sampling time of the dedispersed data $t_{\text{bin}} = 196.608 \mu\text{s}$, for a high DM pulse, the scattering broadening time τ_s has to be taken into account, which can be estimated as following (e.g. Karako-Argaman et al. 2015):

$$\log(\tau_s) \approx a + b \cdot \log(DM) + c \cdot \log^2(DM) - \alpha \cdot \log(\nu), \quad (2)$$

here $a = -3.59$, $b = 0.129$, $c = 1.02$ and $\alpha = -4.4$. The dispersion time inside one frequency channel with a bandwidth $BW_{\text{chan}} = 0.97656248 \text{ MHz}$:

$$\Delta t_{\text{chan}} = 4.7 \mu\text{s} \cdot \frac{BW_{\text{chan}}}{24.414 \text{ kHz}} \cdot \left(\frac{\nu}{350 \text{ MHz}} \right)^{-3} \cdot \frac{DM}{\text{cm}^{-3} \text{ pc}}, \quad (3)$$

must be concerned. Therefore the observed pulse width W_{obs} could be estimated from the intrinsic pulse width $W_{\text{intrinsic}}$ with these broadening, as being

$$W_{\text{obs}} = \sqrt{W_{\text{intrinsic}}^2 + t_{\text{bin}}^2 + \tau_s^2 + \Delta t_{\text{chan}}^2}. \quad (4)$$

The sensitivity of the single pulse detection at a given DM can be estimated from the pulse width W_{obs} and σ of the dedispersed data. The σ of the data flow can be related to the system noise by

$$\sigma = \frac{T_{\text{sys}}}{G_0 \sqrt{n_p \cdot t_{\text{bin}} \cdot BW}}, \quad (5)$$

here T_{sys} is the system noise temperature in units of K, $G_0 = 16.1 \text{ K/Jy}$ is the effective gain of the telescope (Jiang et al. 2020), $n_p = 2$ is the number of polarization summed, t_{bin} is the time of a down-sampled bin, $BW = 437.5 \text{ MHz}$ is frequency bandwidth (MHz) after removed the upper and lower sidebands of 31.25 MHz.

The capability of the single pulse search must therefore consider the observed pulse width and the system noise of σ . For pulses with a high DM and an intrinsic pulse width $W_{\text{intrinsic}}$, one can estimate the minimum

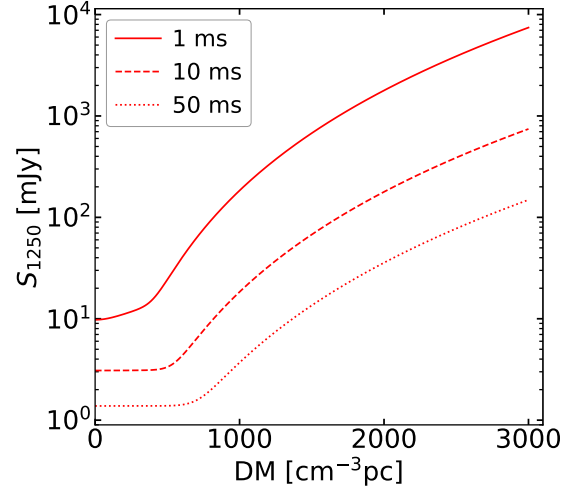


Fig. 2 FAST sensitivity for single pulse search with different intrinsic pulse widths.

flux density of detected pulse at a signal-to-noise ratio of $S/N > R_{\text{min}}$ (Cordes & McLaughlin 2003; Deneva et al. 2016) as being:

$$S_{1250} = R_{\text{min}} \frac{W_{\text{obs}}}{W_{\text{intrinsic}}} \frac{T_{\text{sys}}}{G_0 \cdot \sqrt{n_p \cdot BW \cdot W_{\text{obs}}}}. \quad (6)$$

Taking the minimum detection threshold of $R_{\text{min}} = 7$, one can get the sensitivity curves for different DM values as shown in Fig. 2.

The fluence of each single pulse, F in units of Jy·s at 1250 MHz, is simply the integration of the pulse over the width (t_{bin} , in units of s) as being $F = \sum S_i \cdot t_{\text{bin}}$. The method for estimating the mean flux densities of pulsars with periods estimated is consistent with that described in Section 4 of Paper I (Han et al. 2021).

2.2.3 Period finding

A possible period for detected pulses with the almost same DM has always been searched. If a period is found, the bright pulses obviously come from a pulsar or an RRAT.

For a sequence of TOAs of pulses with almost the same DM, one can get $N(N-1)/2$ differences for those TOAs. We test a number of periods in a range, and check the residual RMS for these TOAs and TOA differences for a given period of P . One would get complete noises for a series of residual RMS if there is no period and periodic derivative. Nevertheless, if there is a period, the very distinct minimum of residual RMS could be found, and the residual is then taken as the uncertainty of so-found period. The data are then fold with the best DM and the period P , and the average pulse profile is obtained. We wrote a small program ‘‘PF’’ for the purpose, and obtained the best periods from TOA sequences for many sources. After we got

this job done, we found that the method is very coincident with that reported by Keane et al. (2010).

For bright pulses and the mean profile of a pulsar or an RRAT, we get their polarization profile by using the package PSRCHIVE (Hotan et al. 2004), after the polarization data are calibrated and the Faraday rotation is corrected (Wang et al. 2022).

3 NEW DISCOVERIES

After processing the GPPS survey data obtained so far, we discover 76 Galactic transient sources, which are all taken as RRATs since they are discovered in single pulses search rather than the periodicity search, see Table 1 for the list.

Among them, we detect 105 pulses from 26 transient sources. Merely a few pulses from each source, as discussed in section 3.1, are not enough for the ‘PF’ to find a period, though we believe they should be RRATs. We simply take these source as the first subclass of newly discovered RRAT with a period to be found. For the other 50 sources, based on the discovered observation or follow-up observations, we classify them into three categories. The first is the prototypes of RRATs, in short ‘proto-RRATs’, from which non-consecutive single pulses are detected in the available observations but a period can be identified from these sporadic bright pulses. In the other periods rather than these with sparse pulses, no significant pulsed emission is detected from any individual period, or only very weak emission is detected from the averaged for many periods. We discovered 16 such proto-RRATs. The second category is extremely nulling pulsars, which have no emission is detected in the most ($\gtrsim 90\%$) of observation duration, but some pulses are detected consecutively for some periods. We discover 10 such extremely nulling pulsars. The last category the weak pulsars with sparse strong pulses. They stay for most of them in a very weak emission state, but occasionally have strong single pulses. The two emission states are very clearly shown in the individual pulses. We discovered 24 weak pulsars with sparse strong pulses.

In the following, we discuss each kind of such newly discovered source first, and then present the polarization observation results for strong pulses or the averaged profiles of detected pulses.

3.1 Galactic transient sources with merely few pulses

Very few pulses have been detected by FAST for 26 transient sources, as listed in the first part of Table 1 and shown in Figure 3 for examples and Figure 23 for pulses of all detected transient sources in the Appendix. Mostly 1 or 2 pulses were detected in 5 or 15 minutes observations, and sometimes even non pulse detected in the following-up ob-

servations for 15 or even 60 minutes. Note that the transient sources listed in Table 1 at least have two pulses, so they have ‘repeating radio bursts’ with almost the same DM, and the DM in Table 1 is *obtained from the strongest pulse*. If only one pulse is detected in the first observation, we have to catch at least another one in the following observations. J1853+0209g, for example, one pulse was detected on 20200812, while no pulse is detected in many sessions such as the 15 minutes observation on 20210627, the 60 minutes observation on 20211014, one 30 minutes observation on 20220602, and one 50 minutes observation on 20221112. Fortunately, one pulse is detected in the 60 minutes observation on 20220824. Therefore, only two single pulses have been detected by FAST observations of in total 290 minutes. For J1855–0154g we get 3 pulses from the 5 minutes survey pointing on 20210907, but none from the following-up observations for 15 minutes on 20211004 and for 60 minutes on 20221116. For all these transient sources, the pulse detection rate is very very low. It is very hard to get a period from the TOAs of so few pulses from all observations of each source.

For these transients, we cannot do much but present the two-dimensional dynamic spectra of the dedispersed pulses, see Figure 3 and Figure 23 in the Appendix. The pulse morphology of these transient sources is rich. In addition to the single peak pulse, we do see that some pulses have two peaks, such as J1828–0003g at 20220803 and 20221114, J1853+0353 on 20210624, or one sharp peak plus a weak peak, e.g. J1847–0046g on 20200606. Pulses detected from one source in different epochs are often different in shape. Some pulses have a very wide profile, such as J1853+0209g, reaching hundreds of milliseconds.

In Table 8 in the Appendix, we list parameters for each pulse, including the TOA of the pulse peak, signal-to-noise ratio of dedispersed pulse R , pulse width in millisecond, and the fluence discussed in Sect.2.2.2. We will discuss the polarization of some strong pulses in Sect.3.5.

The DM values of the pulses from these transient sources are all smaller than that the estimated upper limits given by the Galactic electron distribution models (Cordes & Lazio 2002; Yao et al. 2017), except for J2030+3833g who has a high DM of $417 \pm 6 \text{ pc cm}^{-3}$ which is near the DM upper limit of 402 pc cm^{-3} and 432 pc cm^{-3} given by NE2001 (Cordes & Lazio 2002) and YMW2016 (Yao et al. 2017), respectively. Therefore we conclude that all these transient sources are inside our Milky Way.

3.2 Newly discovered proto-RRATs

Based on the individual pulses detected by the single pulse module from the survey data and also from the longer following-up observations, we get a period from the TOA

Table 1 76 new RRATs discovered via the single pulse module from the GPPS survey data.

Name	gpps No.	P (s)	DM (cm^{-3}pc)	R.A.(J2000) (hh:mm:ss)	Dec(J2000) (\pm dd:mm)	ObsDate/MJD: BeamName	T_{obs} (min)	N_d/N_p	$\langle S \rangle$ (μJy)
(1)	(2)	(3)	(4)	(5)	(6)	(7)	(8)	(9)	(10)
Transient sources with just few pulses, no period has been found yet									
J0637+0332g	0528	...	152(2)	06:37:41	+03:32	20220909/59831: G208.21-1.36-M03P2	5	3/-	
						20230213/59988: J063740+033229-M01	15	0/-	
J1828-0003g	0501	...	193(3)	18:28:53	-00:03	20221114/59897: J182853-000340sp-M01	15	1/-	
						20220803/59794: G30.20+4.91-M19P2	5	1/-	
						20220803/59794: G30.20+4.91-M19P4	5	1/-	
J1847-0046g	0282	...	337(7)	18:47:47	-00:46	20211113/59531: J184711-005148-M19	15	2/-	
						20211031/59518: G31.91+0.42-M06P4	5	1/-	
						20220606/59735: J187446-004620-M01	30	3/-	
J1850-0004g	0280	...	154(1)	18:50:05	-00:04	20220608/59737: J185005-000430-M01	30	4/-	
						20200415/58953: J1849+0001-M09	15	2/-	
						20200902/59094: J1849+0001-M09	15	1/-	
						20210624/59388: J184958-000356sp-M01	15	0/-	
						20221106/59889: J1850-0002-M01	60	1/-	
J1853+0209g	0502	...	350(15)	18:53:07	+02:09	20200812/59073: J1852+0159-M18	15	1/-	
						20210627/59392: J185306+020910sp-M01	15	0/-	
						20211014/59501: J185306+020910sp-M01	60	0/-	
						20220602/59731: J185306+020910-M01	30	0/-	
						20220824/59815: J1853+0209-M01	60	1/-	
						20221112/59895: J1853+0209-M01	50	0/-	
J1853+0353g	0281	...	379(2)	18:53:29	+03:53	20210514/59347: J185404+035848-M13	15	2/-	
						20210624/59388: J185329+035343sp-M01	15	1/-	
J1855-0211g	0526	...	304(3)	18:55:32	-02:11	20230305/60008: J185532-021119-M01	15	1/-	
						20221205/59918: J185556-022129-M16	15	3/-	
						20220810/59801: G31.61-2.12-M16P2	5	1/-	
J1855-0154g	0503	...	417(1)	18:55:09	-01:54	20210907/59464: G31.66-1.69-M01P1	5	3/-	
						20211004/59491: J185509-015406sp-M01	15	0/-	
						20221116/59899: J1855-0154-M01	60	0/-	
						20230321/60024: J1855-0154-M01	60	0/-	
J1855-0054g	0504	...	577(4)	18:55:21	-00:54	20220602/59731: J185521-005410-M01	30	4/-	
						20220210/59678: J185520-005434-M01	15	1/-	
						20211225/59573: G32.45-1.36-M19P1	5	1/-	
						20211225/59573: G32.45-1.36-M19P2	5	1/-	
						20211225/59573: G32.45-1.36-M19P4	5	1/-	
J1855+0033g	0283	...	554(1)	18:55:03	+00:33	20210328/59300: J1855+0033-M01	60	3/-	
						20200328/58935: G34.01-0.68-M16P3	5	1/-	
J1856+0528g	0284	...	307(2)	18:56:23	+05:28	20210826/59452: J185623+052810-M01P1	15	3/-	
						20210608/59372: G38.36+1.61-M10P3	5	2/-	
						20210608/59372: G38.36+1.61-M11P4	5	1/-	
J1859+0832g	0505	...	259(2)	18:59:27	+08:32	20220526/59724: G41.40+2.12-M02P2	5	2/-	
						20221107/59890: J185927+083231sp-M01	15	1/-	
J1900+0908g	0527	...	264(4)	19:00:19	+09:08	20220522/59720: G42.13+2.03-M17P2	5	2/-	
						20221107/59890: J190019+090846sp-M01	15	0/-	
						20230305/60008: J190019+090846-M01	15	0/-	
J1902+0557g	0525	...	414(2)	19:02:56	+05:57	20221018/59870: G39.69+0.17-M05P2	5	2/-	
						20230212/59987: J190255+055718-M01	15	1/-	
J1916+1142Ag	0287	...	260(8)	19:16:59	+11:42	20200302/58910: G46.34-0.17-M04P2	5	1/-	
						20210108/59222: J1917+1142-M01	60	1/-	
J1918+0342g	0506	...	174(5)	19:18:22	+03:42	20211202/59550: G39.54-4.32-M15P3	5	1/-	
						20220329/59667: J191821+034233-M01	15	0/-	
						20220602/57731: J191821+034233-M01	30	1/-	
J1918+1514g	0507	...	134(2)	19:18:57	+15:14	20200531/58999: G49.81+0.93-M15P3	5	2/-	
						20220602/57731: J191857+151422-M01	15	0/-	
						20230228/60003: J191857+151422-M01	15	0/-	
J1921+1629g	0288	...	105(2)	19:21:47	+16:29	20211004/59491: J192147+162934sp-M01	15	2/-	
						20210822/59448: G50.94+1.02-M02P4	5	1/-	
J1924+1734g	0289	...	49(3)	19:24:57	+17:34	20211005/59492: J192457+173434sp-M01	15	3/-	
						20210822/59448: G52.40+0.85-M01P3	5	2/-	

Notes: Column (1)-(2): source name and the GPPS survey discovery number; Column (3)-(4) is the period P (in units of s, if obtained) and DM (in units of cm^{-3}pc) with uncertainty in brackets; Column (5)-(6): beam position of the detection in RA (2000) and Dec(2000); Column (7) is observation date together with MJD and also the beam name; Column (8): observation duration; Column (9): the number of pulses detected together with the number of periods (N_d/N_p) if the period is available; Column (10): the averaged flux density $\langle S \rangle$ (in units of μJy) for detected pulses.

Table 1 – continued.

Name	gpps No.	P (s)	DM (cm^{-3}pc)	R.A.(J2000) (hh:mm:ss)	Dec(J2000) (\pm dd:mm)	ObsDate/MJD: BeamName	T_{obs} (min)	N_d/N_p	$\langle S \rangle$ (μJy)
(1)	(2)	(3)	(4)	(5)	(6)	(7)	(8)	(9)	(10)
J1927+1940g	0290	...	347(2)	19:27:17	+19:40	20190327/58569: G54.31+1.27-M19P4	5	1/-	
						20210624/59388: J192717+194006sp-M01	15	1/-	
						20201120/59173: J1927+1940-M01	15	0/-	
J1932+2126g	0508	...	126(3)	19:32:51	+21:26	20220323/59661: G56.51+1.02-M02P1	5	1/-	
						20220608/59737: J193251+212609-M01	15	1/-	
						20220720/59780: J193251+212609-M01	15	1/-	
J1933+2401g	0291	...	185(3)	19:33:36	+24:01	20210626/59390: J193335+240123sp-M01	15	1/-	
						20210301/59274: G58.86+2.03-M19P2	5	1/-	
J1934+2341g	0292	...	252(2)	19:34:03	+23:41	20210624/59388: J193402+234110sp-M01	15	5/-	
						20210301/59274: G58.86+2.03-M12P2	5	3/-	
						20221106/59889: J1934+2341-M01	15	2/-	
J2001+4209g	0293	...	153(2)	20:01:39	+42:09	20211004/59491: J200139+420904sp-M01	15	2/-	
						20210802/59427: G77.55+6.10-M19P3	5	1/-	
J2005+3154g	0294	...	225(1)	20:05:19	+31:54	20211009/59496: J200519+315400sp-M01	15	1/-	
						20210804/59430: G69.43+0.17-M04P2	5	2/-	
						20210805/59431: G69.43+0.17-M05P4	5	1/-	
						20210805/59431: G69.43+0.17-M13P1	5	3/-	
						20211009/59496: J200530+315600sp-M01	15	2/-	
J2030+3833g	0295	...	417(6)	20:30:31	+38:33	20210317/59290: J203031+383329sp-M01	15	2/-	
						20210624/59388: J203031+383329sp-M01	15	2/-	
						20210220/59265: G77.55-0.34-M09P1	5	2/-	
ProtoRRATs with a good period identified									
J1857+0229g	0296	0.584(3)	574(1)	18:57:19	+02:29	20201108/59161: J1857+0229-M01	60	9/5749	
						20200302/58910: G35.92-0.25-M06P2	5	1/513	
J1858+0453g	0297	3.761(4)	429(1)	18:58:48	+04:53	20210219/59264: J1859+0453-M01	60	7/923	
						20200421/58959: G38.27+0.76-M12P2	5	1/79	
J1859+0251g	0298	3.580(3)	286(3)	18:59:35	+02:51	20210316/59288: J1900+0252-M01	60	14/969	
						20200221/58900: G36.26-0.51-M08P2	5	1/83	
J1904+0621g	0299	1.232(3)	173(1)	19:04:55	+06:21	20210318/59291: J190455+062136sp-M01	15	8/720	
						20201225/59208: G40.03-0.08-M02P1	5	8/243	
						20210213/59258: G40.03-0.08-M02P1	5	2/243	
J1905+0156g	0300	1.085(1)	137(1)	19:05:08	+01:56	20210113/59227: J1905+0156-M01	15	20/818	
						20201127/59180: J1904+0207-M10	15	7/818	
J1905+0558g	0301	0.846(2)	472(1)	19:05:04	+05:58	20210627/59391: J190500+055840sp-M01	15	11/1050	
						20210306/59279: J190452+060345-M03	15	9/1063	
						20210109/59223: J1904+0558-M01	30	3/2127	
						20200219/58898: G39.64-0.25-M08P2	5	1/354	
						20201123/59176: J1904+0558-M01	15	0/1063	
J1908+0911g	0510	5.1661(7)	132(4)	19:08:09	+09:11	20221107/59890: J190808+091144sp-M01	15	8/172	
						20191226/58843: G43.06+0.42-M06P1	5	2/58	
J1916+0937g	0286	7.368(1)	186(2)	19:16:01	+09:37	20221108/59891: J1916+0937-M01	60	10/472	
						20200418/58956: G44.38-1.02-M05P1	5	2/40	
						20201123/59176: J1916+0937-M01	15	1/122	
						20210626/59390: J191600+093701sp-M01	15	4/122	
J1916+1142Bg	0303	1.188(3)	318(8)	19:16:59	+11:42	20210108/59222: J1917+1142-M01	60	7/2929	
						20201123/59176: G46.34-0.17-M04P2	5	3/252	
J1917+0834g	0304	2.933(3)	101(3)	19:17:04	+08:34	20210113/59227: J1917+0834-M01	15	6/303	
						20201123/59176: J1917+0834-M01	15	5/303	
						20200419/58957: G43.55-1.78-M06P4	5	2/102	
J1921+1006g	0511	3.345(9)	362(8)	19:21:44	+10:06	20221107/59890: J192144+100630sp-M01	15	11/262	
						20220821/59812: G45.36-2.20-M17P1	5	2/89	
						20220821/59812: G45.36-2.20-M18P2	5	1/89	
J1924+1446g	0305	1.090(3)	336(3)	19:24:54	+14:46	20201108/59139: J1924+1446-M01	60	9/3080	
						20200426/58964: G50.01-0.59-M15P1	5	1/275	
J1935+1841g	0306	5.529(1)	290(3)	19:35:03	+18:41	20211005/59492: J193502+184128sp-M01	15	7/161	
						20210817/59442: G54.46-0.68-M03P2	5	4/54	
						20220925/59847: J1935+1841-M01	15	3/162	
						20221105/59888: J1935+1841-M01	15	4/162	
						20221128/59911: J1935+1841-M01	15	5/162	
J1948+2314g	0512	1.471(4)	184(3)	19:48:40	+23:14	20221107/59890: J194840+231423sp-M01	15	11/604	
						20220418/59687: G59.99-1.10-M11P1	5	5/203	

Table 1 – continued.

Name	gpps No.	P (s)	DM (cm^{-3}pc)	R.A.(J2000) (hh:mm:ss)	Dec(J2000) (\pm dd:mm)	ObsDate/MJD: BeamName	T_{obs} (min)	N_d/N_p	$\langle S \rangle$ (μJy)
(1)	(2)	(3)	(4)	(5)	(6)	(7)	(8)	(9)	(10)
J2005+3156g	0307	2.146(1)	337(2)	20:05:30	+31:56	20211009/59496: J200530+315600sp-M01 20211009/59496: J200519+315400sp-M01 20210804/59430: G69.43+0.17-M04P1 20210804/59430: G69.43+0.17-M04P2 20210804/59430: G69.43+0.17-M04P4 20210805/59431: G69.43+0.17-M04P1 20210805/59431: G69.43+0.17-M04P2 20210822/59448: G69.43+0.17-M04P2	15 15 5 5 5 5 5 5	6/413 4/413 2/139 2/139 2/139 2/139 2/139 2/139	
J2014+3326g	0524	0.9773(1)	333(2)	20:14:25	+33:26	20230212/59987: J201424+332603-M01 20221201/59914: G71.58-0.51-M10P2	15 5	8/910 5/306	
Extremely nulling pulsars									
J1828-0038g	0509	2.426(3)	70(2)	18:28:15	-00:38	20221114/59897: J182815-003930sp-M01 20220828/59819: J182828-004203-M06 20220828/59819: J182828-004203-M05 20220828/59796: G29.80+4.74-M06P2 20220828/59796: G29.80+4.74-M16P4 20220828/59796: G29.80+4.74-M17P3 20220828/59796: G29.80+4.74-M16P1	15 15 15 15 15 15 15	21/370 14/365 1/371 8/371 5/371 4/371 2/371	
J1842+0114g	0308	4.140(4)	307(8)	18:42:13	+01:14	20210317/59289: J184213+011400sp-M01 20210213/59258: G32.89+2.46-M18P1 20201225/59208: G32.89+2.46-M18P1 20201225/59208: G32.89+2.46-M18P4 20210213/59258: G32.89+2.46-M18P4	15 5 5 5 5	23/215 5/72 5/72 4/72 2/72	8.9
J1845-0008g	0309	1.268(3)	143(3)	18:45:08	-00:08	20210626/59390: J184508-000800sp-M01 20200422/58960: G32.01+1.27-M19P2 20200422/58960: G32.01+1.27-M19P3 20201121/59174: J1845-0007-M01P1 20210707/59401: J184508-000800sp-M01 20210109/59223: J1845-0007-015P1	15 5 5 15 15 30	39/700 7/242 2/242 0/710 0/710 0/710	9.6
J1855+0240g	0310	1.224(3)	397(3)	18:55:13	+02:40	20210626/59390: J185513+024047sp-M01 20200321/58929: G35.63+0.42-M08P3 20201121/59174: J1855+0240-M01 20210111/59225: J1855+0240-M01	15 5 15 30	5/725 2/245 2/725 0/1470	1.3
J1858-0113g	0513	1.532(1)	280(4)	18:58:52	-01:13	20220403/59671: J185852-011306-M01P1 20220127/59606: G32.74-2.03-M11P2 20220127/59606: G32.74-2.03-M11P4	15 5 5	16/578 6/195 7/195	7.8
J1911+1017g	0302	1.337(1)	162(2)	19:11:12	+10:17	20201123/59176: J1911+1017b-M01 20200321/58929: G44.53+0.25-M15P2	15 5	12/664 10/231	
J1921+0851g	0234	0.957(5)	101(2)	19:21:11	+08:51	20210429/59332: G44.23-2.29-M11P4 20210624/59388: J192111+085133sp-M01	5 15	16/307 51/926	72.9
J1921+1632g	0311	0.493(1)	164(2)	19:21:37	+16:32	20211004/59491: J192136+163201sp-M01 20210822/59448: G50.94+1.02-M02P1	15 5	5/580 1/195	
J1935+1901g	0407	0.897(1)	365(2)	19:35:50	+19:01	20220329/59667: J193550+190159-M01 20211107/59525: G54.80-0.93-M18P2	15 5	11/990 9/334	6.4
J1940+2203g	0312	11.906(1)	59(9)	19:40:49	+22:03	20210109/59223: J1940+2203-M01 20201123/59176: J1940+2203-M01 20200426/58964: G58.22-0.25-M05P4 20200426/58964: G58.22-0.25-M05P3 20220925/59847: J1940+2203-M01 20221107/59890: J1940+2203-M01 20221128/59911: J1940+2203-M01	30 15 5 5 15 15	9/150 2/75 1/25 1/25 0/75 0/75 3/75	
Newly discovered weak pulsars with sparse strong pulses									
J1840-0245g	0313	1.502(1)	277(2)	18:40:14	-02:45	20211004/59491: J184014-024556sp-M01 20210816/59442: G29.41+1.36-M13P3	15 5	4/591 2/206	6.7
J1843-0051g	0314	0.580(1)	573(3)	18:43:32	-00:51	20211009/59496: J184332-005100sp-M01 20210811/59437: G31.27+1.36-M01P1	15 5	31/1528 13/532	6.0
J1845+0326g	0521	0.968(1)	144(1)	18:45:42	+03:26	20230218/59993: J184542+032600-M01 20221002/59854: G35.53+2.80-M15P3 20221002/59854: G35.53+2.80-M15P4	15 5 5	32/919 2/309 3/309	3.3
J1845+0417g	0515	1.697(6)	164(3)	18:45:33	+04:17	20221111/59894: J184533+041730sp-M01 20220524/59722: G35.97+3.39-M09P4 20220524/59722: G35.97+3.39-M09P3	15 5 5	34/524 6/170 2/170	3.1

Table 1 – *continued and ended.*

Name	gpps No.	P (s)	DM (cm^{-3}pc)	R.A.(J2000) (hh:mm:ss)	Dec(J2000) (\pm dd:mm)	ObsDate/MJD: BeamName	T_{obs} (min)	N_d/N_p	$\langle S \rangle$ (μJy)
(1)	(2)	(3)	(4)	(5)	(6)	(7)	(8)	(9)	(10)
J1849+0619g	0522	2.011230(3)	110(1)	18:49:35	+06:19	20230228/60003: J184935+061900-M01 20221001/59853: G38.56+3.30-M14P1 20221111/59894: J184950+062304-M04	15 5 15	4/442 1/149 1/442	6.2
J1851+0051g	0315	4.027(2)	575(5)	18:51:40	+00:51	20210207/59252: J1852+0051-M01 20200303/58911: G33.77+0.42-M04P1 20201228/59211: J1851+0056-M03	60 5 20	12/833 1/74 1/297	2.7
J1853–0130g	0316	1.945(1)	344(1)	18:53:07	–01:30	20211004/59491: J185307–013012sp-M01 20210901/59458: G31.76–0.85-M10P3	15 5	15/454 1/154	6.4
J1856+0029g	0317	0.376(3)	234(3)	18:56:49	+00:29	20210524/59357: J1856+0029-M01 20200422/58960: G33.96–1.10-M18P3	60 5	23/8943 1/798	2.6
J1859+0239Bg	0529	0.848740(3)	624(4)	18:59:18	+02:39	20220529/59728: J1859+0239-M01 20221227/59940: J1859+0239-M01 20230125/59969: J1859+0239-M01 20221118/59901: J185918+023926sp-M01 20211226/59574: J1859+0239-M01 20230102/59946: J1859+0239-M01 20230217/59992: J1859+0239-M01 20230121/59965: J1859+0239-M01 20221103/59886: J1859+0239-M01 20221222/59935: J1859+0239-M01	15 5 15 15 15 5 5 5 5 5	1/1060 1/353 1/1060 0/1060 0/1060 0/353 0/353 0/353 0/353 0/353	
J1900–0152g	0516	1.384(6)	314(2)	19:00:56	–01:52	20221109/59892: J190056–015215sp-M01 20220812/59803: G32.25–3.05-M19P2	15 5	14/642 7/216	14.5
J1900+0732g	0318	1.709(1)	226(1)	19:00:15	+07:32	20210626/59390: J190015+073203sp-M01 20200512/58980: G40.57+1.36-M18P4	15 5	8/519 2/175	4.0
J1903+0319g	0319	1.854(3)	307(3)	19:03:14	+03:19	20210508/59341: J1903+0319-M01 20200521/58989: G37.29–1.27-M17P2	60 5	11/1872 1/161	5.1
J1906+0335g	0226	1.296(1)	213(1)	19:06:48	+03:35	20210707/59401: J190649+033508-M01 20210627/59391: J190648+033500sp-M01 20210606/59370: G37.97–1.78-M05P1	15 15 5	34/685 25/685 9/238	8.0
J1907+0555g	0320	3.159(1)	150(5)	19:07:27	+05:55	20201101/59154: J1907+0555-M01 20200514/58982: G39.93–0.93-M19P2	60 5	31/1062 1/94	7.2
J1911+0310g	0517	1.3326(5)	167.7(8)	19:11:18	+03:10	20221111/59894: J191118+031005sp-M01 20220706/59765: G38.22–2.88-M13P2	15 5	11/667 7/225	7.7
J1912+1000g	0321	3.053(4)	147(4)	19:12:46	+10:00	20210113/59227: J1912+1000-M01 20201123/59176: J1912+1000-M01 20201206/59189: G43.55–1.78-M06P4	15 15 5	12/290 5/290 2/98	3.7
J1915+1045g	0518	1.546(2)	123(3)	19:15:32	+10:45	20221107/59890: J191532+104524sp-M01 20200219/58898: G45.21–0.25-M03P4 20201205/59918: J191532+104524-M01	15 5 15	15/575 1/194 11/575	3.3
J1919+1113g	0322	0.766(5)	288(2)	19:19:27	+11:13	20210113/59227: J1919+1113-M01 20201121/59174: J1919+1113-M01 20200509/58977: G46.24–1.02-M05P2	15 15 5	9/1159 6/1159 2/391	4.8
J1921+1227g	0323	1.598(1)	259(2)	19:21:22	+12:27	20211004/59491: J192122+122745sp-M01 20210805/59431: G47.37–0.93-M07P1 20220629/59758: J192133+123801-M11	15 5 15	4/556 1/187 12/556	0.3
J1927+1849g	0389	0.3121(1)	200(3)	19:27:46	+18:49	20220329/59667: J192746+184917-M01 20220210/59620: J1928+1852-M06P4 20220306/59644: J192733+185434-M03	15 5 15	13/2848 2/961 11/2848	20.8
J1938+1748g	0523	7.1060(2)	56(1)	19:38:30	+17:48	20230218/59993: J193829+174846-M01 20221004/59856: G54.31–1.95-M15P3	15 5	11/125 2/42	1.8
J1940+2231g	0324	5.682(2)	198(7)	19:40:55	+22:31	20201123/59176: J1940+2231-M01 20200421/58960: G58.62–0.08-M05P2 20220925/59847: J1940+2231-M01 20221115/59898: J1940+2231-M01 20221128/59911: J1940+2231-M01	15 5 15 15 15	8/156 4/52 5/156 3/156 9/156	2.9
J1948+2438g	0519	1.9031(2)	450(4)	19:48:23	+24:38	20221107/59890: J194823+243817sp-M01 20220708/59767: G61.16–0.59-M07P2	15 5	1/467 1/157	5.0
J1956+2911g	0520	3.8163(2)	265(2)	19:56:36	+29:11	20220329/59667: J195635+291113-M01 20210912/59469: G66.10+0.34-M04P2	15 5	11/233 3/78	1.9

value of pulses for 50 transient sources (see Sect. 2.2.3), see the second part of Table 1 for the list. We therefore

confirm that these 16 sources are characterized as proto-RRATs with occasionally emitted pulses. With a newly

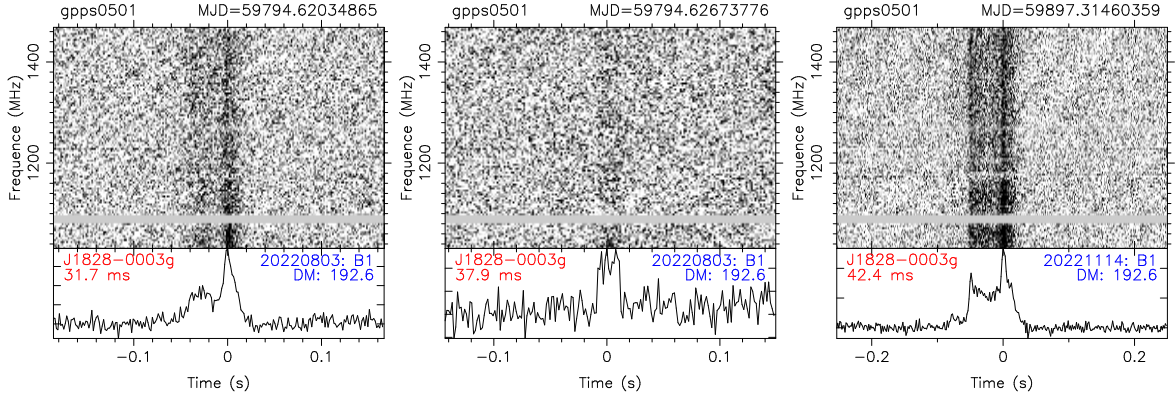


Fig. 3 Examples for the merely 3 pulses detected by the FAST at three epochs from a new FAST transient source, J1828-0003g. See Figure 23 in the Appendix for all 105 pulses detected by FAST from 26 radio transient sources. The two-dimensional dynamic spectrum over the frequency in the band and observation time is shown in the top-subpanel, and the de-dispersed averaged profile is shown in the bottom sub-panel. The GPPS object number is given on the top of the panel on the left, and epoch is marked on the right. The name of object and the pulse width (in ms) are marked in the top-left inside the lower sub-panel, observation date together with the pulse number (number after B) and the also DM value are marked in the top-right.

found period, the detected pulses can be well aligned, see an example in Figure 4. Such plots for newly discovered RRATs in the GPPS survey are shown in Figure 24 in the Appendix. In general, we can get much better average profiles for these detected pulses over 3σ , but cannot detect significant emissions from other periods though they are all added together. Such proto-RRATs cannot be detected via general normal pulsar periodicity search, and their integrated profiles over all periods in an observation session do not have a good S/N.

For some proto-RRATs with several observation sessions, the pulse detect rate is somehow a constant, such as about 24 pulses per hour for J2005+3156g. For some RRATs, the pulse strengths and the detection rates vary a lot, see N_d/N_p and T_{obs} in Table 1 for J1905+0558g as examples. For some RRATs, however, a period is obtained fortunately from few detected pulses. For example, both J1857+0229g and J1924+1446g have only one pulse detected in the 5 minutes survey data, and their periods are obtained from only 9 pulses detected from the expensive one hour observations. No such fortune is available for many transient sources discussed above, such as J1850-0004g, J1855+0033g and J1916+1142Ag.

3.3 Newly discovered extremely nulling pulsars

In addition to detecting sparse pulses from RRATs discussed above, the single pulse search module can also pick up successive pulses for several periods but merely emerge in a small fraction of observation time, so that they cannot be picked out via the periodicity pulsar search. No detection of the pulsed flux for other periods than bright pulses

implies their nature of very nulling. We get 10 new extremely nulling pulsars from the single pulse searching, as listed in the third part of Table 1. Figure 5 shows one example, while all newly discovered very nulling pulsars are shown in Figure 25 in the Appendix.

Such extremely nulling pulsars have an advantage for period determination. Catching the emission active episode sometimes is not easy for some objects, so none detection of any pulses ($N_p=0$) in some observation sessions for e.g. PSR J1845-0008g and J1855+0240g is possible, see Table 1. PSR J1845-0008g is a particularly interesting nulling pulsar. We detect pulses in three sessions, but not the other three. For PSR J1855+0240g, successive pulses are merely detected in a short episode during the 15-minute observation.

The mean flux density (S) of these pulsars in Table 1, calculated from the averaged flux over all periods in the observation session, should be taken as the upper limit.

3.4 Weak pulsars with sparse strong pulses

For 24 weak pulsars listed in the last part of Table 1, the single pulse search module can also pick up sparse strong pulses from the 5 minutes snapshot observations. The normal pulsar searching cannot pick up these objects due to the low single-to-noise ratio. They may be detected as a pulsar with the same DM and period from the following-up 15 minutes tracking observations. Figure 6 shows one example, and plots for all the 24 weak pulsars are presented in Figure 26 in the Appendix.

Some newly discovered pulsars are remarkable in some aspects. PSR J1849+0619g (GPPS0522) is dis-

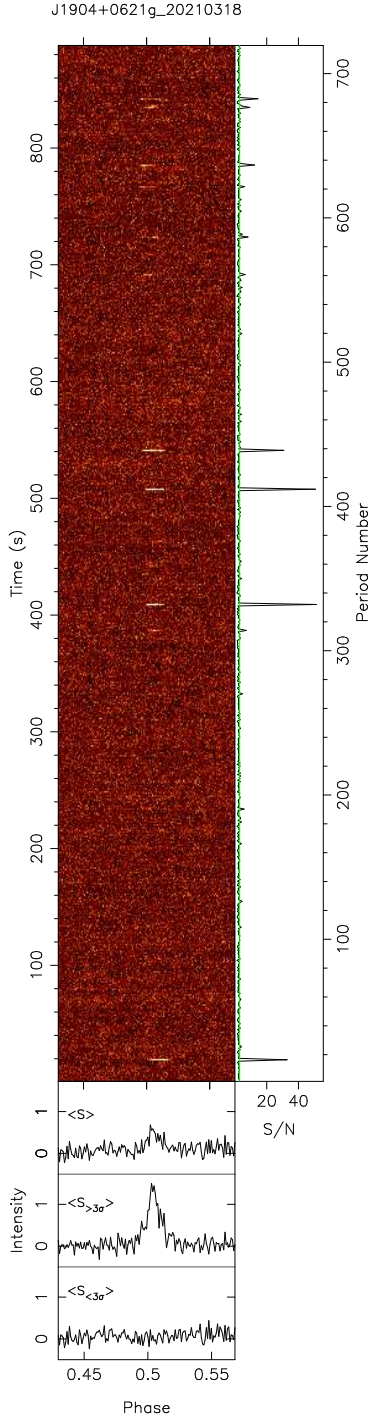


Fig. 4 An example of a newly discovered RRAT, PSR J1904+0621g. Plots for 16 newly discovered RRATs are presented in Figure 24 in the Appendix. Pulse-stack is shown in the main left panel, with only a few pulses occasionally emit. The right panel shows the curve of S/N over pulse number (see Sect.2.2.2), with the sigma calculated from a given width of off-pulse phase range. Three sub-panels below the main panel are the averaged profiles of all periods, of single pulses with the signal-to-noise ratio $> 3\sigma$ and $< 3\sigma$.

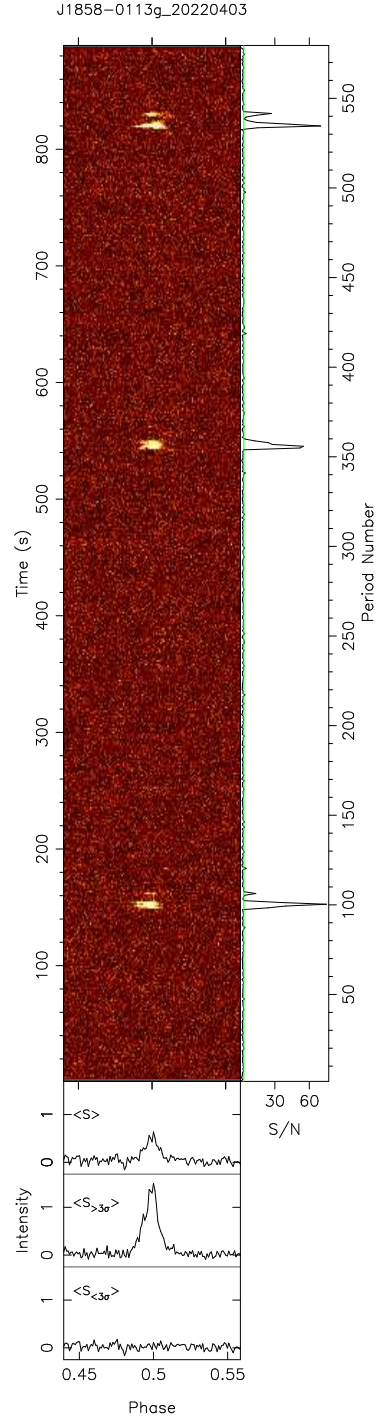


Fig. 5 Same as Figure 4 but for an example of extremely nulling pulsar, J1858-0113g, discovered by the GPPS survey. Plots for all observations of newly discovered nulling pulsars are presented in Figure 25 in the Appendix.

covered via the single pulse search, one pulse in G38.56+3.30-M14P1 on 20221001 and another one pulse in J184950+062304-M04 on 20221111 with the same DM of 110 ± 1 pc cm $^{-3}$. Together with the 4 pulses discovered in a recent verification observation on

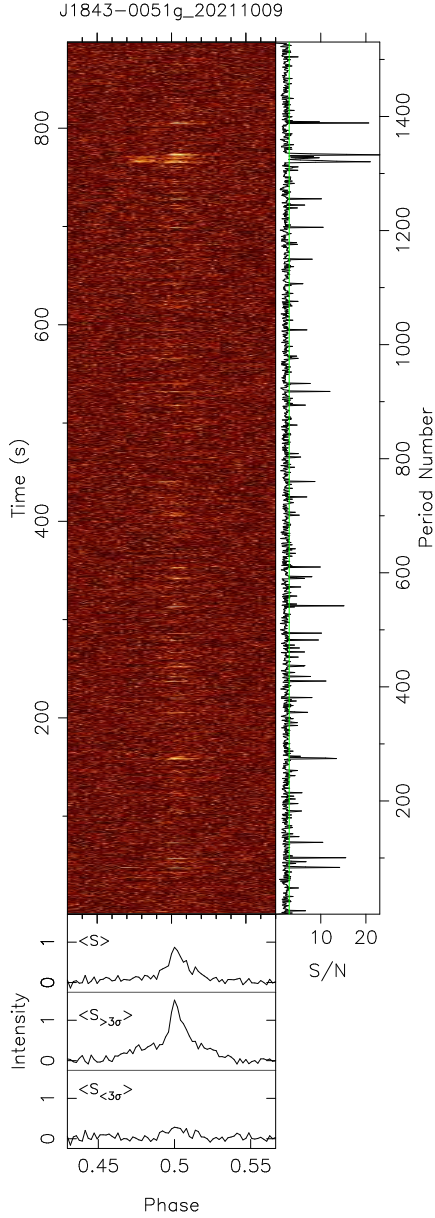


Fig. 6 Same as Figure 4 but for an example of a weak pulse with sparse bright pulses. Plots for many such new weak pulsars discovered by catching their bright pulses are presented in Figure 26 in the Appendix.

20230228, the period is found from this observation that is about 2.011230 s via the careful period search at this DM. PSR J1859+0239Bg (GPPS0526) is discovered by only one pulse on 20220529 in the data for timing PSR J1859+0239Ag (GPPS0091, i.e. PSR J1859+0239g reported in the paper I Han et al. 2021). This new pulsar has only one pulse detected in each of the three sessions, 20220529, 20221227 and 20230125. Its period was found via the periodicity searching on 20230125 though with a very weak S/N (see Figure 26 in Appendix), but not confirmed by the folded profiles with the same period

Table 2 Polarization properties of individual pulses for the newly discovered transient sources.

Name	ObsDate:No.	L/I (%)	V/I (%)	$ V /I$ (%)	RM (rad m ⁻²)
J1828-0003g	20221114:B1	40.5	-4.1	18.4	5.7(36)
J1850-0004g	20200415:B1	48.0	-13.2	16.4	-286(10)
	20200902:B1	49.1	-30.7	29.7	-317(9)
	20220608:B1	73.4	12.3	13.1	-298(1)
	20220608:B3	44.9	-15.9	15.4	-302(9)
J1853+0209g	20221106:B1	38.2	-3.9	0.0	-286(7)
J1853+0353g	20220824:B1	57.4	-1.6	2.7	-27(10)
J1855-0211g	20210624:B1	63.4	2.3	14.7	381(13)
J1855+0033g	20221205:B1	31.5	1.8	12.0	715.9(46)
	20221205:B2	61.1	12.1	10.0	711.8(44)
	20221205:B3	31.3	-2.2	13.5	712.1(37)
	20230305:B1	50.3	4.9	27.9	725.3(14)
J1859+0832g	20210328:B2	53.5	17.5	15.3	381(9)
J1859+0832g	20221107:B1	80.1	-8.8	8.5	1004(2)
J1918+0342g	20211202:B1	57.4	-8.4	20.2	208(5)
J1921+1629g	20211004:B1	52.7	18.5	18.1	362(4)
	20211004:B2	52.5	17.7	16.6	368(3)
J1924+1734g	20211005:B3	51.4	7.5	10.9	108(6)
J1934+2341g	20210624:B5	58.5	0.4	1.4	133(3)
J2005+3154g	20211009:B2	54.5	-70.4	70.2	-132(9)

on 20211226, 20230102 and 20230125. PSR J1938+1748g has a period of 7.106 s, while the folded pulse-width is 8.7 ms which means an extremely narrow pulse with a duty cycle of only about 0.082% or 0.29 degrees in the rotation phase longitude. PSR J1956+2911g is also a source with a narrow pulse width of only 3.7 ms, or 0.36 degrees in the rotation phase longitude. PSR J1921+1227g has a low mean flux density of about 0.28 μ Jy, which is probably one of the weakest pulsars. The pulse-stacks of PSR J1843-0051g and J1856+0029g show mode-changing with bright wider pulses detected only in some episodes and weaker narrow pulses in other periods. They are similar to the case of the known pulsar PSR J1938+2213 with an occasionally bright mode, see Section 5. PSR J1927+1849g was first picked up as 2 single pulses from the single pulse search in the 5 minutes observation, and the two tracking observations show a wide profile with these sparse narrow bright pulses.

3.5 Polarization of new sources

Fortunately, polarization data are recorded for all tracking observations for verification of the detected single pulses. Following Han et al. (2021) and Wang et al. (2022), we calibrate the polarization data, and obtain the polarization profiles for some strong single pulses of the transient sources (see Figure 7) and the mean polarization profiles of bright pulses of the newly discovered proto-RRATs, extremely nulling pulsars and weak pulsars (see Figures 8, 9 and 10). We derive the polarization properties and also the Faraday rotation measures (RMs) of the bright pulses for the transient sources, as listed in Table 2, and of the mean for bright pulses of RRATs, nulling pulsars and weak pulsars

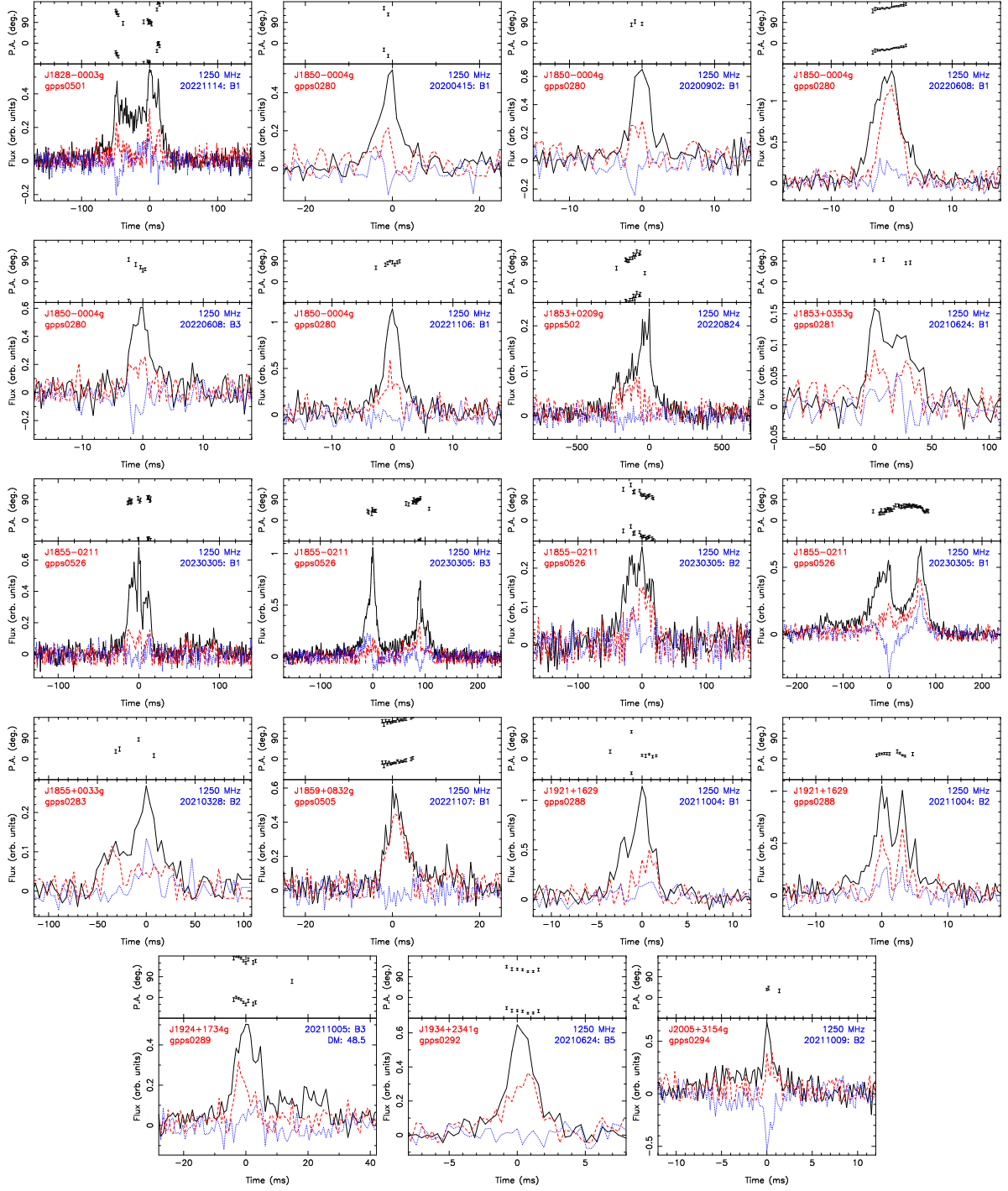


Fig. 7 Polarization profiles of strong pulses from newly discovered transient sources. The upper sub-panel is for polarization angle (PA), and bottom sub-panel is for pulse profiles of total intensity I (solid line), linear polarization angle L (dashed line) and circular polarization V (dotted line). Source name, the source number in GPPS survey, observe date, pulse number on that day are marked inside the bottom sub-panel.

as listed in Table 3. The new measurements of RMs can be used for revealing the interstellar magnetic fields (Han 2017; Han et al. 2018; Xu et al. 2022a).

Some features of these polarization profiles of transient sources are remarkable. Pulse No.1 of J1850-0004g

observed on 20220608 is highly linearly polarized, with the polarization angles (PAs) clearly sweep up. So do the pulse on 20220824 of J1853+0209g and pulse No.1 on 20221107 of J1859+0832g. The PAs in part of the profiles sweep down are seen in the pulse No.1 on 20221114 of

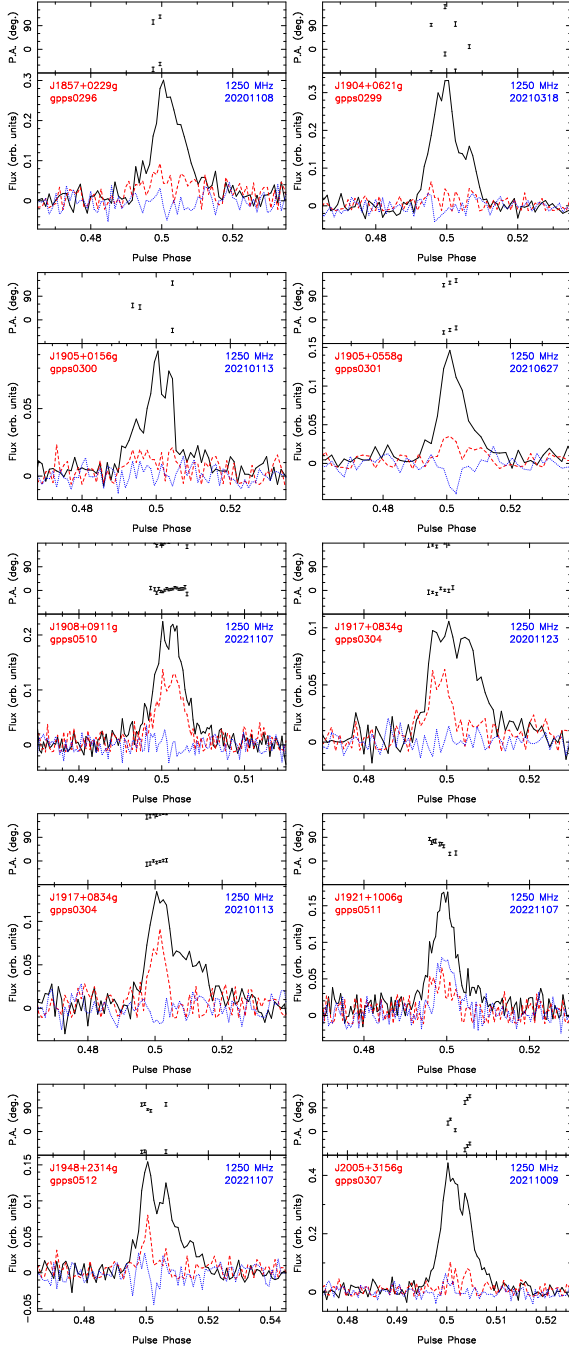


Fig. 8 The same as Figure 7 but for the integrated polarization profiles of the bright pulses of newly discovered RRATs in the GPPS survey.

J1828–0003g, pulse No.3 on 20211005 of J1924+1734g and pulse No.5 on 20210824 of J1934+2341g. Such PA sweeping is a typical feature of pulsar signals produced in pulsar magnetosphere. Therefore we trust that the pulses of these transient sources are produced by neutron stars, and they are probably just bright pulses of undetectable weaker pulsars, see more discussion of FAST observations of previously known RRATs below.

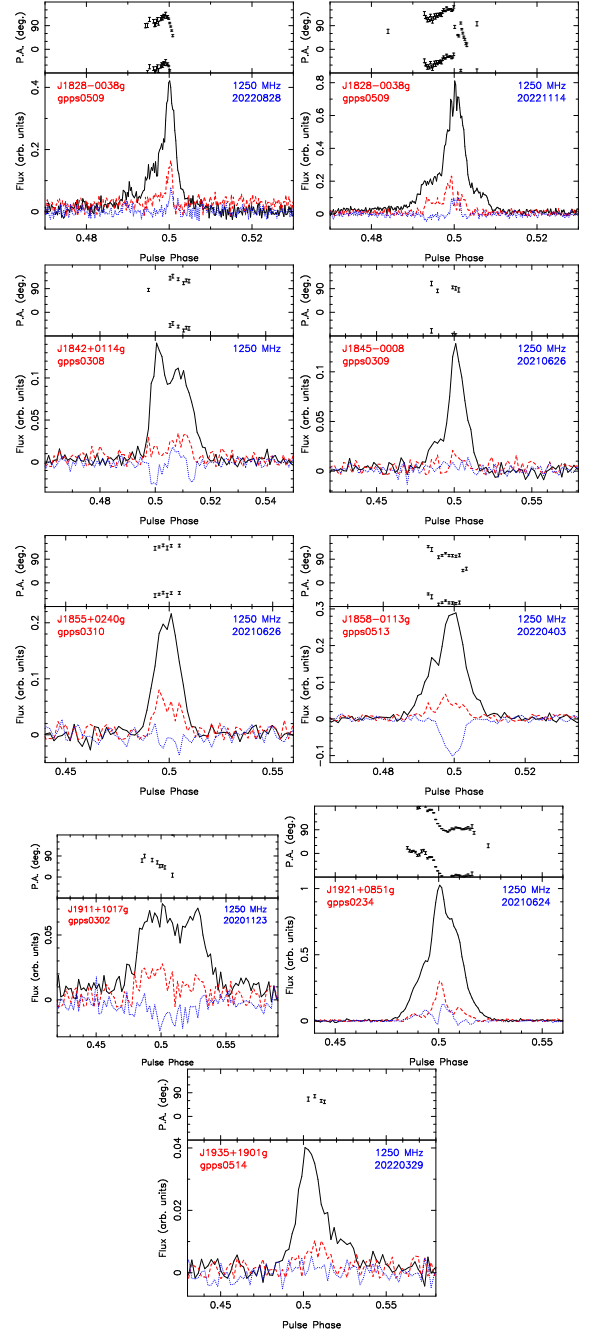


Fig. 9 The same as Figure 7 but for the integrated polarization profiles of the bright pulses of newly discovered extremely nulling pulsars in the GPPS survey.

The polarized profiles of the pulse No.2 on 20221009 of J2005+3154g have a highly circular polarization of $V/I = -0.702$.

As seen in Table 2 and 3, for pulses detected from one source or observed at different days, their RMs are consistent with each other within uncertainties. The largest RM value is detected for the pulse No.1 on 20221107 of J1859+0832g, which is $1004 \pm 2 \text{ rad m}^{-2}$ for the pulse with

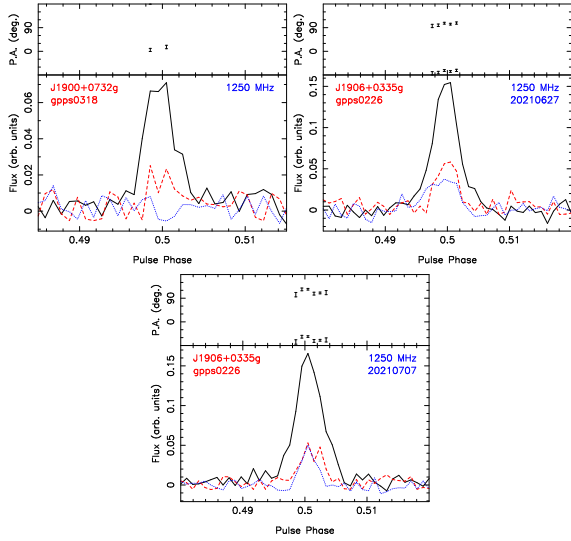


Fig. 10 The same as Figure 7 but for the integrated polarization profiles of the bright pulses of newly discovered weak pulsars in the GPPS survey.

Table 3 Polarization properties of new pulsars with bright pulses.

Name	ObsDate	W_{50} (ms)	L/I (%)	V/I (%)	$ V /I$ (%)	RM (rad m ⁻²)
RRATs with a good period identified						
J1857+0229g	20201108	5.7	37.4	8.2	6.6	34(12)
J1904+0621g	20210318	9.6	22.8	4.4	7.2	-238(25)
J1905+0156g	20210113		42.7	10.4	19.8	-84(5)
J1905+0558g	20210627	6.6	25.0	-19.8	18.0	431(20)
J1908+0911g	20221107	18.9	57.0	-0.7	5.0	73(2)
J1917+0834g	20201123	37.2	51.0	0.0	6.8	192(3)
	20210113	22.9	53.3	-6.8	8.5	180(4)
J1921+1006g	20221107	19.6	38.5	36.0	34.5	489(8)
J1948+2314g	20221107	14.4	35.6	6.0	7.5	70(4)
J2005+3156g	20211009	12.6	21.5	1.5	3.3	-283(6)
Extremely nulling pulsars						
J1828-0038g	20220828	8.3	31.6	6.4	6.6	33(2)
	20221114	12.4	24.9	0.8	6.5	36.7(9)
J1842+0114g	20210317	60.7	33.0	4.9	10.6	119(5)
J1845-0008g	20210626	14.9	18.9	5.0	2.8	24(9)
J1855+0240g	20210626	16.7	33.1	-6.6	9.3	99(6)
J1858-0113g	20220403	13.5	18.9	-25.6	25.5	673(3)
J1911+1017g	20201123	70.5	38.0	-19.1	20.0	261(14)
J1921+0851g	20210624	14.0	16.7	6.3	8.2	381.3(8)
J1935+1901g	20220329	14.0	31.1	5.4	2.1	82(8)
Newly discovered weak pulsars with occasionally strong pulses						
J1900+0732g	20210626	6.7	35.3	1.9	5.3	372(17)
J1906+0335g	20210627	6.3	37.5	26.4	26.4	203(4)
	20210707	6.3	27.4	19.5	19.8	205(4)

a DM of 259 ± 2 pc cm⁻³. The result is understandable that this object is located near the Galactic plane in the spiral arm tangent where the interstellar magnetic fields could be very strong (Han 2017; Han et al. 2018; Xu et al. 2022a).

No question that the polarization profiles of the mean bright pulses of RRATs, nulling pulsars and weak pulsars are more or less similar to polarization of normal pulsars (Wang et al. 2022).

4 OBSERVATIONS OF KNOWN RRATs

Sensitive observations of previously known RRATs can help to understand the enigma of RRATs.

In the visible sky area of FAST, there are more than 60 previously known RRATs. Since these RRATs were discovered via detection of sparse strong pulses by other telescopes (McLaughlin et al. 2006; Hessels et al. 2008; Deneva et al. 2009; Keane et al. 2010; Burke-Spolaor & Bailes 2010; Burke-Spolaor et al. 2011; Keane et al. 2011; Coenen et al. 2014; Stovall et al. 2014; Karako-Argaman et al. 2015; Deneva et al. 2016; Keane et al. 2018; Patel et al. 2018; Tyul'bashev et al. 2018b,a; Good et al. 2021; Dong et al. 2022), very sensitive observations by FAST may reveal possible weaker pulses from these rotating neutron stars. Some known RRATs have basic parameters (period, DM and position) with a poor accuracy, and our new observations with the FAST snapshot observations can improve these parameters (see Table 6), as done for other pulsars in the first paper (see Han et al. 2021).

With the observations of the GPPS survey and also the project for the known pulsar positioning (PT2021_0051, PI: J. Xu) and the projects for known RRATs studies (PT2021_0151, PI: D.J. Zhou), we have got 59 RRATs observed by chance or by targeting observations, and detected 48 RRATs (see the list in Table 6). 11 RRATs have been observed but not detected (see Table 7), among which 8 RRATs could not be detected in targeted observations and the other 3 could not be detected in the snapshot observations for the GPPS survey. It is possible that these RRATs were not active when they were observed by FAST, e.g. for J1911+00 only 0.31 pulses hr⁻¹ in the original discovery paper. Some RRATs were discovered at a very low-frequency band, and do not have enough flux at the L-band for the FAST to detect, e.g. J0534+3407. Otherwise, non-detection could be caused by the very large uncertain position.

For 48 known RRATs we detect, their parameters are presented in Table 6, and period, DM or position accuracy has been improved for 28 RRATs. The period of an RRAT is obtained either from the TOAs of single pulses or even via a normal periodic search for the survey data (see Table 6). The spin period of J0156+0358, J1857+0719 and J1905+0414 are obtained for the first time here by our FAST observations. The periods of J1838+0414 and J1924+1006 were 3.640 s and 5.281 s, respectively, in the discovery paper for the PALFA¹⁴, however, we detect the periods of 1.330681 s and 4.619757 s by analyzing the TOA of the detected single pulses in our FAST data with the period analysis program *PF*. The DM values of these RRATs were estimated by using some bright

¹⁴ <http://www.naic.edu/~palf/newpulsars/>

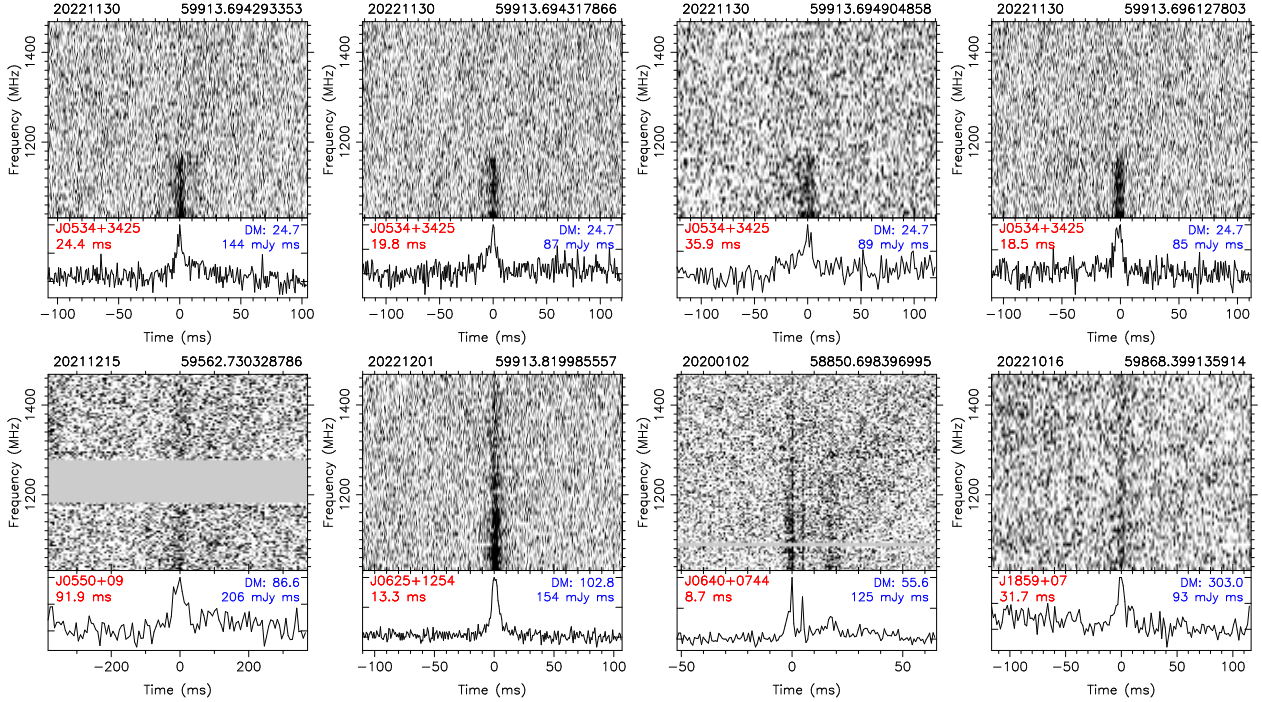


Fig. 11 The same as Figure 3 but for no period is found for previously known RRATs J0534+3425, J0550+09, J0625+1254, J0640+0744 and J1859+07. Some channels in dynamic spectra are removed due to RFI.

single pulses, and we get DMs of 10 RRATs improved. J1945+2357 (J1946+24) was reported to have a DM of 96 pc cm^{-3} (Deneva et al. 2009), but our FAST observations give a much better determined DM as being $87.53 \pm 0.18 \text{ pc cm}^{-3}$. For some RRATs, their position can be constrained by the FAST observations to a half beam size of FAST (see discussion in Sect.4 and Sect.5 of Han et al. 2021), and we get positions of 19 RRATs, significantly improved from these in references. Their new names accordingly to the latest coordinates are given in the first column in Table 6.

We emphasize that most of the previously known RRATs are very bright for the FAST, as indicated by the high detection percentage of individual pulses over the 3σ criteria as listed in column (10). Nevertheless, for 1 known RRAT, we detect only 4 pulses, and for other 4 known RRATs, we detect only one pulse each. PSR J0534+3425 was first discovered at 111 MHz (Tyul’bashev et al. 2018b), and we detect 4 pulses in a 5-minute tracking observation of the GPPS survey, but no pulse was detected in the following 15 monitoring observation. For these four pulses, only signals below 1180 MHz are detected in our observations. Considering the low DM of about 24.7 pc cm^{-3} , the detection in a partial band is likely to be caused by interstellar scintillation. No period can be found from our FAST observation yet. PSR J0550+0948 was reported by Deneva et al. (2016) with $P = 1.745 \text{ s}$ and $DM = 86.6 \text{ pc cm}^{-3}$. Only one weak pulse is de-

tected by FAST with $S/N = 17.2$ during the snapshot observation on 20211215 around a candidate position in the beam of J0550+0900-M02P3. PSRs J0550+0948 (Deneva et al. 2016), J0625+1254 (Patel et al. 2018), J0640+0744 (Tyul’bashev et al. 2018b) and J1859+0759 (Patel et al. 2018) have no previously known period. In our FAST observation, only one pulse is detected in a 5 minutes observation for each source with $S/N=17.2$, $S/N=32.8$, $S/N=25.0$ and $S/N=15.0$, respectively. For these sources, we cannot get a period from our data even after folding for J0550+0948. The dynamic spectra for these eight pulses are shown in Figure 11.

For the other 43 known RRATs detected by FAST, the folded data according to the period and DM show that 25 of them are just normal pulsars (see Figure 12), 5 of them are very nulling pulsars (see Figure 13), and others are pulsars with sparse strong pulses (see Figure 14). In the following, we discuss such these cases in detail.

4.1 Known RRATs as normal pulsars

Because of extremely high sensitivity of the FAST, individual pulses of 25 previously known RRATs are detected over a large fraction of observation time, and they appear as just normal pulsars as shown in Figure 12 though bright pulses or nulling features occasionally emerge. It is understandable that when the detection threshold is tens times or hundreds times worse than the current 3σ thresh-

Table 6 FAST observations of Previously Known RRATs: Polarization Parameters

Name	L/I (%)	V/I (%)	$ V /I$ (%)	RM (rad m ⁻²)
Just a pulsar with nulling features in FAST observations:				
J0302+2252	24.2	-0.3	6.4	-7.20(3)
J0608+1635	14.7	10.2	9.9	-106(2)
J0625+1714	42.7	-1.1	7.1	107(2)
J1538+2345	47.7	-5.9	6.9	9.2(2)
J1843+0118	44.5	-8.8	9.0	49(5)
J1843+0527	22.8	0.4	10.5	221(5)
J1849+0106	31.3	-5.8	6.0	107.4(6)
J1850+1532	49.0	-17.7	22.4	67(7)
J1853+0427	33.2	15.3	15.9	379.9(5)
J1856+0912	40.1	0.9	8.7	618.3(7)
J1905+0902	20.7	1.7	2.2	520(3)
J1908+1351	27.6	-8.3	10.2	634(2)
J1909+0641	15.8	-4.1	8.7	-18(2)
J1915+0639	20.5	-10.2	10.9	201(6)
J1919+1745	41.3	2.4	3.9	520.0(5)
J1952+3021	10.8	-3.0	2.7	-8(2)
J1958+3033	16.5	1.5	7.5	-15(3)
J2000+2920	22.5	-4.0	5.1	63.3(3)
J2008+3758	31.8	0.5	3.4	277(2)
J2033+0042	15.0	-2.2	4.1	-71.2(3)
Extremely nulling pulsars in FAST observations:				
J0103+5354	26.1	6.5	6.4	-56(4)
J1717+0305	39.3	-3.1	6.8	22(4)
J1720+0040	17.9	-1.0	9.5	1(5)
J1839-0141	27.6	-16.1	17.3	355.8(3)
J1928+1725	95.9	-1.8	2.4	215.6(5)
Very weak pulsars with sparse strong pulses in FAST observations:				
J0623+1536	46.5	-7.2	11.1	28.1(3)
J0627+1612	78.9	-4.2	0.0	166(8)
J0628+0909	31.4	15.9	16.7	129.4(3)
J1848+1516	40.8	-2.1	15.2	240.4(6)
J1854+0306	52.7	-2.4	3.4	-43.3(5)
J1905+0414	63.5	-4.0	11.6	1089(3)
J1924+1006	50.1	-3.2	2.7	425(4)
J1945+2357	38.0	13.3	20.3	20(8)

old of FAST observations, only a few strong pulses would be detected, and they would definitely appear as RRATs as shown in original discovery papers (McLaughlin et al. 2006; Cordes et al. 2006; Deneva et al. 2009; Patel et al. 2018), and a period of an RRAT may be hard to find, for example, J1849+0106 and J1908+1351 by Arecibo, see the web-page¹⁵.

Some interesting features are revealed in our FAST observations. For example, nulling for a small fraction of periods in the single pulse series is observed for J1919+1745, and even one weak dwarf pulse has been detected (see Fig. 27). Some pulsars are very normal so that we can see a quasi-periodic intensity modulation in their single pulse sequence, such as J1915+0639 and J1952+3021, or subpulse drifting, such as J1843+0527 and J1952+3021. Analyses of the single pulse behaviors for a large number of pulsars will be reported by Y. Yan et al.(2023, in preparation).

¹⁵ see <http://www.naic.edu/~palfa/newpulsars/>

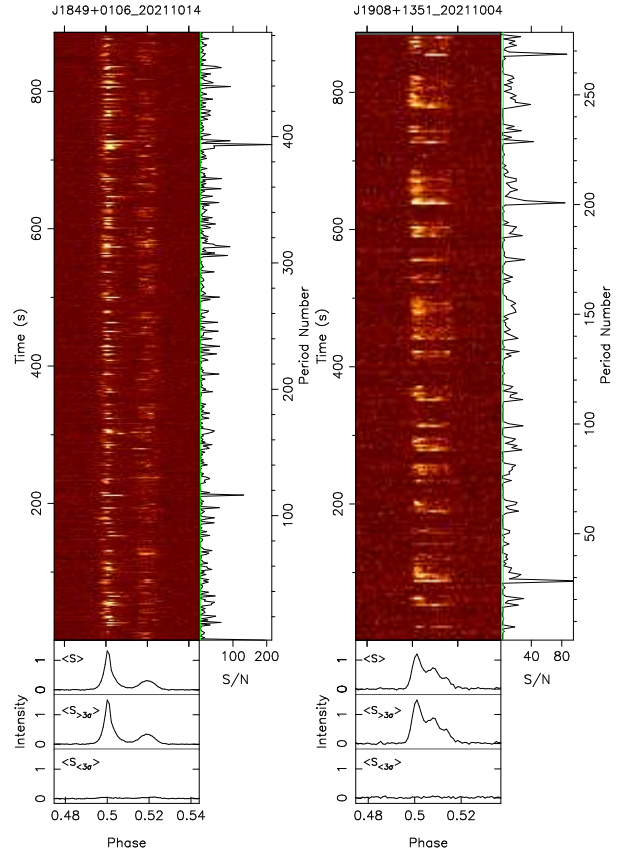


Fig. 12 Two examples (J1849+0106 and J1908+1351) for the known RRATs shown as normal pulsars in the FAST observations though some bright pulses occasionally emerge. All such cases are presented in Figure 27 in Appendix.

4.2 Known RRATs as extremely nulling pulsars and pulsars with sparse strong pulses

Five previously known RRATs appear as extremely nulling pulsars in the FAST observation as shown in Figure 13. For example, the PSR J0103+5354 and J1839-0141 have only one, J1717+0305 and J1928+1725 have two brief continuous radiation episodes, and J1720+0040 have several interspersed emission fractions in our observations. Outside the active episodes, no detectable pulse is found in FAST data.

We have got the other 13 known RRATs observed by the FAST, and they generally appear as many sparse strong pulses as shown in Figure 14 and also shown Figure 29, much more pulses than in their original discovery papers. They ‘must’ be RRATs in the eyes of other telescopes. In our FAST observations, we can get them easily detected not only by single pulse search module, and most of them can be picked out through normal pulsar searches.

Some objects are worth to give a note. PSR J1720+0040 is an interesting RRAT. We detect 7 pulses

Table 7 Previously known RRATs observed but not detected by FAST observations

Name	Ref.	R.A.(J2000)	Dec(J2000)	P	DM	FAST	FAST beam Name /ObsDate	T _{Obs}
(1)	(2)	(3)	(4)	(5)	(6)	(7)	(8)	(9)
		(hh:mm:ss)	(dd:mm)	(s)	(cm ⁻³ pc)	Project ID		(min)
J0544+20	[1]	05:44:12	+20:50		56.9	PT2021_0151	J0544+2000-M01 /20211210	5
J1059-01	[2]	10:59	-01:02		18.7	PT2021_0151	J1059-0100-M01 /20211209	5
J1433+00	[1]	14:33:30	+00:28		23.5	PT2021_0151	J1433+0000-M01 /20211210	5
J1554+18	[1]	15:54:17	+18:04		24.0	PT2021_0151	J1554+1800-M01 /20211210	5
J1603+18	[1]	16:03:34	+18:51	0.503	29.7	PT2021_0151	J1603+1800-M01 /20211210	5
J1611-01	[3]	16:11	-01:28	1.297	27.2	PT2021_0151	J1611-0100-M01 /20211210	5
J1911+00	[4]	19:11:48	+00:37	6.94	100	PT2021_0151	J1911+0000-M01 /20220126	3
J1912+08	[5]	19:12:57	+08:29		96	GPPS	G42.91-0.85-M02P3 /20200514	5
J1917+11	[6]	19:17:01	+11:42		38.0	PT2020_0155	J1917+1142-M01 /20210108	60
J1928+15	[5]	19:28:20	+15:13		242.0	GPPS	G50.69-1.10-M06P1 /20200528	5
J2007+20	[3]	20:07	+20:21	4.634	67.0	GPPS	G59.74-6.44-M07-P3 /20210710	5

References in Column (2): [1] = [Deneva et al. \(2016\)](#); [2] = <http://astro.phys.wvu.edu/rratalog/>; [3] = [Karako-Argaman et al. \(2015\)](#); [4] = [McLaughlin et al. \(2006\)](#) [5] = <http://www.naic.edu/~palfa/newpulsars/> [6] = [Tyul'bashev et al. \(2018b\)](#). In column (8), observations with a beam name starting with 'G' were made by the GPPS survey, and others with 'J' by applied FAST PI projects.

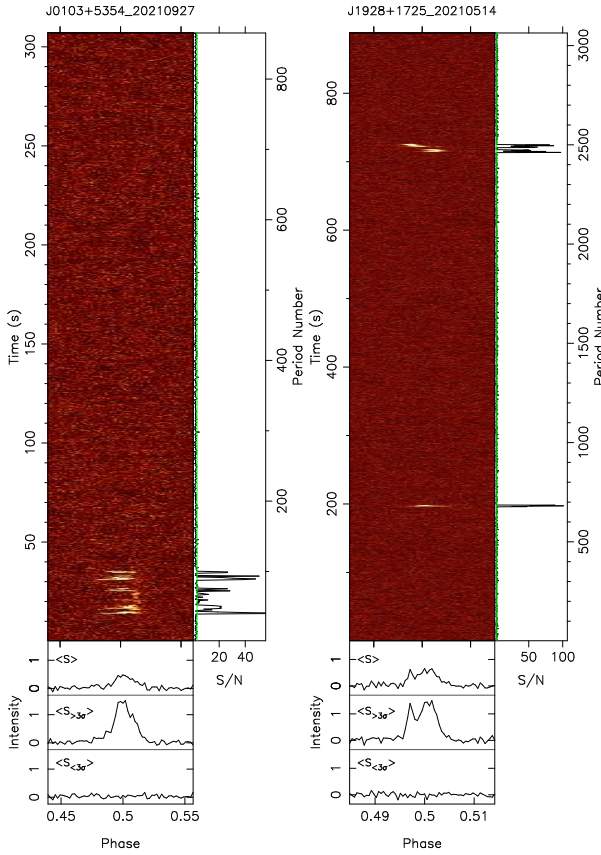


Fig. 13 The same as Figure 12 but for two examples of the known RRATs shown as extremely nulling pulsars. All such cases are presented in Figure 28 in Appendix.

during a 305 s observation (see Figure 14), and we fortunately can get its period as being 3.356875 s. We can determine the position according to the position of the snapshot beam with significant pulse signal detection. The occasional brightened state, for example, has been recently detected for PSR J1938+2213 ([Chandler 2003](#); [Sun et al. 2022](#)), which is shown in Figure 16. The single pulses in

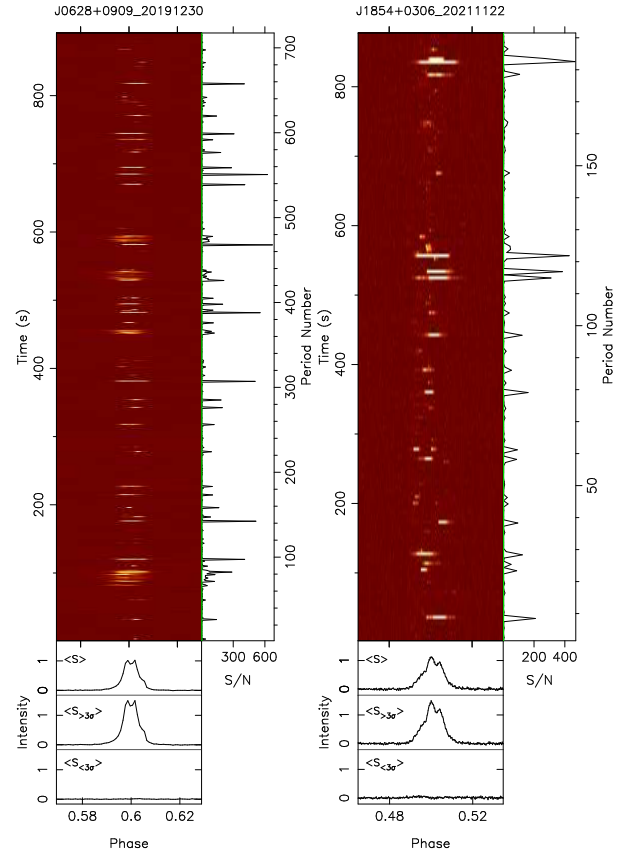


Fig. 14 Two examples for the known RRATs shown as generally very weak pulsars with sparse strong pulses. See all such cases Figure 29 in Appendix.

the bright state are suddenly 100 times brighter. If it is observed by a small telescope, probably only the brightened part would be observable, it could be shown as an extremely nulling pulsar, like PSR J1839-0141 ([Lu et al. 2019](#)) and PSR B0823+26 ([Sobey et al. 2015](#)) which have a 'bright' mode that regularly emits bright pulses and a 'quiet' mode that occasionally emits weak pulses. PSR

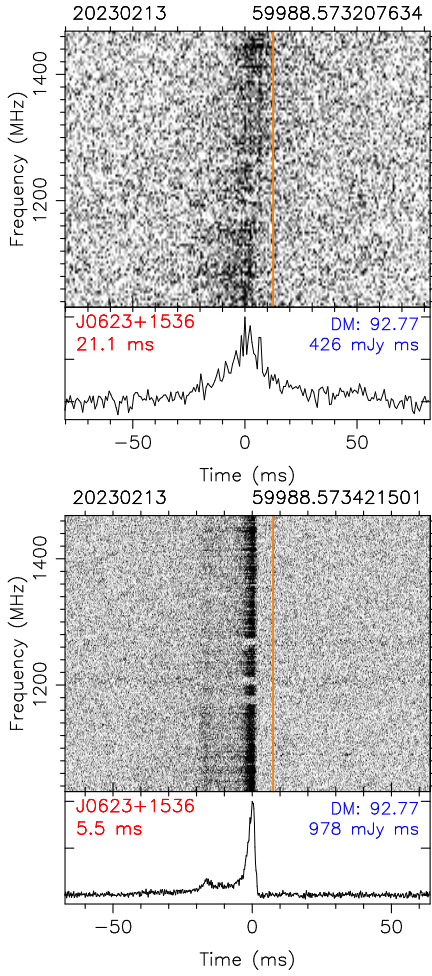


Fig. 15 The same as Figure 3 but for two single pulses of PSR J0623+1536, dedispersed by using the DM of $92.77 \text{ cm}^{-3} \text{ pc}$. A dark yellow vertical line is used to indicate the proper dedispersion for the two pulses. The dynamic spectrum of the upper one for the period No.330 shows that emission first appears at the lower part of frequency band but later the emission appears at the higher part of the band. The other pulse in the lower panel for the period No.337 does not show such a frequency drifting.

J1946+1449 (J1946+14) (Deneva et al. 2016) is also shown RRAT-like pattern that emission is intermittent, and we detect few bright pulses. If they are observed by a not-so-sensitive telescope, they must be classified as RRATs as being pulsars with sparse strong pulses.

J0623+1536 is a known RRAT J0623+15 discovered in PALFA survey (Patel et al. 2018) with the previously given DM of $92.5 \pm 1.6 \text{ cm}^{-3} \text{ pc}$. In the 15-minute observation on 20230213, ten single pulses have been detected. We analyze and get a DM of $92.77 \pm 0.24 \text{ cm}^{-3} \text{ pc}$ and a period of about 2.638545(18) s. Interestingly, the single pulse at the period No.330 shows the emission frequency drifting in the dynamic spectrum, while other pulses are very

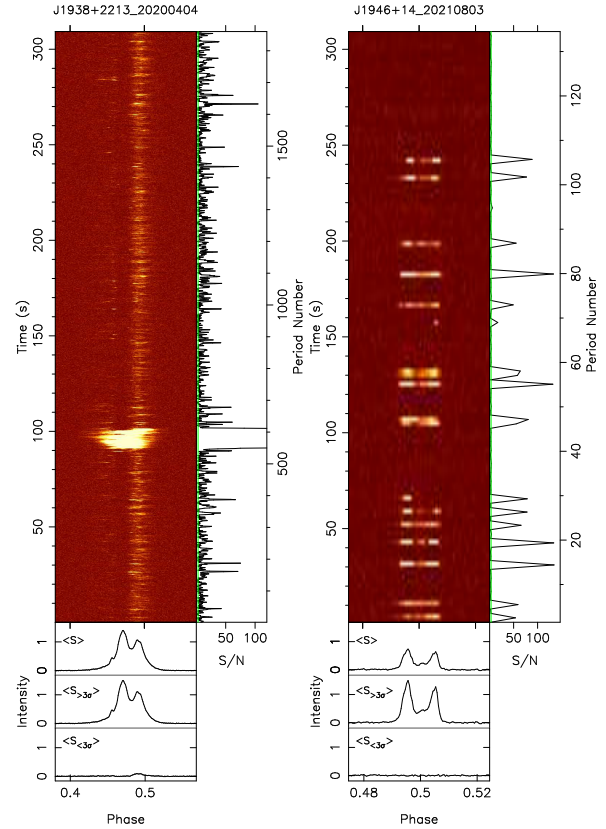


Fig. 16 Same as Figure 12, but for special RRAT-like pulsars. The left plot for J1938+2213 has zoomed in for the maximum of S/N to 120.

normal without any drifting, see Figure 15. The dynamic spectrum of this anomalous pulse shows well-dedispersed structures with the DM of $92.77 \text{ cm}^{-3} \text{ pc}$. Such a phenomenon has been identified for some bursts of FRBs (Hessels et al. 2019; Zhou et al. 2022) but rarely seen in pulsars. The previously known case is the emission drifting structure of PSR J0953+0755 at low frequency (Bilous et al. 2022).

4.3 Polarization of known RRATs

When these known RRATs were observed by FAST, the polarization signals are recorded. We use the standard polarization calibration procedure (Wang et al. 2022) and process all data. We obtain the polarization profiles of these known RRATs as shown in Figure 17, Figure 18 and Figure 19. To maximize the signal to noise ratio, we have to ignore these periods with undetectable signal, i.e. only work on the periods with a signal of $S/N > 3$. We extract polarization information from the Faraday RMs as listed in Table 6.

As one can see from these polarization profiles, in general, they are not unusual compared to normal pulsar profiles. For these RRATs which appear as normal pulsars

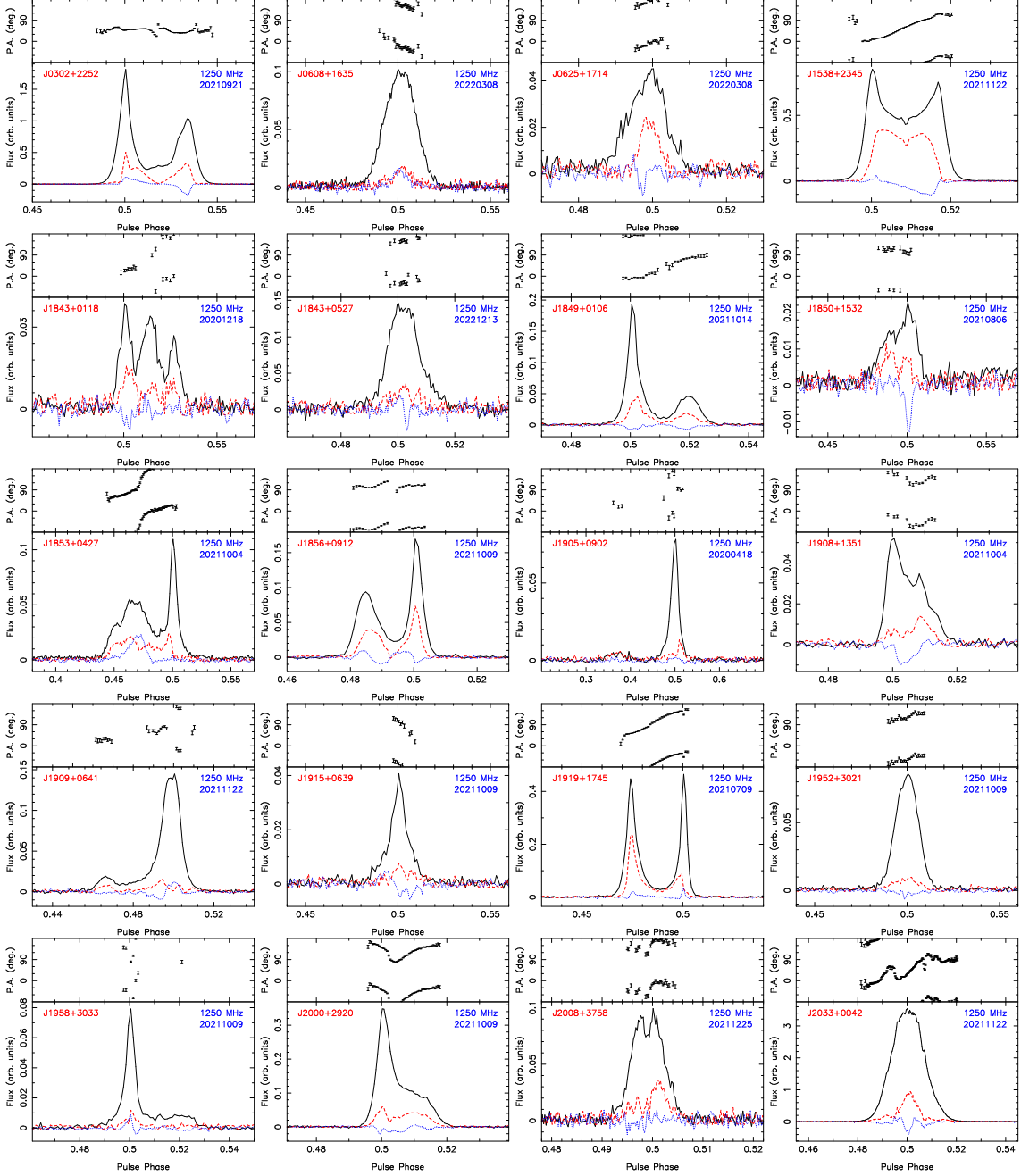


Fig. 17 The polarization angle and integrated polarization profiles of single pulses with S/N > 3.0 of known RRATs as normal pulsars.

in the FAST observations, the PA curves of J1849+0106, J1853+0427 and J1919+1745 show a smooth variation with an ‘S’ shape. Some pulsars show a steep polarization angle sweep at the profile center with a reversal of circular polarization, such as J0302+2252 and J1856+0912. The J1850+1532 has a highly circular polarized component. Orthogonal polarized modes have been detected in the PA curve of J1538+2345.

For five RRATs as extremely nulling pulsars very interesting is the extremely highly linear polarization

of J1928+1725 with a flat PA curve (see Figure 18). For pulsars with sparse strong pulses, because of limited periods accumulated, it is hard to say the profiles in Figure 19 are stabilized. Interestingly the RM value for J1905+0414, which has a large RM value of $1090 \pm 3 \text{ rad m}^{-2}$. Combined with the DM of this RRAT 383.0 pc cm^{-3} , the averaged magnetic fields in the line of sight to this distant RRAT is $1.232 \times 1090/383 = 3.5 \mu\text{G}$. This seems to be fine (Han 2017) for a pulsar at a spiral

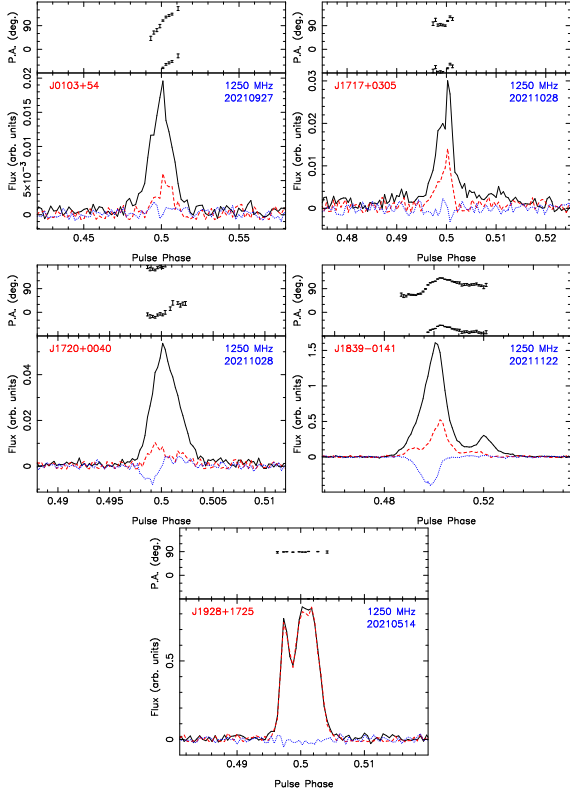


Fig. 18 Same as Figure 17 but for known RRATs as just pulsars with extremely nulling features.

arm tangent at $(l, b) = (38.246^\circ, -1.079^\circ)$. J1720+0040 and J1848+1516 also have reversal of circular polarization.

4.4 Sparse Strong pulses and polarization

For previously known RRATs, it is important to verify if these sparse strong pulses are very outstanding from the energy distribution of normal pulses, and if they have very different polarization from normal pulses.

For known RRATs with a sufficient number (> 300) of single pulses observed by FAST so that a well-defined average pulse profile has been obtained, we obtain the energy distribution of their single pulses. For each pulse, we sum the individual pulse energy in the on-pulse range, and then obtain the average energy of all single pulses. The energy of all individual pulses is then normalized by the averaged energy. As shown in Figure 20, the pulse energy distributions of the known RRATs rarely show any points with a scaled energy greater than 10 if they are believed as normal pulses, except for J0302+2252 and J1915+0639 which seems to be very unusual with two more peaks in the distribution in addition to the main component for nulling pulses around zero. For RRATs as extremely nulling pulsars, the distribution has a component for nulling together with a few periods with a high-energy tail for emission. For RRATs with sparse strong pulses, J0628+0909,

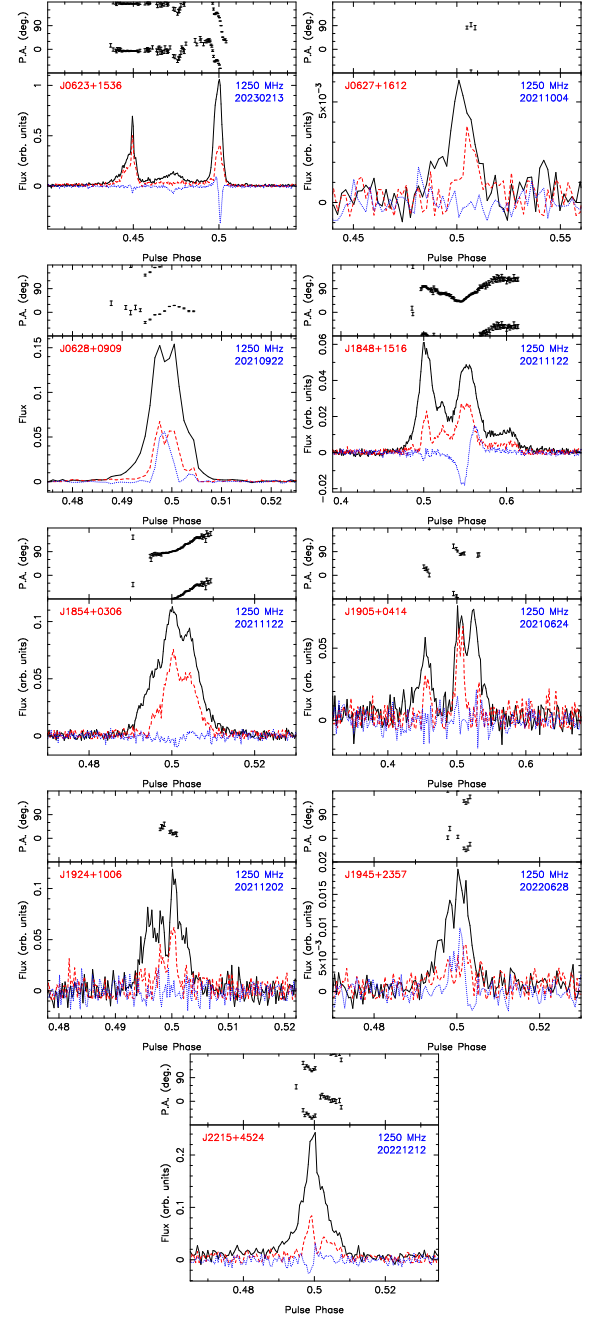


Fig. 19 Same as Figure 17 but for known RRATs with sparse strong pulses.

J1848+1515 and J1905+0414 and also J1913+1330, we do see these sparse pulses with unusual energy.

Figure 21 compares the polarization profiles for the normal weak pulses and these sparsely strong pulses, in the two sides of the normalized energy distributions Figure 20. In principle their number distributions should be fitted with a log-normal energy distribution. However, such fitting cannot be done well since only a small number of bright pulses are available. The sparse strong pulses can therefore be distinguished from the weak pulses in the distribution

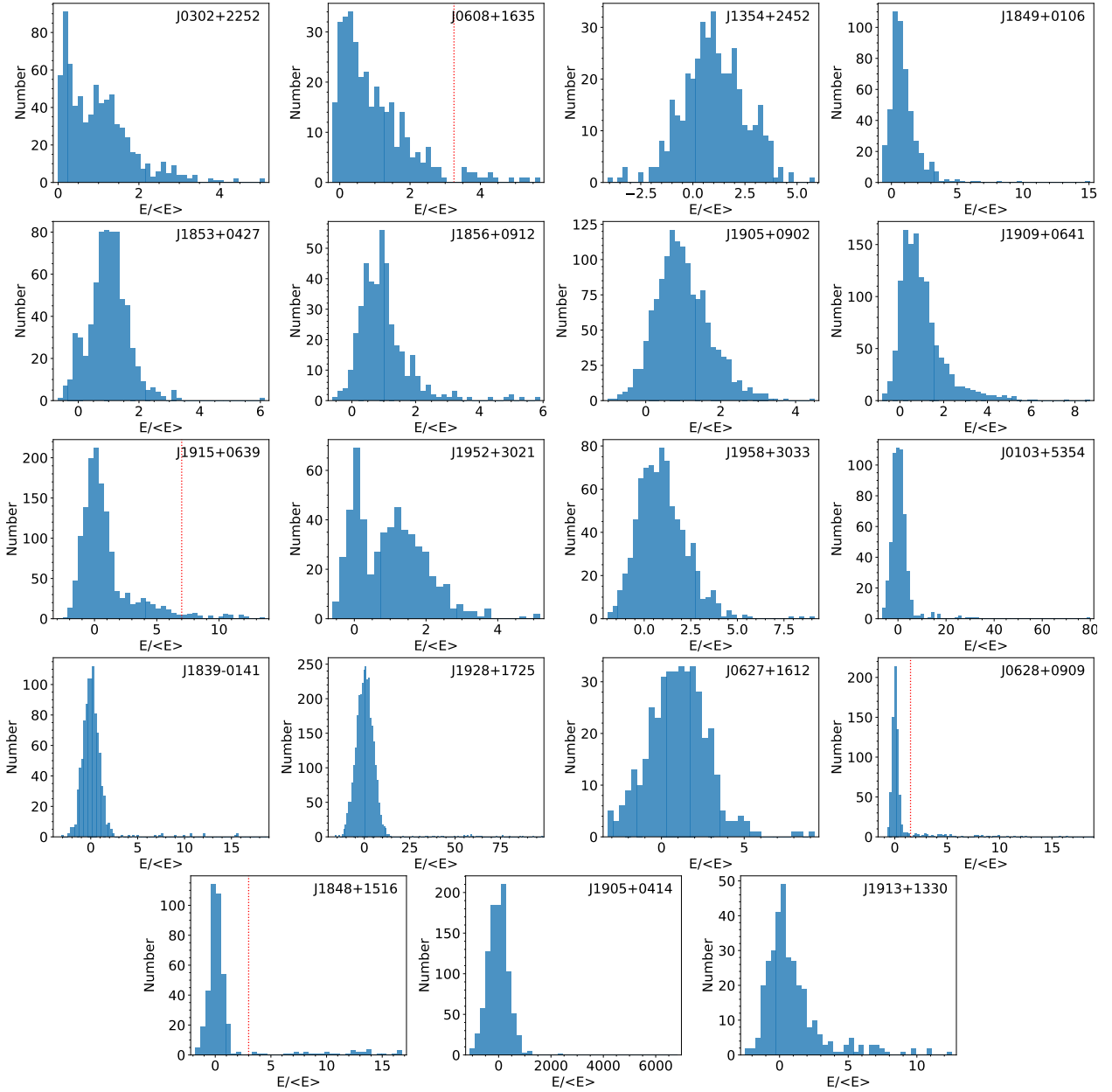


Fig. 20 The energy distributions of individual pulses for known RRATs with FAST observations for more than 300 pulses, normalized by the mean energy of all observed periods. The vertical line indicates an easy criterion to separate normal pulses and sparsely strong pulses, for them the polarization profiles are compared in Figure 21.

roughly by the lowest valley. We find that the polarization profiles from these small number of strong pulses in the high-energy tail have the same or the orthogonal polarized modes for their polarization angle distributions for weaker pulses, except for the case of PSR J1915+0639 which is hardly to understand. This indicates that mostly there is no difference between polarization profiles for sparse strong pulses and mean polarization profiles of normal pulses.

5 DISCUSSIONS AND CONCLUSIONS

We developed an efficient single pulse searching module for generating DM-time images and target detection with AI, so that it is computationally fast. Two processing strategies, the full bandwidth and the two halves of observation band of FAST are processed independently for single pulse search which can improve the detection of narrow or steep-spectrum pulses. We apply this new single pulse search module to the FAST GPPS survey, and discovered 76 new RRATs in our Galaxy. Among them, 26 sources have only

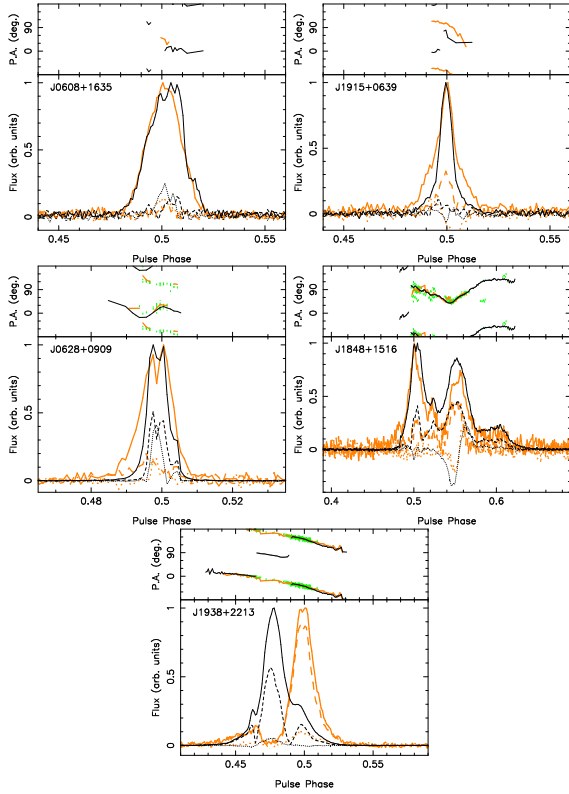


Fig. 21 Polarization profiles of sparsely strong pulses (black thin lines) are compared with those of normal weaker pulses (thick lines), see the criteria marked in the energy distribution in Figure 20, except for J1938+2213 for the bright pulses of $S/N > 200$ in Figure 16. In the top sub-panel the PA values in dark green come from bright pulses with linearly polarized intensities $> 10\sigma$, black and orange lines are respectively for the averaged PA values of bright and weak pulses. The bottom sub-panel is for the total power (solid line), linear polarization (dashed line) and circular polarization (dotted line), with the profile peaks normalized to the unity.

several pulses detected by FAST, so that their rotation period cannot be derived from the limited duration of FAST tracking observations. We have got 16 sources identified as proto-RRATs which have sparse strong pulses with a recognized period. 10 sources of them are apparently extreme nulling pulsars, and the other 24 sources are weak pulsars with sparse strong pulses.

For many newly discovered transient sources, the occasional strong emission state can help them to be found if the pulses are strong enough over the detection threshold. This has some implications. One is there must be a large neutron star population in our Galaxy to uncover but mostly undetectable. Second, single pulse searching is a desired step to catch them. Third, the occasionally bright-

ened emission state of these neutron stars must be related to some physical conditions which must be understood.

Noticed that these 76 transient objects here, including 12 objects discovered by the single pulse search that reported in the paper I (Han et al. 2021) are about 15% of newly discovered pulsars. In the other words, at least 15% of neutron stars would not be detected from the traditional periodicity signal search. Therefore, the single pulse search is important on revealing a large population of unknown RRATs, i.e. these pulsars with sporadic strong pulses.

The RRAT detection percentage of the FAST GPPS survey is much larger than the percentage of the known RRATs compared to all known pulsars, which is only 5% for all known RRATs, including extremely nulling pulsars and weak pulsars with sparse strong pulses. Detection of RRATs by FAST data leads us to find pulsars at the sub- μJy level. For some of them, we cannot get enough pulses to figure out the period yet. Finding their period by multiple observations or by increasing the duration of FAST observation is very necessary.

Figure 22 shows the distribution for the period and mean flux density of newly discovered transient sources in this paper compared to values for the known RRATs and the other pulsars with a period of larger than 0.1 s in the first FAST GPPS paper (Han et al. 2021). The mean flux densities of these newly discovered sources are much lower than that of the known RRATs and even the GPPS pulsars. Most of them have a mean flux density of few μJy , and J1921+1227g even has the lowest mean flux density of about $0.28\mu\text{Jy}$. This demonstrates the population of weak radiate neutron stars inside the Milky Way to be discovered. For the Probability density functions (PDFs) and cumulative distribution functions (CDFs), there is no significant difference in period distribution between these transient sources and the previously known RRATs. The difference between the FAST GPPS pulsars and these RRATs is prominent, which apparently caused by different selection effects from the search method. Any pulsars discovered by the normal periodical search are not classified as RRATs. On the other hand, the single pulse detection also has limitations. The identification of extremely narrow transient (< 1 ms, like the ultranarrow burst of FRB 20191107B, Gupta et al. 2022) or even narrower band radiation in FRB, has to be improved in the future. The detection efficiency of signals at the boundary of the DM-time images has to be improved.

Extremely sensitive observations are fundamental to understand the transient sources, especially RRATs. Observations of the known RRATs by using FAST could detect more weak pulses, in addition to previously detected sparse strong pulses. In our FAST GPPS survey area, a large number of known RRATs have the FAST data

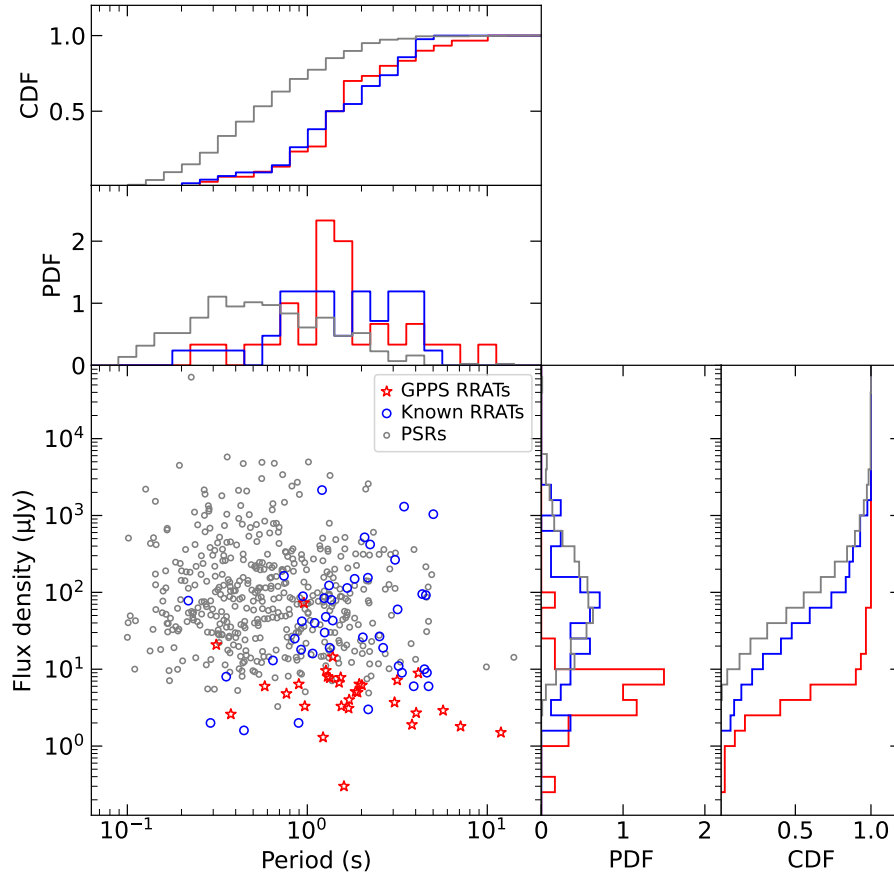


Fig. 22 The distribution for the period and mean flux density of the newly discovered transient sources in this paper (red), compared with the known RRATs (blue) and the other pulsars in the GPPS survey Paper I (gray, Han et al. 2021). In the top and right panels are the cumulative distribution functions (CDFs) and the probability density functions (PDFs) for the period and mean flux density, respectively.

recorded already. Together with other FAST projects, we have got 48 known RRATs detected by FAST. Four of them have only one pulse detected in our FAST observations and another 1 has four pulses detected in a five minutes observation session but not confirmed in the verification observation. 25 known RRATs are simply normal pulsars in the FAST observations, 5 of them are extremely nulling pulsars, and 13 objects are weaker pulsars with sparse strong pulses. Polarization observations show no unusual difference of these strong pulses from weaker pulses.

We therefore conclude that most RRATs are simply weaker pulsars with sparse strong pulses or very nulling pulsars. The sensitivity of the telescope and long observations are the key to understand the enigma of RRATs.

Acknowledgements This project, as one of five key projects, is being carried out by using FAST, a Chinese national mega-science facility built and operated by the National Astronomical Observatories, Chinese Academy of Sciences. J. L. Han is supported by the National Natural Science Foundation of China (NSFC, Nos. 11988101 and

11833009) and the Key Research Program of the Chinese Academy of Sciences (Grant No. QYZDJ-SSW-SLH021); D. J. Zhou is supported by the Cultivation Project for the FAST scientific Payoff and Research Achievement of CAMS-CAS. H. G. Wang, C. Wang, P. F. Wang and X. P. You are supported by NSFC No. 12133004; P. F. Wang, C. Wang and H. G. Wang are also partially supported by the National SKA program of China No. 2020SKA0120200. In addition, C. Wang is also partially supported by NSFC No. U1731120; P. F. Wang is also partially supported by the NSFC No. 11873058; H. G. Wang is also partially supported by the Guangzhou Science and Technology Project No. 202102010466; Jun Xu is partially supported by NSFC No. U2031115.

AUTHORS CONTRIBUTIONS

The FAST GPPS survey is a key science project of FAST led by J. L. Han. D. J. Zhou realized the single pulse search module and related software under the supervision of J. L. Han, and processed all data presented in this paper. J. L.

Han coordinated the teamwork and coordinated computational resources, and also in charge of writing this paper. Jun Xu observed some RRATs in his project and contributed the data of some known RRATs. Chen Wang designed the survey observation plan for the GPPS survey, and fed all targets for each observation session and verification observations. P. F. Wang realized the polarization processing pipeline which is used in this paper. Tao Wang initialized and realized parts of the data preparing module. P. F. Wang and Jun Xu made fundamental contributions to the construction and maintenance on the computation platform. W. C. Jing, Xue Chen, Yi Yan and W. Q. Su joined many group discussions and commented on the results of this paper. H. Q. Gan, P. Jiang and J. H. Sun ensured the success of FAST observations. Other people jointly propose or monitor the project. All authors contributed to the finalization of the paper.

DATA AND SOFTWARE AVAILABILITY

Original FAST observational data will be open sources according to the FAST data 1-year protection policy. The folded and calibrated data for sources in this paper can be obtained from authors by kind requests. Pulsar profile data presented and the source codes in this paper are available on the webpage of the GPPS survey <http://zmtt.bao.ac.cn/GPPS/>.

References

- Abhishek Malusare N., Tanushree N., Hegde G., Konar S., 2022, *JApA*, **43**, 75 2, 3
- Agarwal D., Aggarwal K., Burke-Spolaor S., Lorimer D. R., Garver-Daniels N., 2020, *MNRAS*, **497**, 1661 4
- Bezuidenhout M. C., et al., 2022, *MNRAS*, **512**, 1483 2
- Bhattacharyya B., et al., 2018, *MNRAS*, **477**, 4090 2, 3
- Bilous A. V., et al., 2022, *A&A*, **658**, A143 23
- Bochkovskiy A., Wang C.-Y., Liao H.-Y. M., 2020, YOLOv4: Optimal Speed and Accuracy of Object Detection ([arXiv:2004.10934](https://arxiv.org/abs/2004.10934)) 5
- Burke-Spolaor S., Bailes M., 2010, *MNRAS*, **402**, 855 2, 17, 18, 19
- Burke-Spolaor S., et al., 2011, *MNRAS*, **416**, 2465 2, 17
- Butler R. P., Marcy G. W., 1996, *ApJ*, **464**, L153 2
- Caleb M., et al., 2019, *MNRAS*, **487**, 1191 2
- Cameron A. D., Barr E. D., Champion D. J., Kramer M., Zhu W. W., 2017, *MNRAS*, **468**, 1994 2
- Chandler A. M., 2003, PhD thesis, CALIFORNIA INSTITUTE OF TECHNOLOGY 18, 19, 22
- Coenen T., et al., 2014, *A&A*, **570**, A60 2, 17
- Cordes J. M., Lazio T. J. W., 2002, arXiv e-prints, [pp astro-ph/0207156](https://arxiv.org/abs/astro-ph/0207156) 7
- Cordes J. M., McLaughlin M. A., 2003, *ApJ*, **596**, 1142 2, 6
- Cordes J. M., et al., 2006, *ApJ*, **637**, 446 2, 18, 19, 21
- Cui B. Y., Boyles J., McLaughlin M. A., Palliyaguru N., 2017, *ApJ*, **840**, 5 2, 3, 18, 19
- Deneva J. S., et al., 2009, *ApJ*, **703**, 2259 2, 17, 18, 19, 20, 21
- Deneva J. S., et al., 2016, *ApJ*, **821**, 10 2, 6, 17, 18, 19, 20, 22, 23
- Devine T. R., Goseva-Popstojanova K., McLaughlin M., 2016, *MNRAS*, **459**, 1519 4
- Dong F., 2021, PhD thesis, University of British Columbia, [doi:http://dx.doi.org/10.14288/1.0396957](https://doi.org/10.14288/1.0396957), <https://open.library.ubc.ca/collections/ubctheses/24/items/1.0396957> 18, 19
- Dong F. A., et al., 2022, arXiv e-prints, [p. arXiv:2210.09172](https://arxiv.org/abs/2210.09172) 2, 17, 18, 19
- Fishman G. J., Meegan C. A., 1995, *ARA&A*, **33**, 415 1
- Good D. C., et al., 2021, *ApJ*, **922**, 43 2, 17
- Gupta V., Flynn C., Farah W., Bailes M., Deller A. T., Day C. K., Lower M. E., 2022, *MNRAS*, **514**, 5866 27
- Han J. L., 2017, *ARA&A*, **55**, 111 15, 17, 24
- Han J. L., Manchester R. N., van Straten W., Demorest P., 2018, *ApJS*, **234**, 11 15, 17
- Han J. L., et al., 2021, *RAA*, **21**, 107 2, 3, 5, 6, 14, 17, 18, 19, 20, 27, 28
- Hankins T. H., Kern J. S., Weatherall J. C., Eilek J. A., 2003, *Nature*, **422**, 141 2
- Hessels J. W. T., Ransom S. M., Kaspi V. M., Roberts M. S. E., Champion D. J., Stappers B. W., 2008, in Bassa C., Wang Z., Cumming A., Kaspi V. M., eds, AIPC Vol. 983, 40 Years of Pulsars: Millisecond Pulsars, Magnetars and More. pp 613–615 ([arXiv:0710.1745](https://arxiv.org/abs/0710.1745)), [doi:10.1063/1.2900310](https://doi.org/10.1063/1.2900310) 2, 17
- Hessels J. W. T., et al., 2019, *ApJ*, **876**, L23 23
- Hewish A., Bell S. J., Pilkington J. D. H., Scott P. F., Collins R. A., 1968, *Nature*, **217**, 709 2
- Hotan A. W., van Straten W., Manchester R. N., 2004, *PASA*, **21**, 302 7
- Hsu J. A., Jiang J. C., Xu H., Lee K. J., Xu R. X., 2023, *MNRAS*, **518**, 1418 2
- Jiang M., Cui B. Y., Schmid N. A., McLaughlin M. A., Cao Z. C., 2017, *ApJ*, **847**, 75 18, 19
- Jiang P., et al., 2020, *RAA*, **20**, 064 3, 6
- Karako-Argaman C., et al., 2015, *ApJ*, **809**, 67 2, 4, 6, 17, 18, 19, 22
- Karastergiou A., Hotan A. W., van Straten W., McLaughlin M. A., Ord S. M., 2009, *MNRAS*, **396**, L95 2, 3
- Keane E. F., Ludovici D. A., Eatough R. P., Kramer M., Lyne A. G., McLaughlin M. A., Stappers B. W., 2010, *MNRAS*, **401**, 1057 2, 7, 17, 18, 19

- Keane E. F., Kramer M., Lyne A. G., Stappers B. W., McLaughlin M. A., 2011, *MNRAS*, **415**, 3065 2, 3, 17, 18, 19
- Keane E. F., et al., 2018, *MNRAS*, **473**, 116 2, 17
- Kondratiev V. I., McLaughlin M. A., Lorimer D. R., Burgay M., Possenti A., Turolla R., Popov S. B., Zane S., 2009, *ApJ*, **702**, 692 2
- Lorimer D. R., 2011, SIGPROC: Pulsar Signal Processing Programs (ascl:1107.016) 2
- Lorimer D. R., Bailes M., McLaughlin M. A., Narkevic D. J., Crawford F., 2007, *Science*, **318**, 777 2
- Lorimer D. R., Camilo F., McLaughlin M. A., 2013, *MNRAS*, **434**, 347 18, 19
- Lower M. E., et al., 2020, *MNRAS*, **494**, 228 18, 19
- Lu J., et al., 2019, *SCPMA*, **62**, 959503 2, 22
- Luo R., et al., 2020, *Nature*, **586**, 693 3
- Lynch R. S., et al., 2013, *ApJ*, **763**, 81 18, 19
- Lyne A. G., McLaughlin M. A., Keane E. F., Kramer M., Espinoza C. M., Stappers B. W., Palliyaguru N. T., Miller J., 2009, *MNRAS*, **400**, 1439 3
- Magro A., Karastergiou A., Salvini S., Mort B., Dulwich F., Zarb Adami K., 2011, *MNRAS*, **417**, 2642 5
- Mayor M., Queloz D., 1995, *Nature*, **378**, 355 2
- McLaughlin M. A., et al., 2006, *Nature*, **439**, 817 2, 17, 18, 19, 21, 22
- McLaughlin M. A., et al., 2009, *MNRAS*, **400**, 1431 3, 18, 19
- Men Y. P., et al., 2019, *MNRAS*, **488**, 3957 4
- Michilli D., Hessels J. W. T., 2018, SpS: Single-pulse Searcher (ascl:1806.013) 4
- Michilli D., et al., 2018, *MNRAS*, **480**, 3457 4, 18, 19
- Michilli D., et al., 2020, *MNRAS*, **491**, 725 18, 19
- Mickaliger M. B., McEwen A. E., McLaughlin M. A., Lorimer D. R., 2018, *MNRAS*, **479**, 5413 2
- Nan R., et al., 2011, *IJMPD*, **20**, 989 2, 3
- Nice D. J., et al., 2013, *ApJ*, **772**, 50 18, 19
- Niu C.-H., et al., 2021, *ApJ*, **909**, L8 3
- Niu C. H., et al., 2022, *Nature*, **606**, 873 3
- Pan Z., et al., 2021, *ApJ*, **915**, L28 3
- Parent E., et al., 2018, *ApJ*, **861**, 44 2
- Parent E., et al., 2022, *ApJ*, **924**, 135 18, 19
- Patel C., et al., 2018, *ApJ*, **869**, 181 2, 4, 17, 18, 19, 20, 21, 23
- Petroff E., et al., 2014, *ApJ*, **789**, L26 5
- Ransom S., 2011, PRESTO: Pulsar Exploration and Search TOolkit (ascl:1107.017) 2, 4
- Redmon J., Farhadi A., 2018, arXiv 5
- Sanidas S., et al., 2019, *A&A*, **626**, A104 18, 19
- Serylak M., et al., 2021, *MNRAS*, **505**, 4483 18, 19
- Sobey C., et al., 2015, *MNRAS*, **451**, 2493 22
- Staelin D. H., 1969, *IEEE Proceedings*, **57**, 724 2
- Stovall K., et al., 2014, *ApJ*, **791**, 67 2, 17
- Sun S.-N., Yan W.-M., Wang N., Yuen R., 2021, *RAA*, **21**, 240 2
- Sun S. N., Yan W. M., Wang N., Wang H. G., Wang S. Q., Dang S. J., 2022, *ApJ*, **934**, 57 22
- Tange O., 2018, GNU Parallel 2018. Ole Tange, doi:10.5281/zenodo.1146014, <https://doi.org/10.5281/zenodo.1146014> 5
- Tyul'bashev S. A., Tyul'bashev V. S., Oreshko V. V., Logvinenko S. V., 2016, *Astronomy Reports*, **60**, 220 18, 19
- Tyul'bashev S. A., et al., 2018a, *Astronomy Reports*, **62**, 63 2, 17
- Tyul'bashev S. A., Tyul'bashev V. S., Malofeev V. M., 2018b, *A&A*, **618**, A70 2, 17, 18, 19, 20, 22
- Tyul'bashev S. A., Pervukhin D. V., Kitaeva M. A., Tyul'basheva G. E., Brylyakova E. A., Chernosov A. V., 2022, *A&A*, **664**, A37 2
- Wang C.-Y., Bochkovskiy A., Liao H.-Y. M., 2021a, in Proceedings of the IEEE/CVF Conference on Computer Vision and Pattern Recognition (CVPR). pp 13029–13038 5
- Wang P., et al., 2021b, *SCPMA*, **64**, 129562 3
- Wang P. F., et al., 2022, *RAA*, Submitted 3, 7, 14, 17, 23
- Weltevrede P., Stappers B. W., Rankin J. M., Wright G. A. E., 2006, *ApJ*, **645**, L149 2
- Xu J., Han J. L., Wang P. F., Yan Y., 2022a, *SCPMA*, **65**, 129704 15, 17
- Xu H., et al., 2022b, *Nature*, **609**, 685 3
- Yao J. M., Manchester R. N., Wang N., 2017, *ApJ*, **835**, 29 7
- Zhang C. F., et al., 2021, *MNRAS*, **503**, 5223 4
- Zhou D. J., et al., 2022, *RAA*, **22**, 124001 5, 23
- Zhu W., et al., 2020, *ApJ*, **895**, L6 3, 5

APPENDIX

The single pulse search module for the GPPS survey uncovers many radio transient sources in the sky.

Table 8 (published in the online version of this paper) list parameters for each pulse, including the TOA of the pulse peak, signal-to-noise ratio of dedispersed pulse R , pulse width in millisecond, and the fluence discussed in Sect.2.2.2.

Figure 23 (published in the online version of this paper) show all water-fall plots for 26 radio transients with only a few pulses detected for each source, including the 3 example plots in Fig. 3.

Figure 24 (published in the online version of this paper) show plots for 16 RRATs discovered in the GPPS survey, while Figure 4 is only one example.

Figure 25 (published in the online version of this paper) show plots for 10 extremely nulling pulsars as dis-

covered in the GPPS survey, while Figure 5 is only one example.

Figure 26 (published in the online version of this paper) show plots for 24 weak pulsars with sparse strong pulses discovered in the GPPS survey, while Figure 6 is only one example.

Figure 27 (published in the online version of this paper) show plots for 25 previously known RRATs shown as normal pulsars in the FAST observations, while Figure 12 just two examples.

Figure 28 (published in the online version of this paper) show plots for 5 previously known RRATs shown as extremely nulling pulsars in the FAST observations, while Figure 13 just two examples.

Figure 29 (published in the online version of this paper) show plots for 13 previously known RRATs shown as pulsars with sparse strong pulses in the FAST observations, while Figure 14 just examples respectively.

Table 8 Properties of single pulses for newly discovered transient sources with few pulses detected by FAST.

ObsDate	No.	TOA (MJD)	R	W (ms)	F (mJy ms)
(1)	(2)	(3)	(4)	(5)	(6)
J0637+0332g = gpps0528					
20220909	1	59831.03261773	9.9	7.6	47.8
	2	59831.03501918	10.6	12.2	45.8
	3	59831.03555291	11.7	8.8	40.0
J1828-0003g = gpps0501					
20200803	1	59794.62034865	40.5	31.7	600.5
	1	59794.62673776	16.1	37.9	143.3
20221114	1	59897.31460359	95.6	42.4	1830.0
J1847-0046g = gpps0282					
20211031	1	59518.38408605	7.6	12.1	60.9
20211113	1	59531.34693849	11.4	43.5	111.7
	2	59531.35255450	31.8	17.0	483.1
20220606	1	59735.77706666	32.9	26.8	572.8
	2	59735.78296057	22.4	13.9	367.9
	3	59735.78746444	12.9	34.1	178.5
J1850-0004g = gpps0280					
20200415	1	58953.93718024	22.6	5.8	147.0
	2	58953.93992108	25.0	6.9	206.0
20200902	1	59094.53330366	21.3	7.7	107.7
20220608	1	59737.77205668	62.2	7.4	479.8
	2	59737.77357873	23.8	7.1	176.5
20221006	1	59889.35833273	35.5	7.4	122.0
	3	59737.77825393	22.9	15.8	163.3
	4	59737.78097067	16.9	10.1	120.4
J1853+0209g = gpps0502					
20200812	1	59073.58342402	30.9	120.6	773.9
20220824	1	59815.56281964	60.7	217.7	1923.4
J1853+0353g = gpps0281					
20210514	1	59347.82755635	11.8	42.6	166.7
	2	59347.83650747	22.0	64.6	415.1
20210624	1	59388.76374658	26.1	57.4	476.0
J1855-0211g = gpps0526					
20220810	1	59801.62433801	9.6	74.7	85.9
20221205	1	59918.27588921	57.1	25.5	660.7
20221205	2	59918.27671860	33.0	41.0	466.9
20221205	3	59918.28352914	77.9	48.0	1695.7
20221205	1	60008.03900500	111.3	102.5	3474.8
J1855-0154g = gpps0503					
20210514	1	59464.52884265	18.6	12.0	134.9
	2	59464.52880855	21.4	10.2	170.4
	3	59464.52884265	12.9	9.1	78.5
J1855-0054g = gpps0504					
20220210	1	59678.94763145	26.1	61.9	529.6
20220602	1	59731.78531778	9.9	55.9	93.2
	2	59731.78540454	14.6	30.1	204.0
	3	59731.78846381	19.3	108.0	391.2
	4	59731.78994988	22.4	79.1	434.5
J1855+0033g = gpps0283					
20200328	1	58935.98123561	15.9	53.2	112.5
20210328	1	59300.95680323	11.9	11.6	72.7
	2	59300.97261027	32.3	46.0	436.2
	3	59300.98378786	33.8	19.3	338.2
J1856+0528g = gpps0284					
20210608	1	59372.79606129	12.7	86.2	99.5
	2	59372.79608372	12.2	47.6	70.4
	3	59372.79920230	10.5	50.3	69.9
20210826	1	59452.57993757	17.0	87.8	169.8
	2	59452.58749961	13.0	43.5	86.8
	3	59452.58950899	10.4	84.9	65.6

Notes: Column (1)-(3): Observation date, pulse number, TOA of pulse peak in MJD; Column (4)-(6): signal-to-noise ratio, and pulse width in ms and also the fluence.

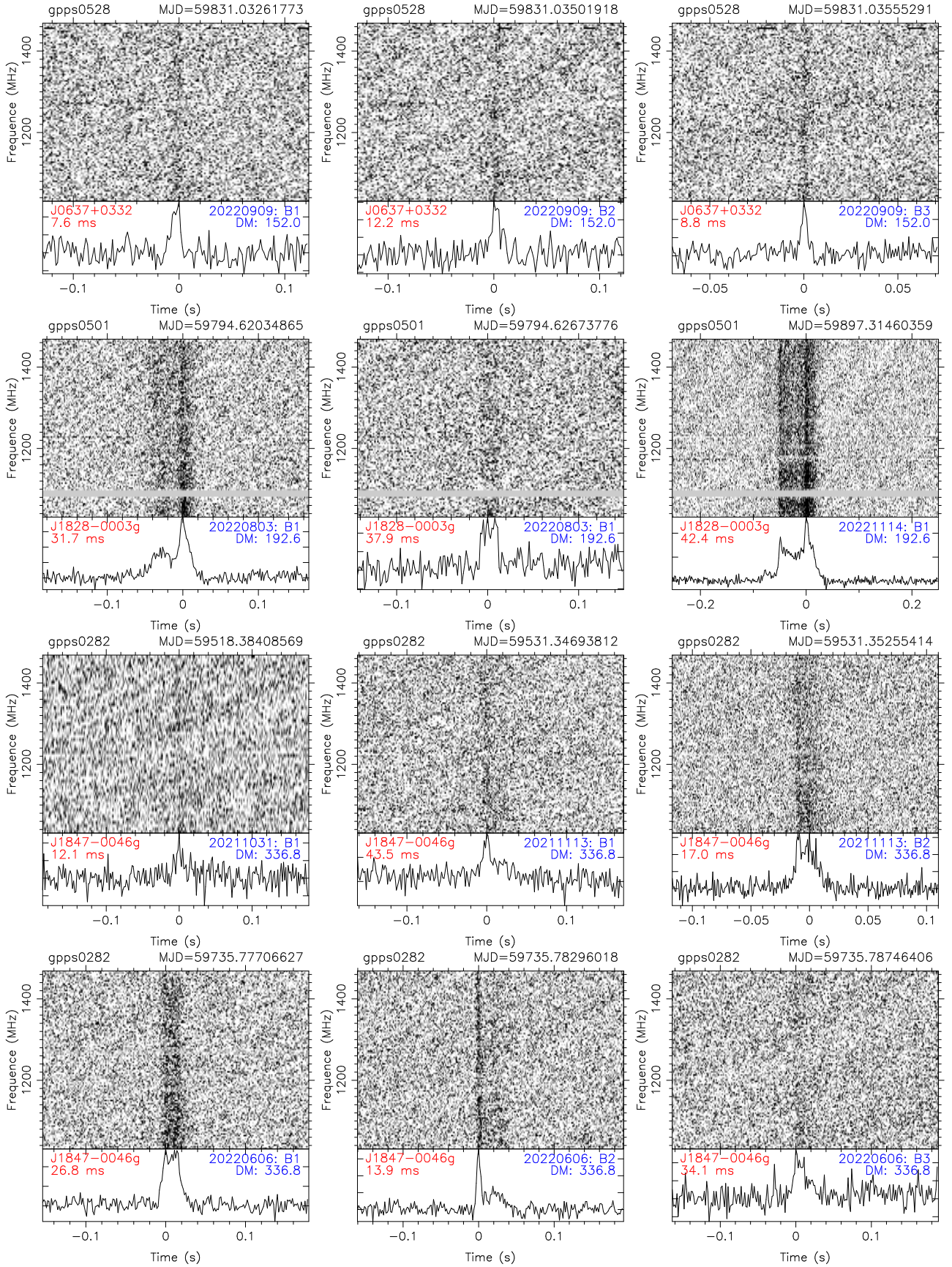


Fig. 23 The same as Figure 3 but for 105 pulses detected by FAST from 26 radio transient sources.

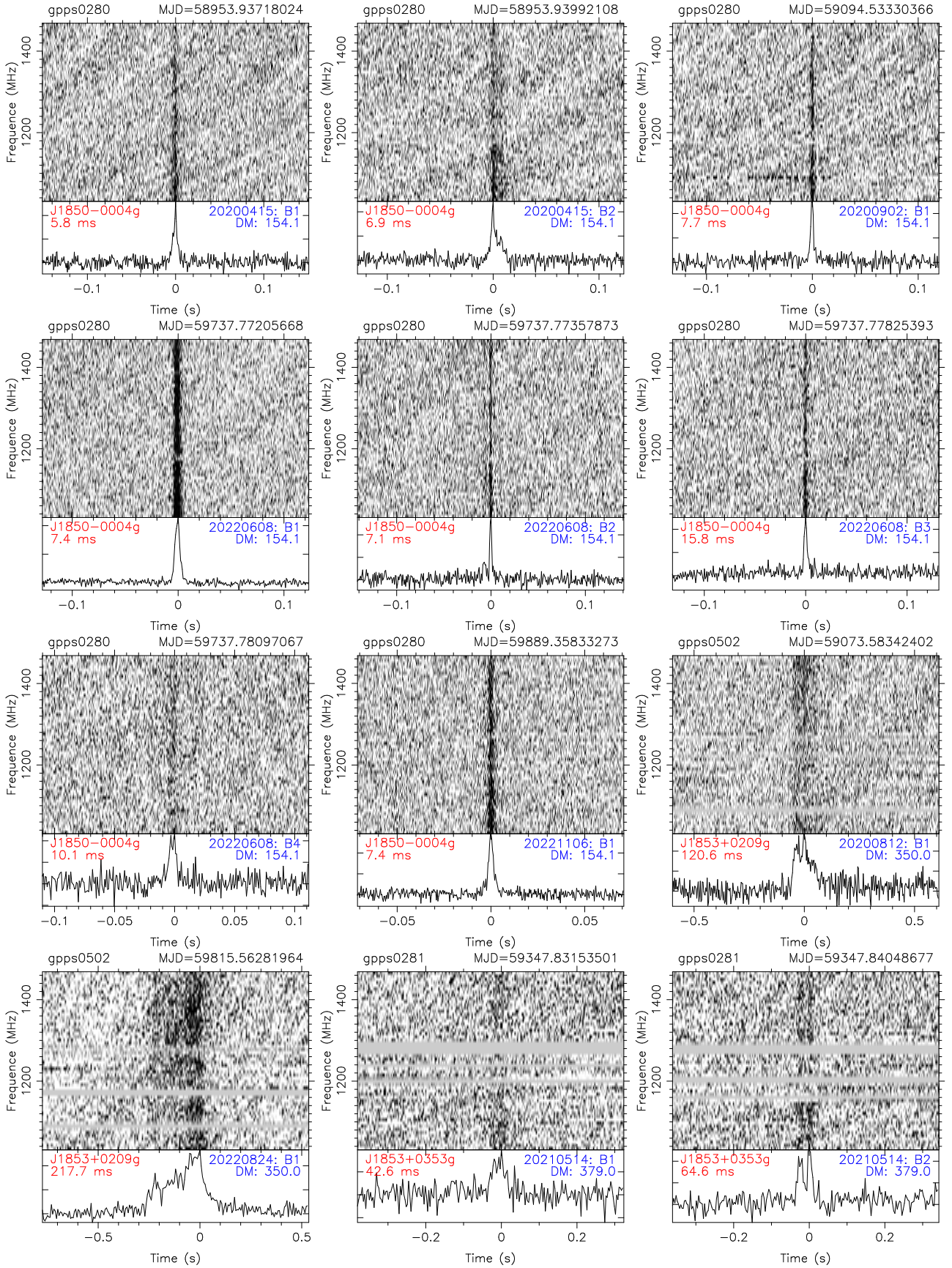


Fig. 23 (Continued.)

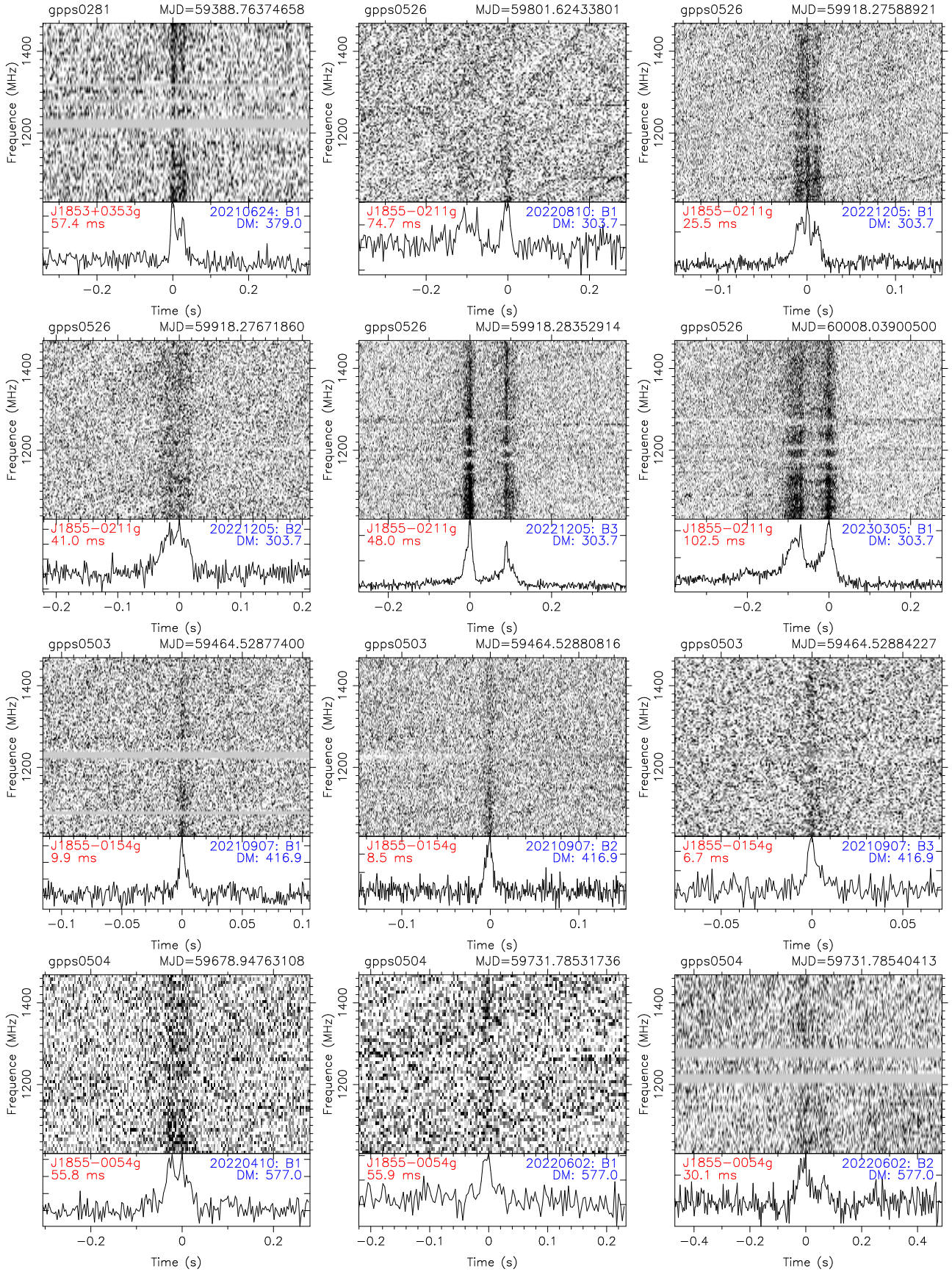


Fig. 23 (Continued.)

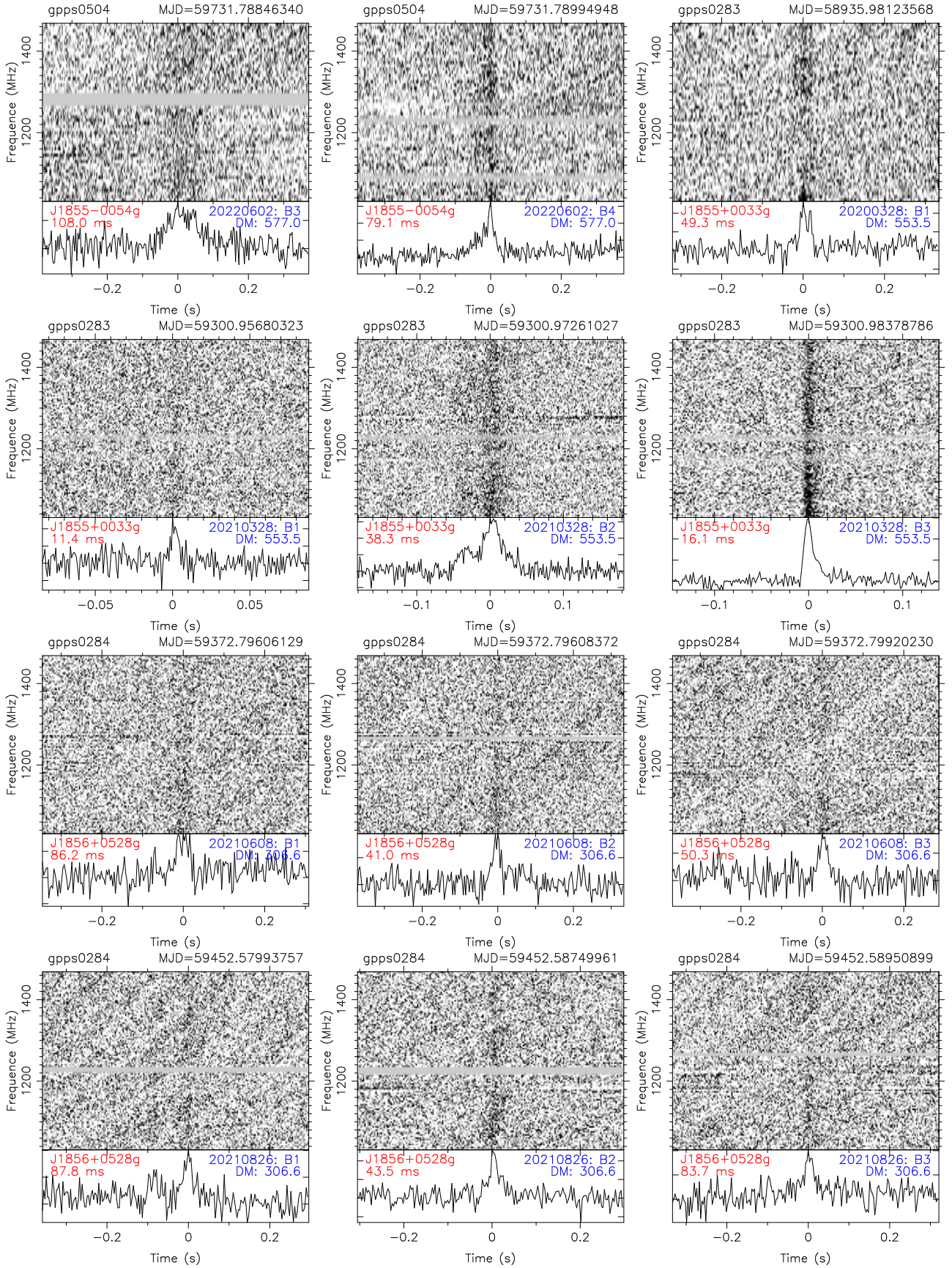


Fig. 23 (Continued.)

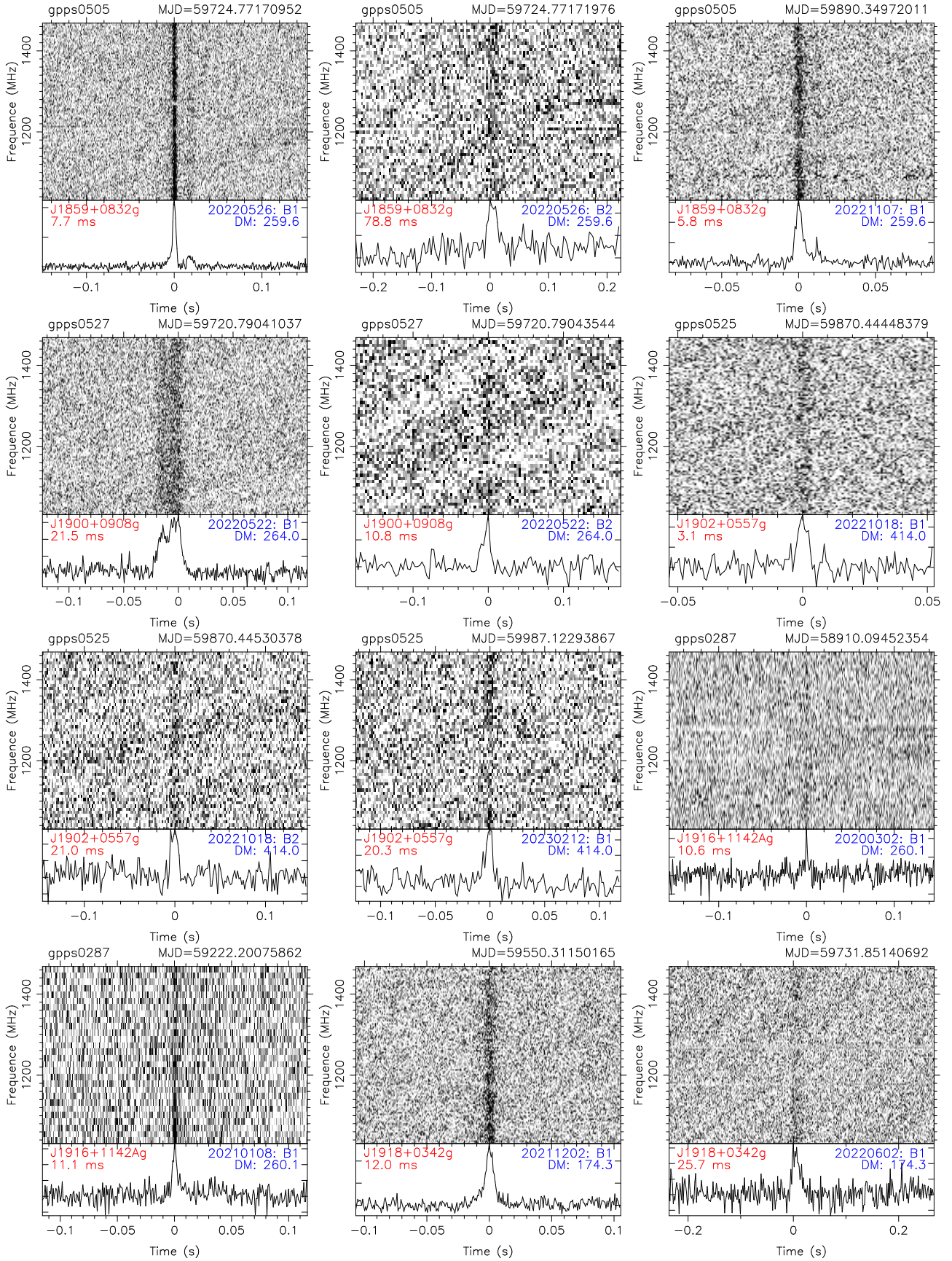


Fig. 23 (Continued.)

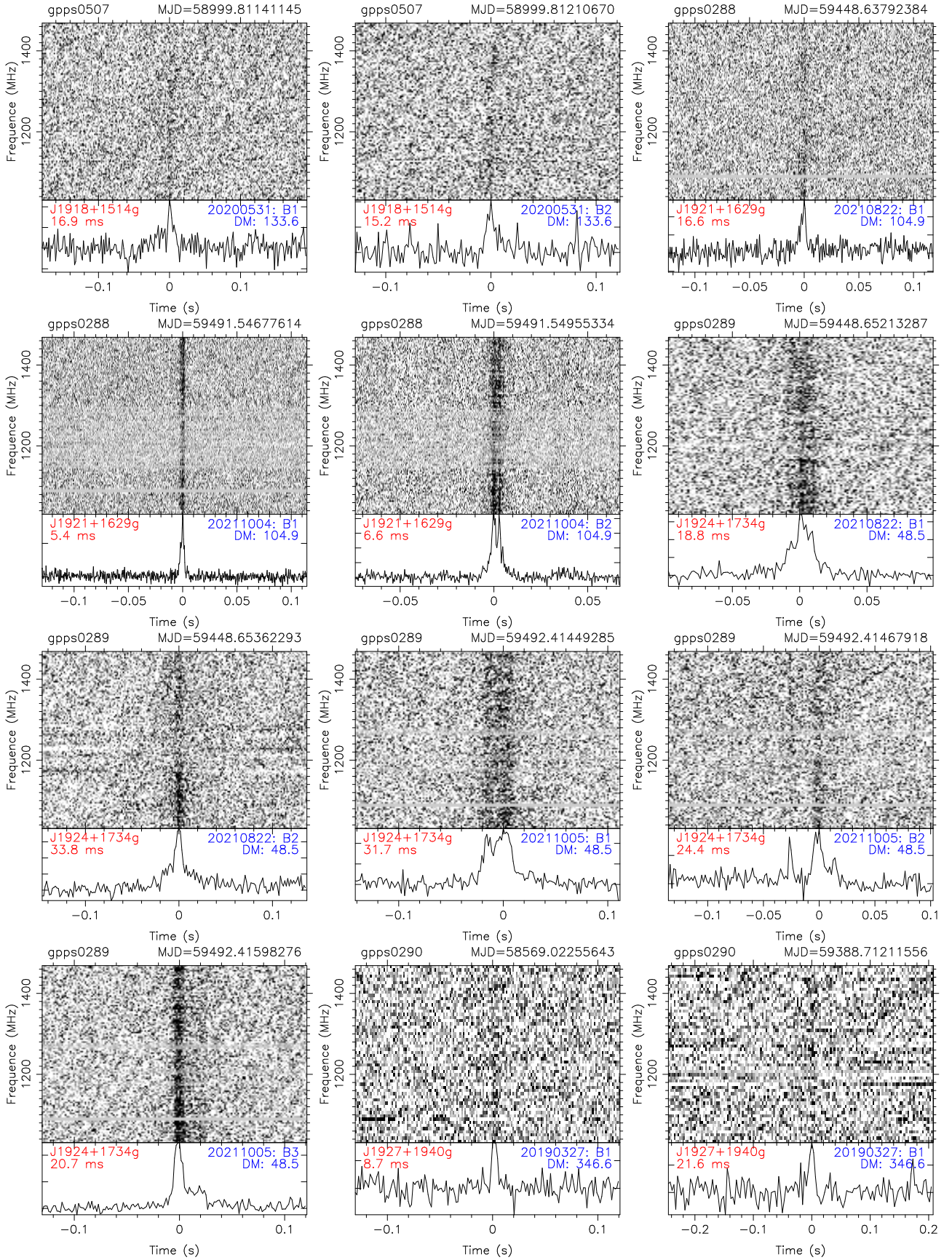


Fig. 23 (Continued.)

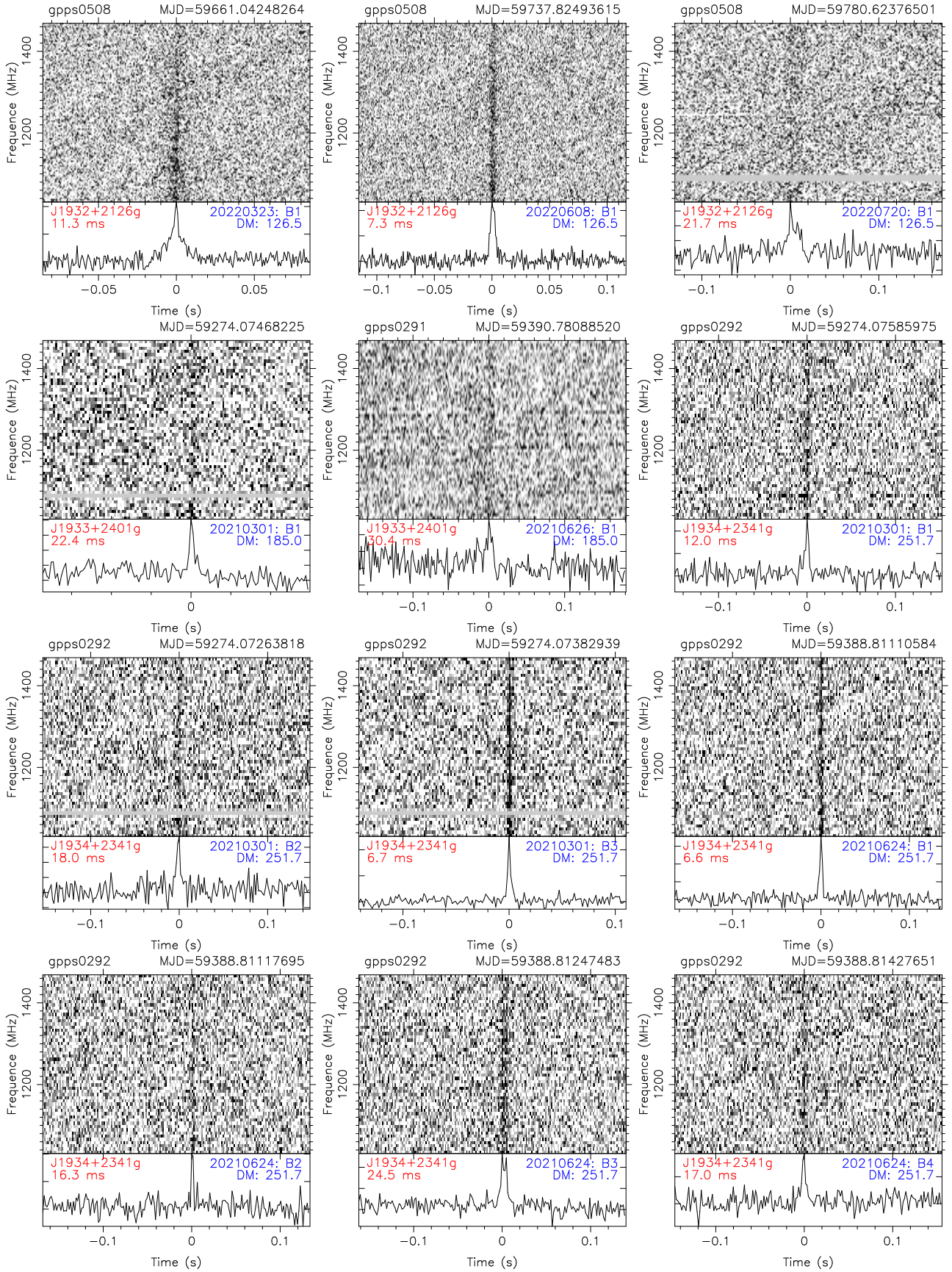


Fig. 23 (Continued.)

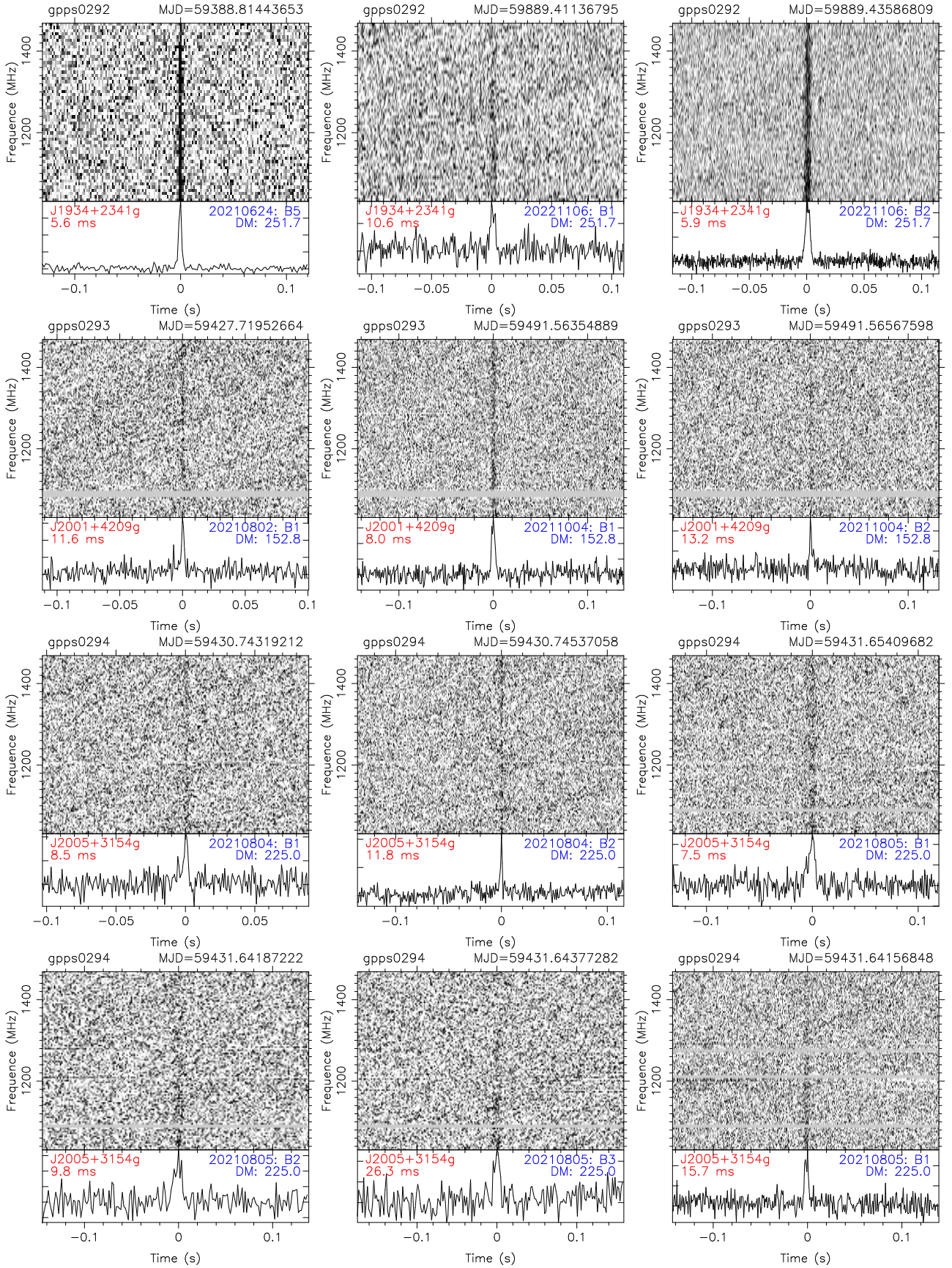


Fig. 23 (Continued.)

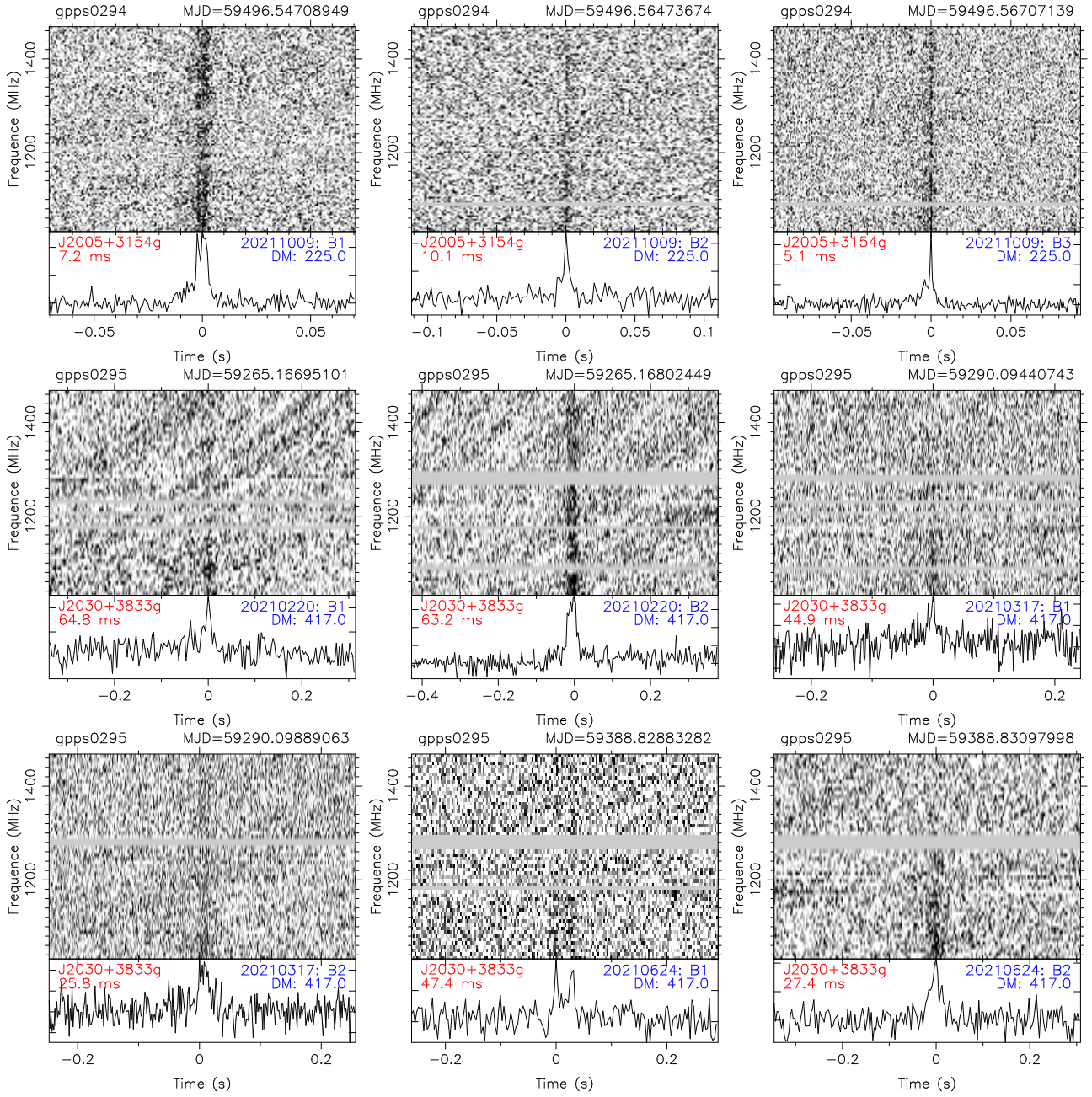


Fig. 23 (Continued.)

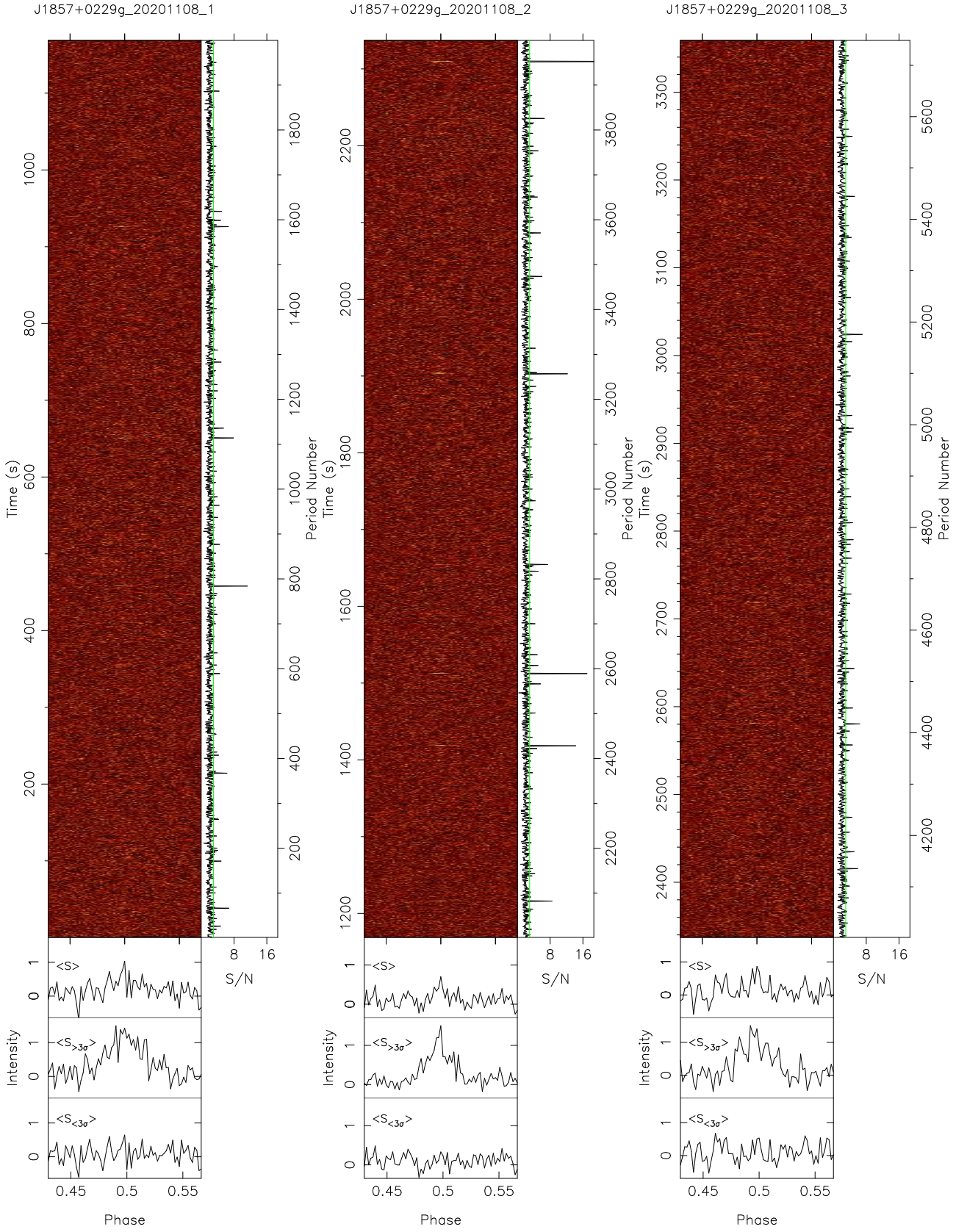


Fig. 24 The same as Figure 4 but for 16 proto-RRATs discovered in the GPPS survey.

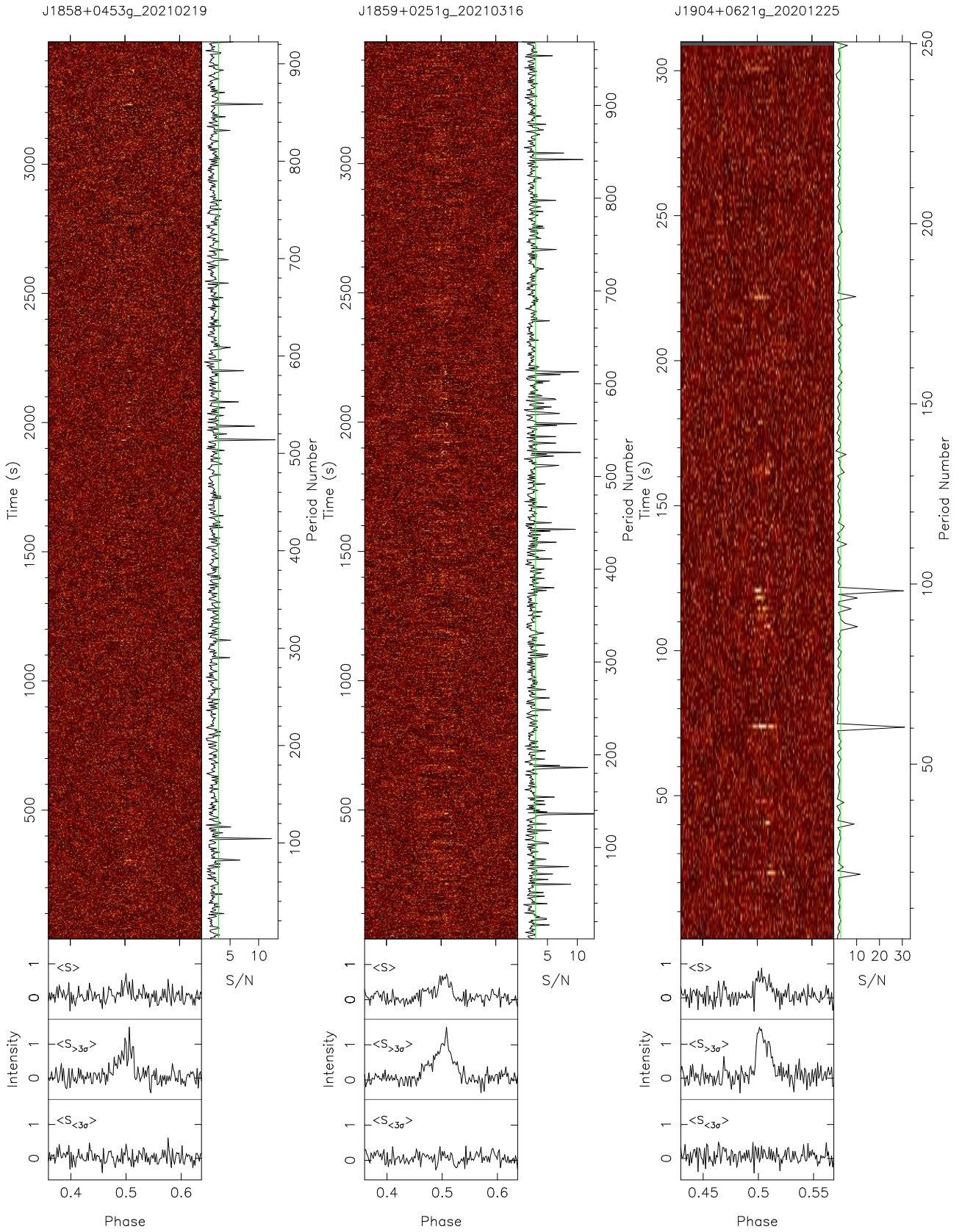


Fig. 24 – continued.

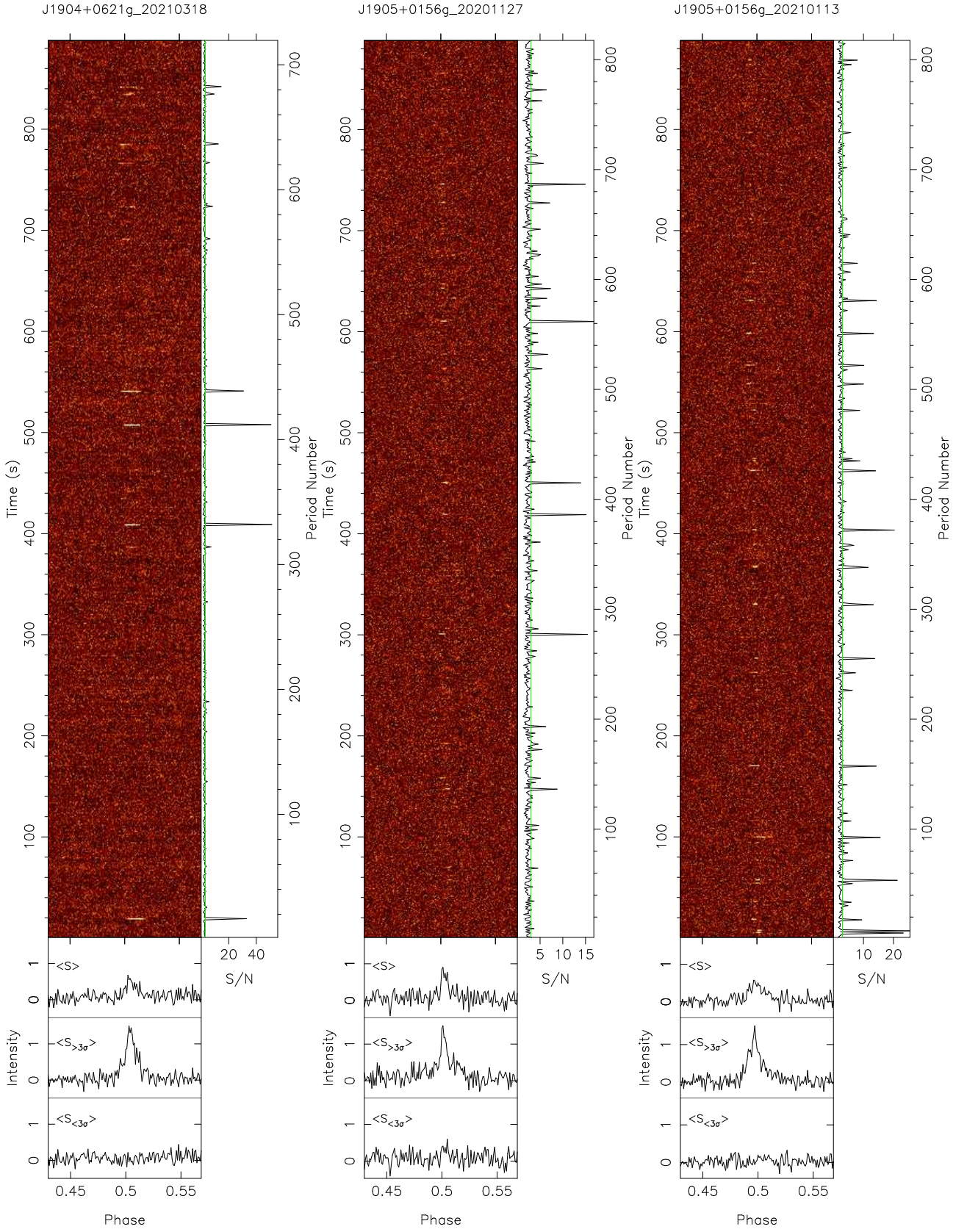


Fig. 24 – continued.

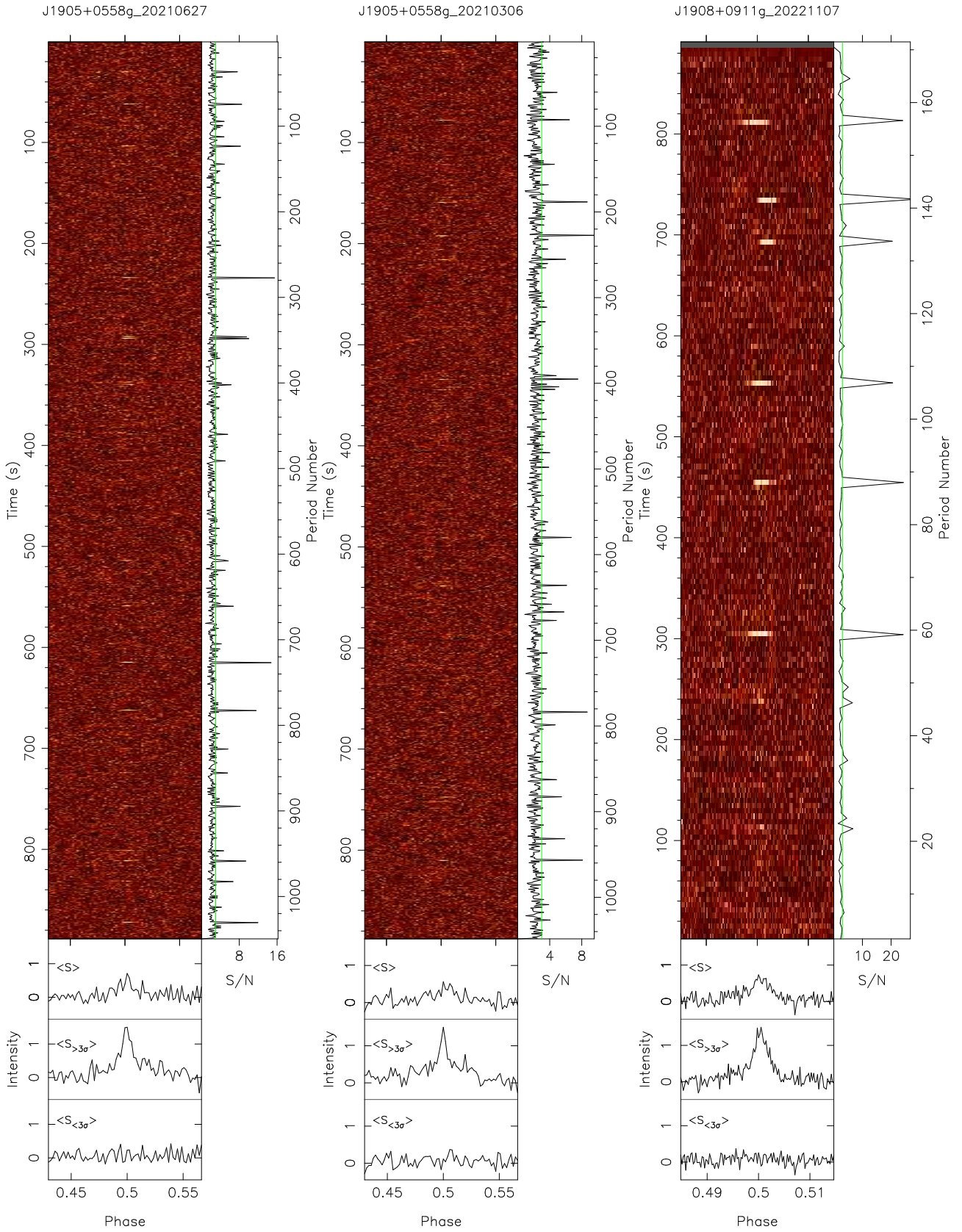


Fig. 24 – continued.

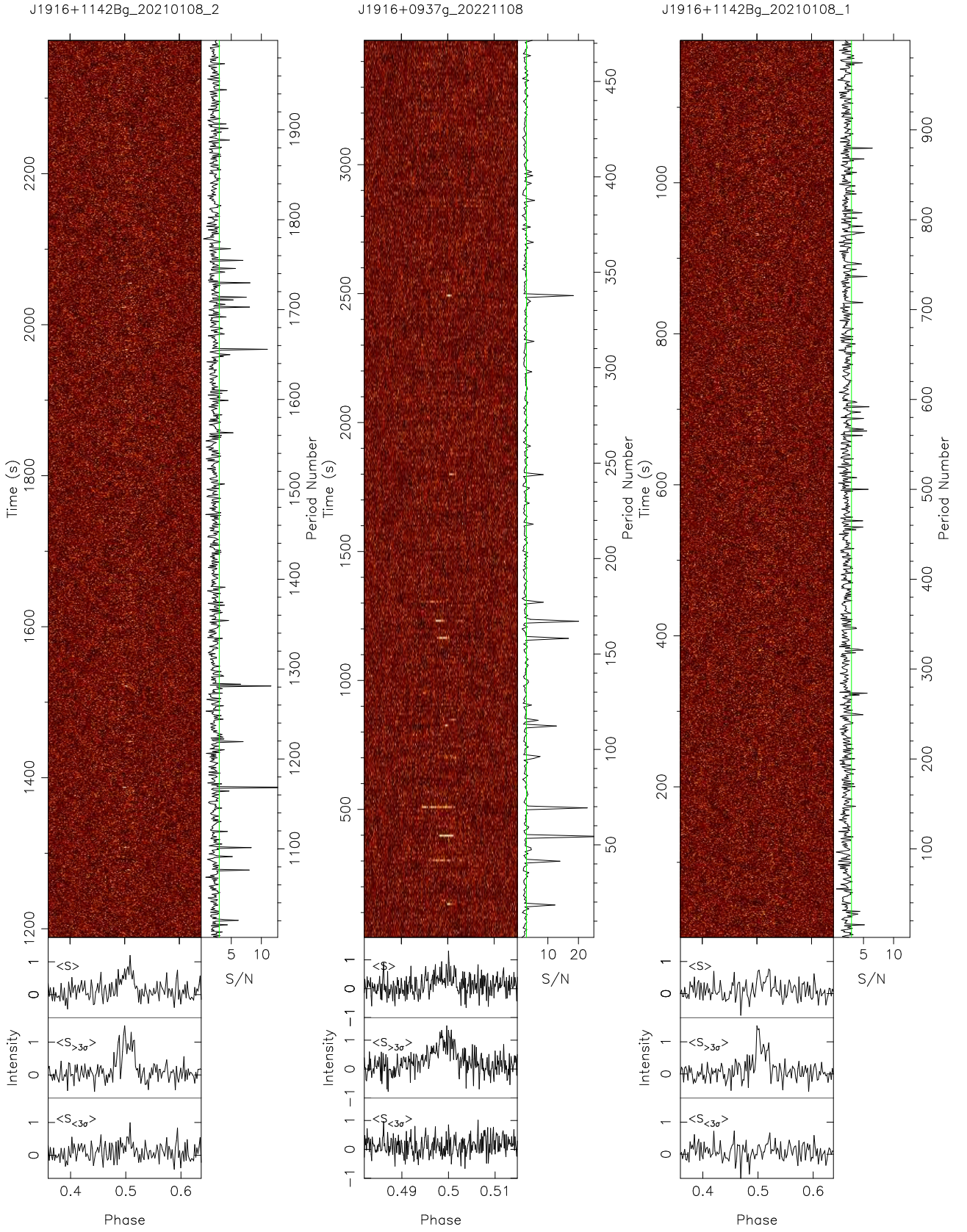


Fig. 24 – continued.

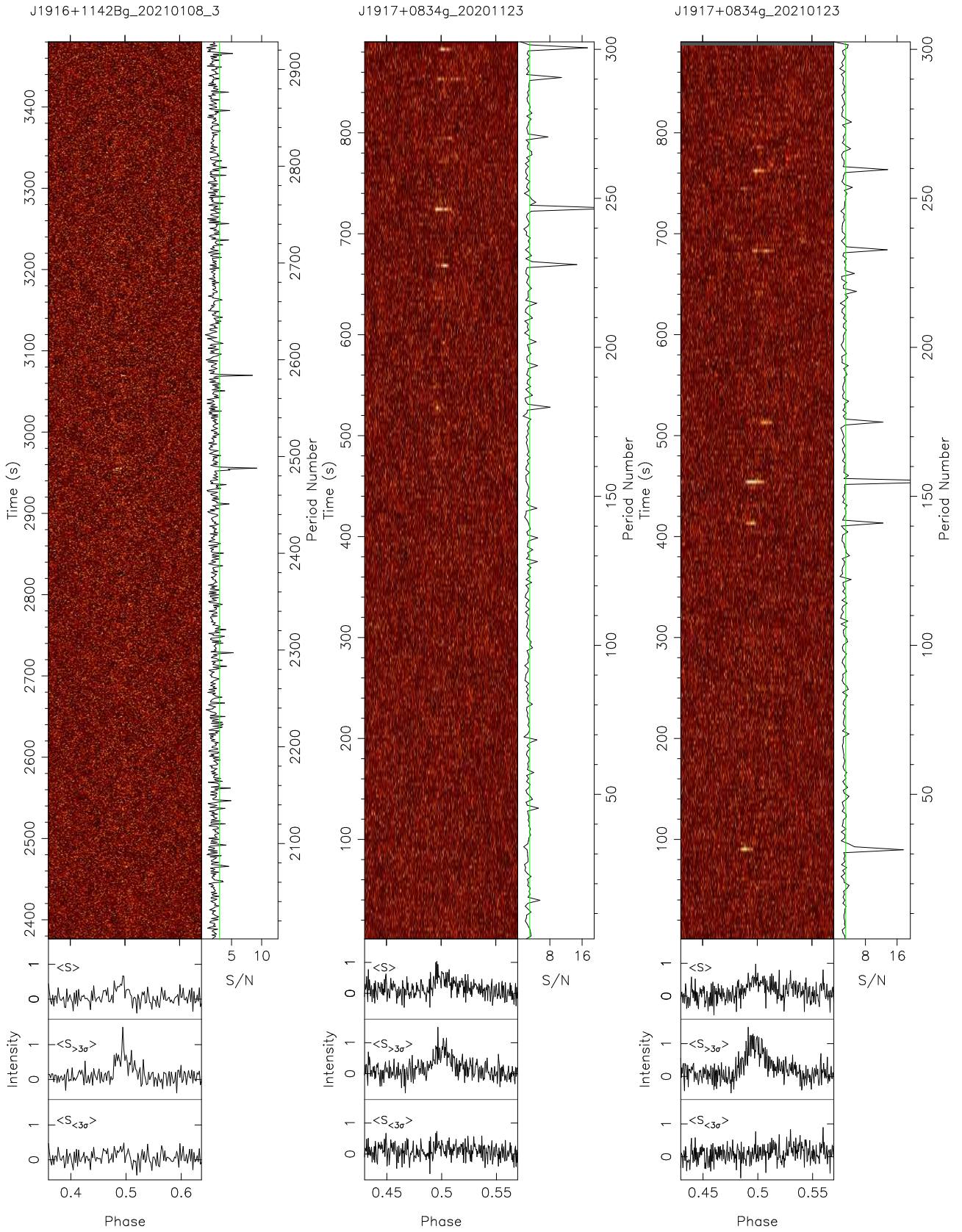


Fig. 24 – continued.

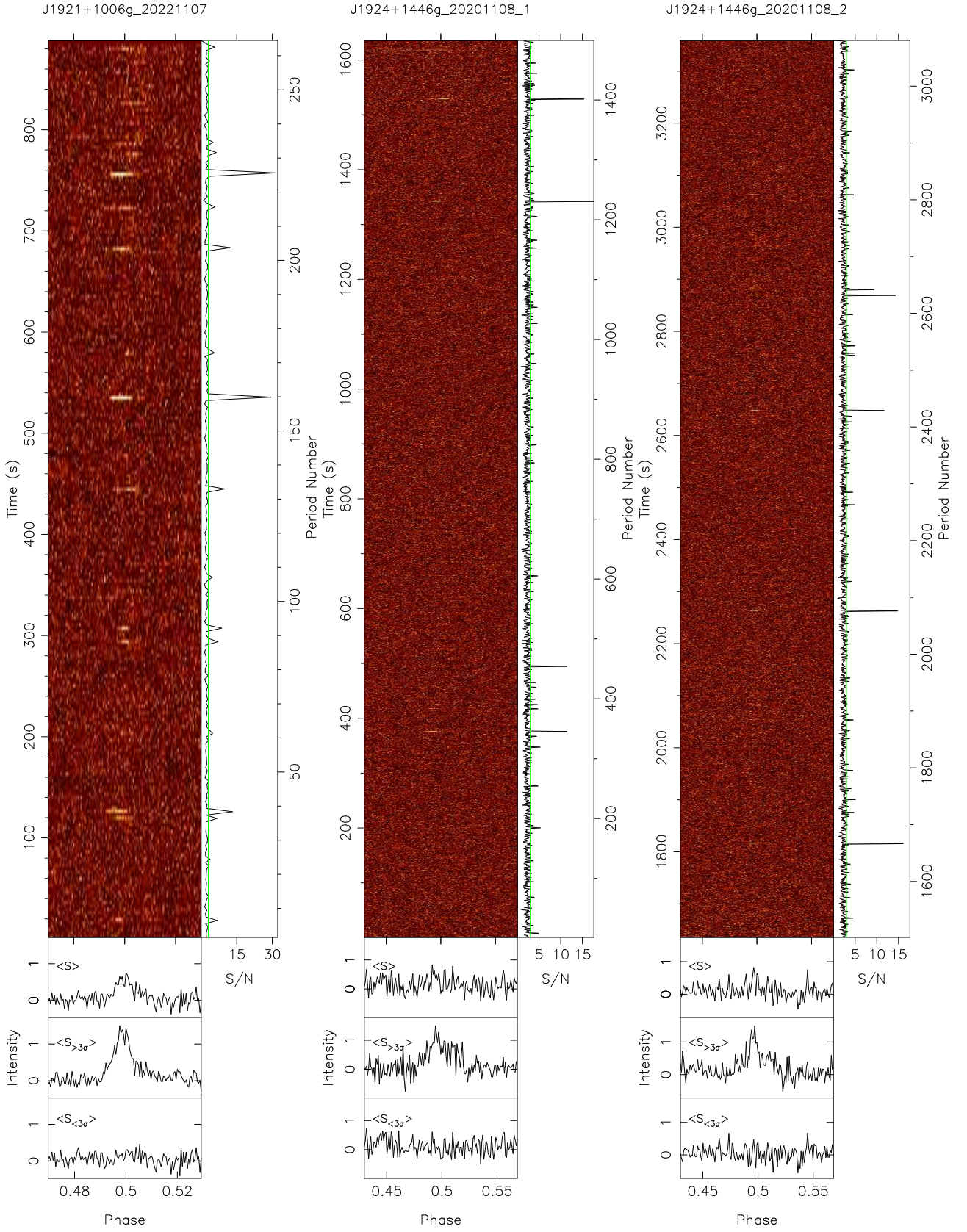


Fig. 24 – continued.

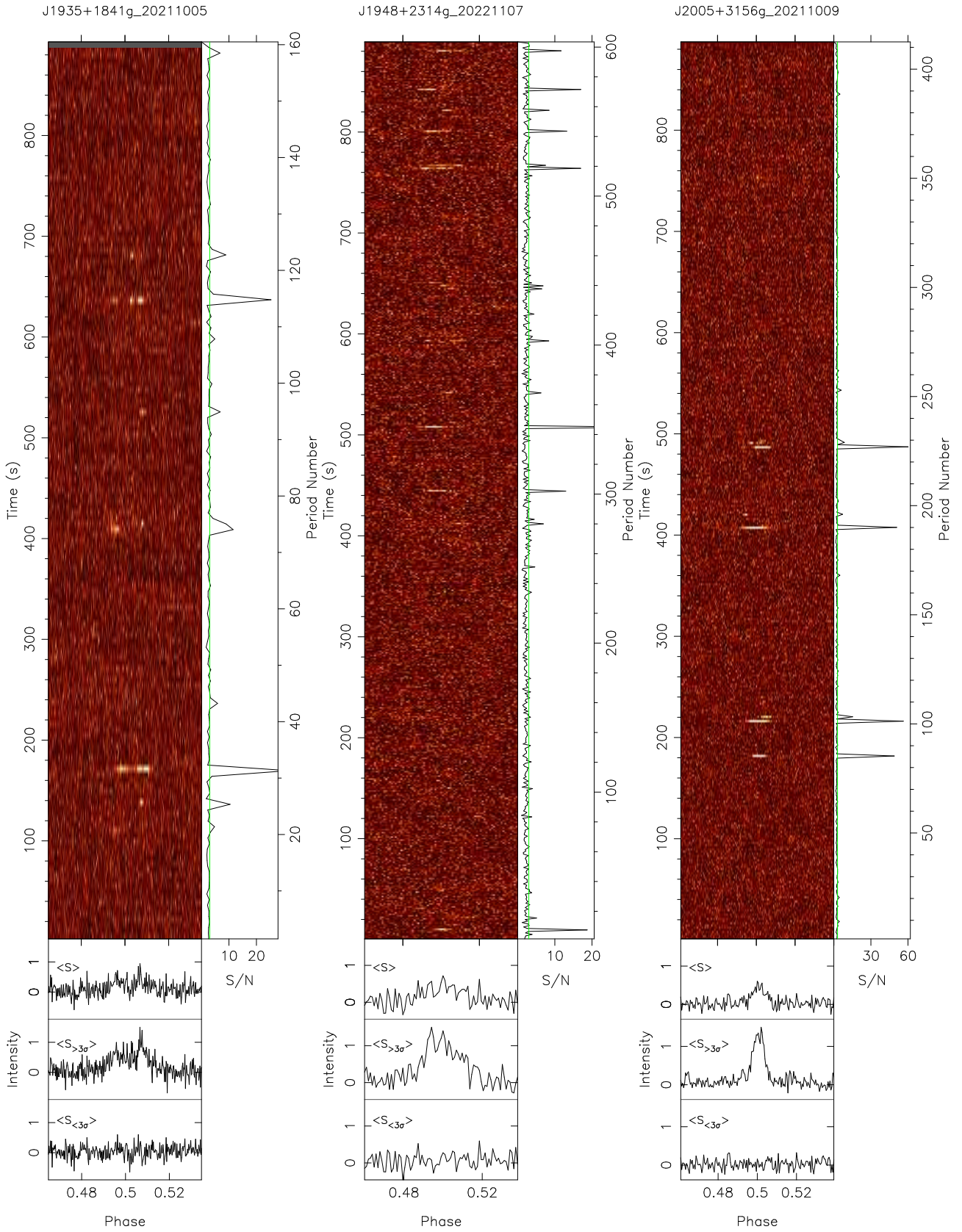


Fig. 24 – continued.

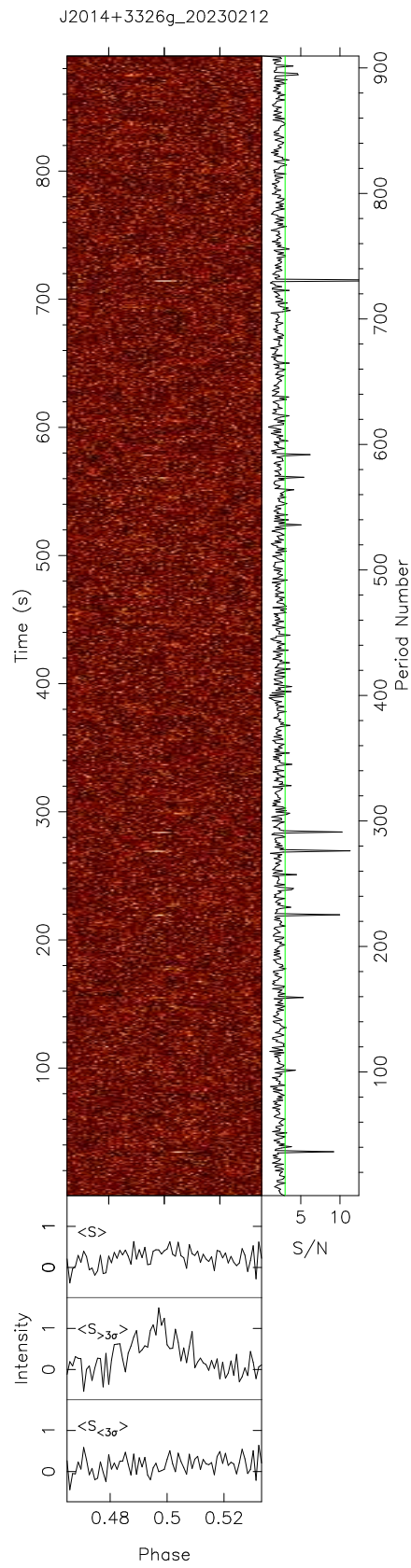


Fig. 24 – continued.

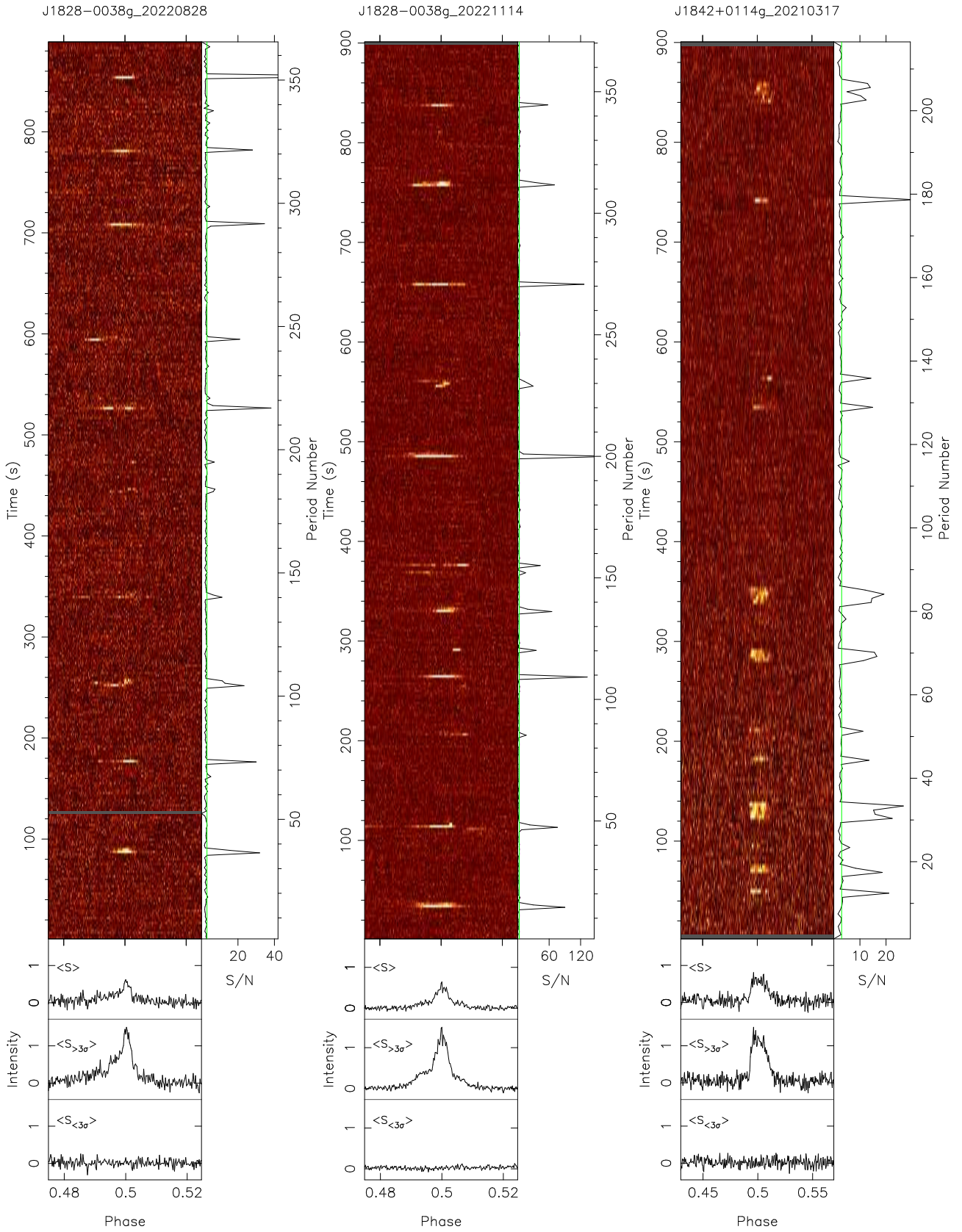


Fig. 25 Very nulling pulsars discovered by GPPS.

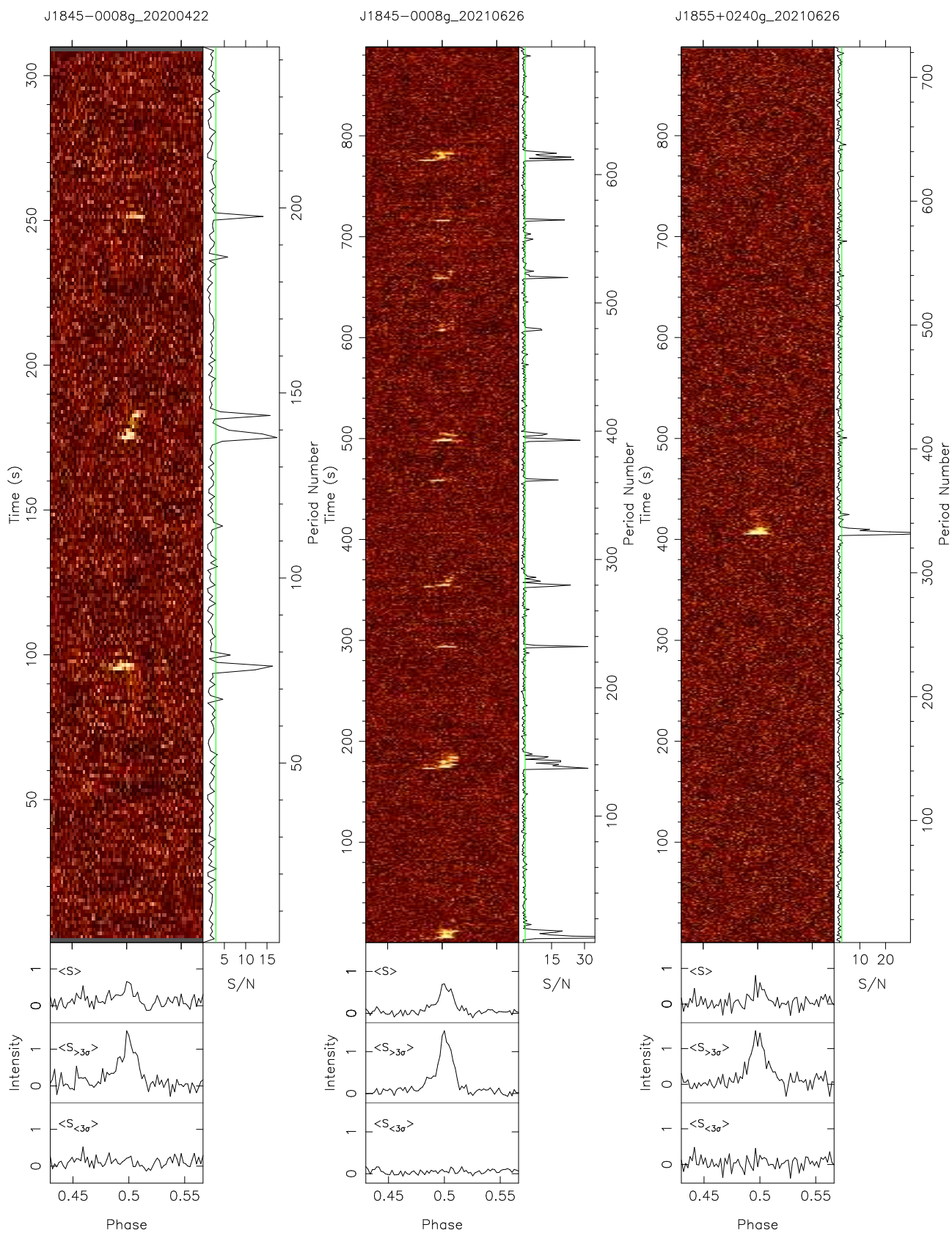


Fig. 25 – continued.

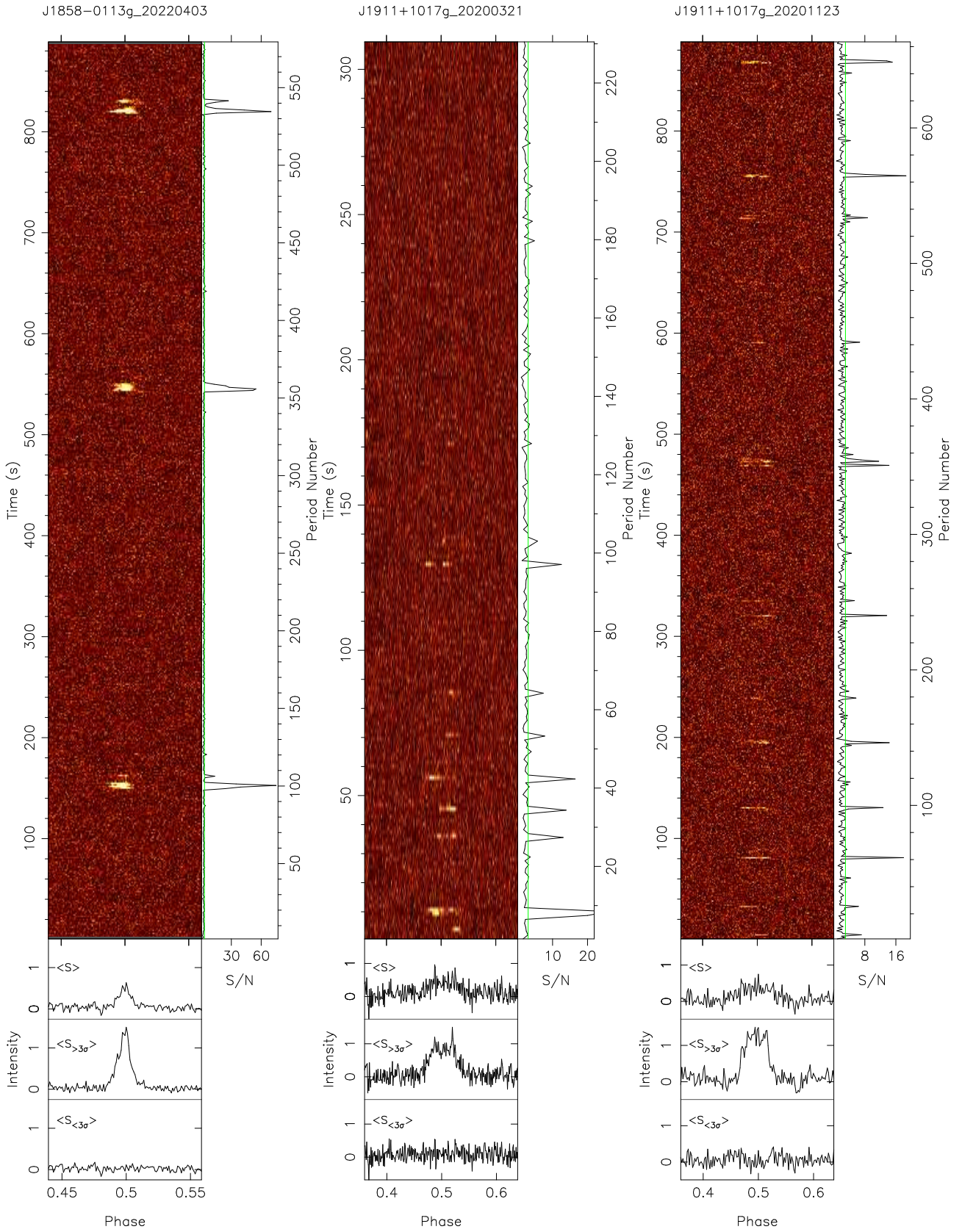


Fig. 25 – continued.

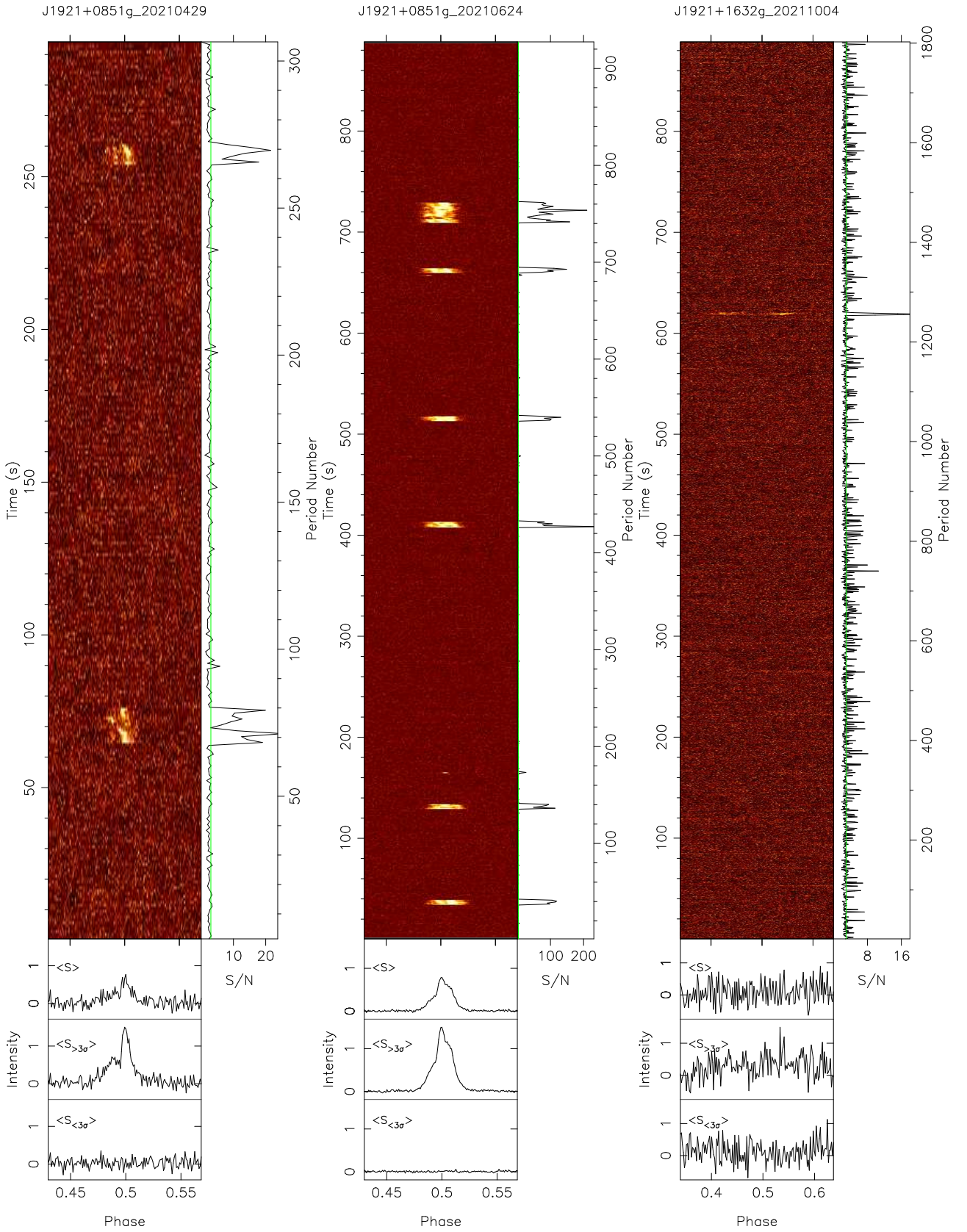


Fig. 25 – continued.

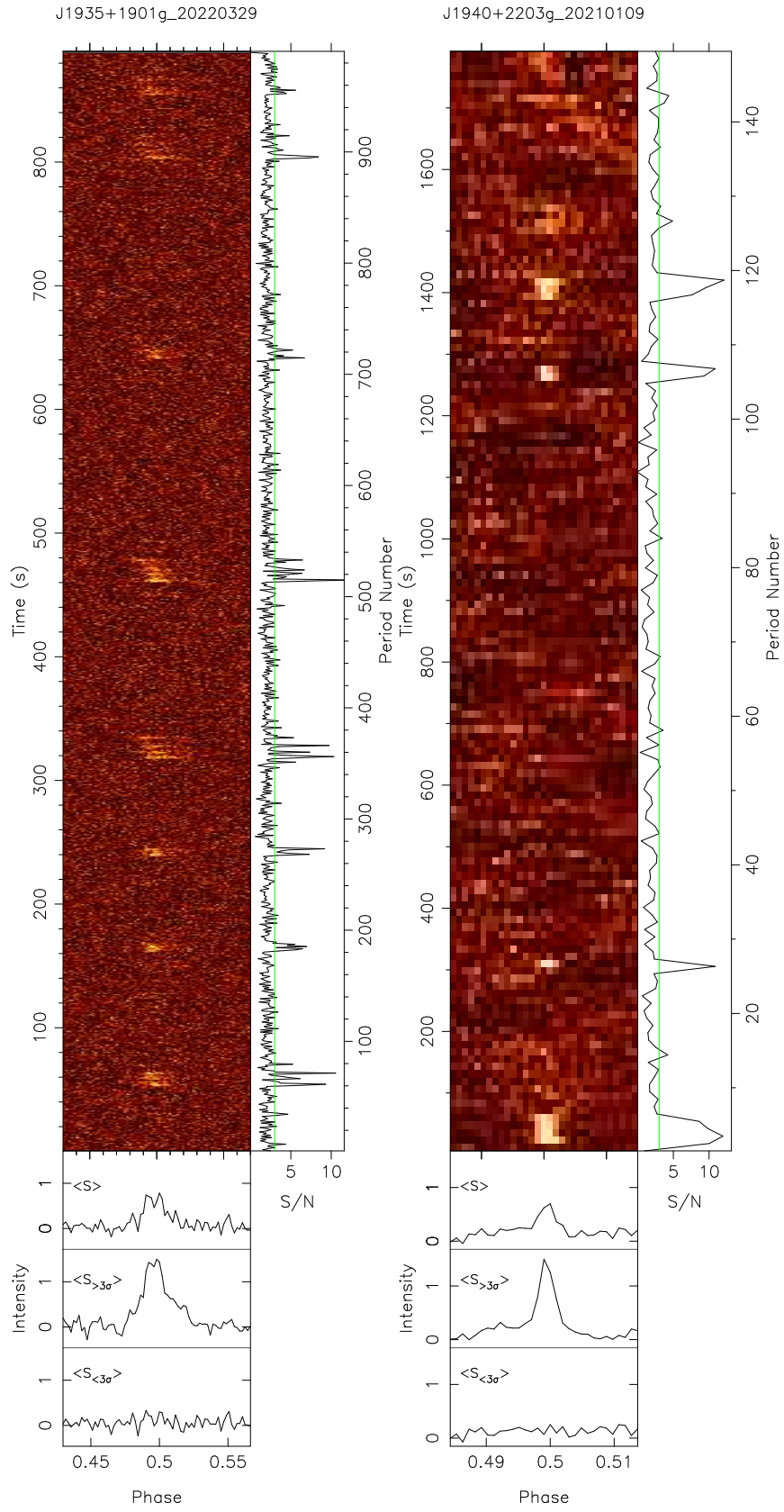


Fig. 25 – continued.

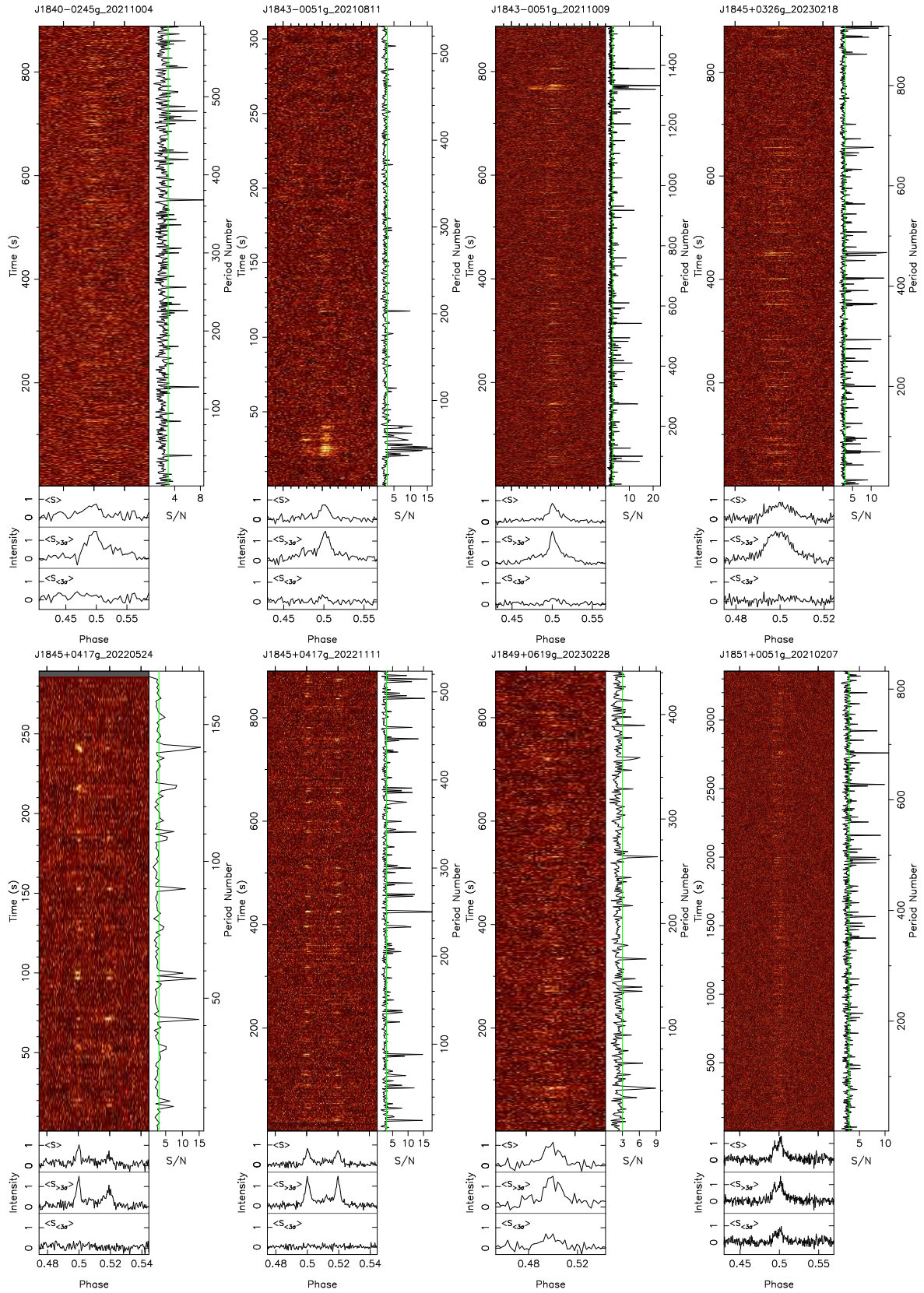


Fig. 26 Weak pulsars by GPPS.

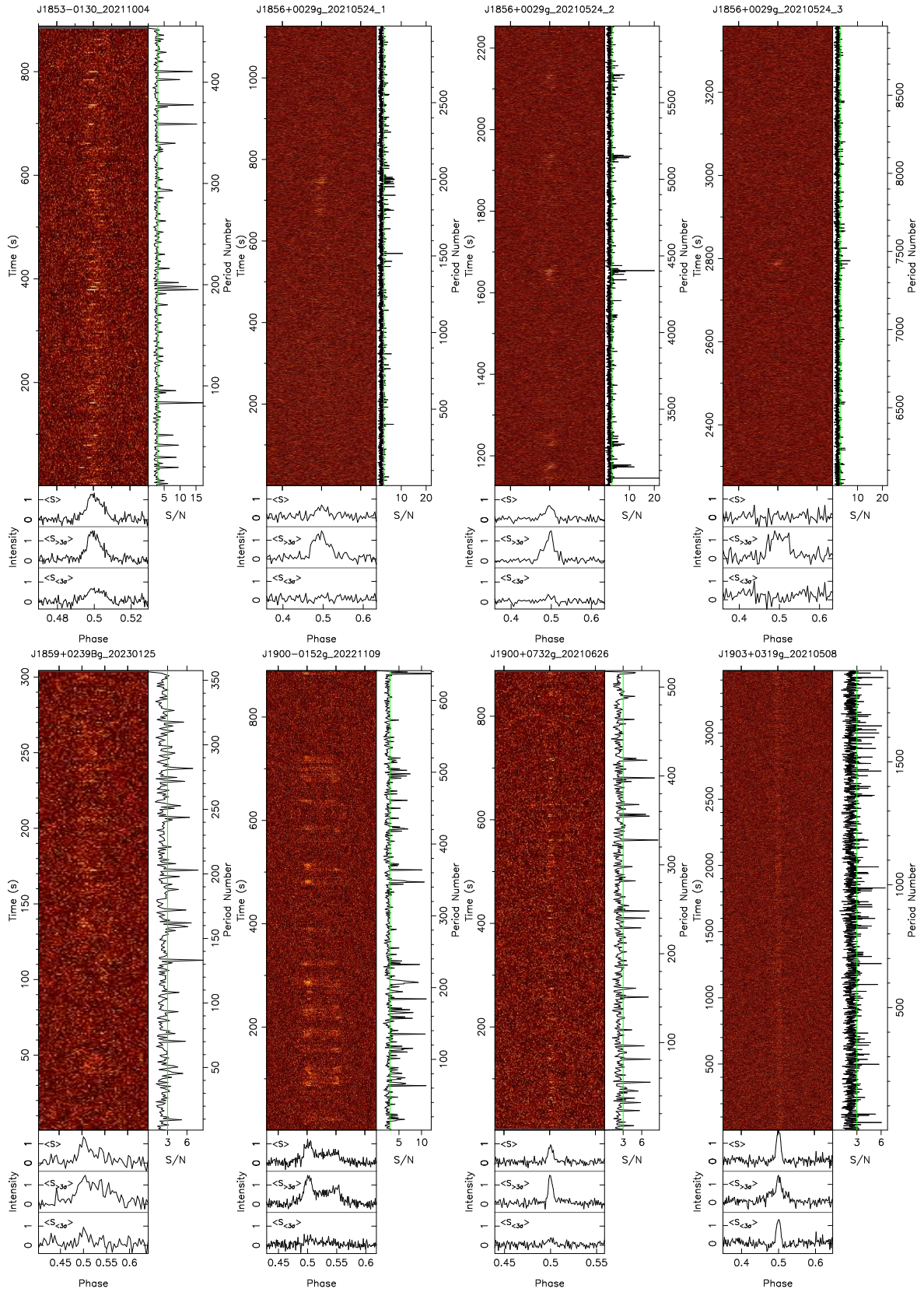


Fig. 26 – continued.

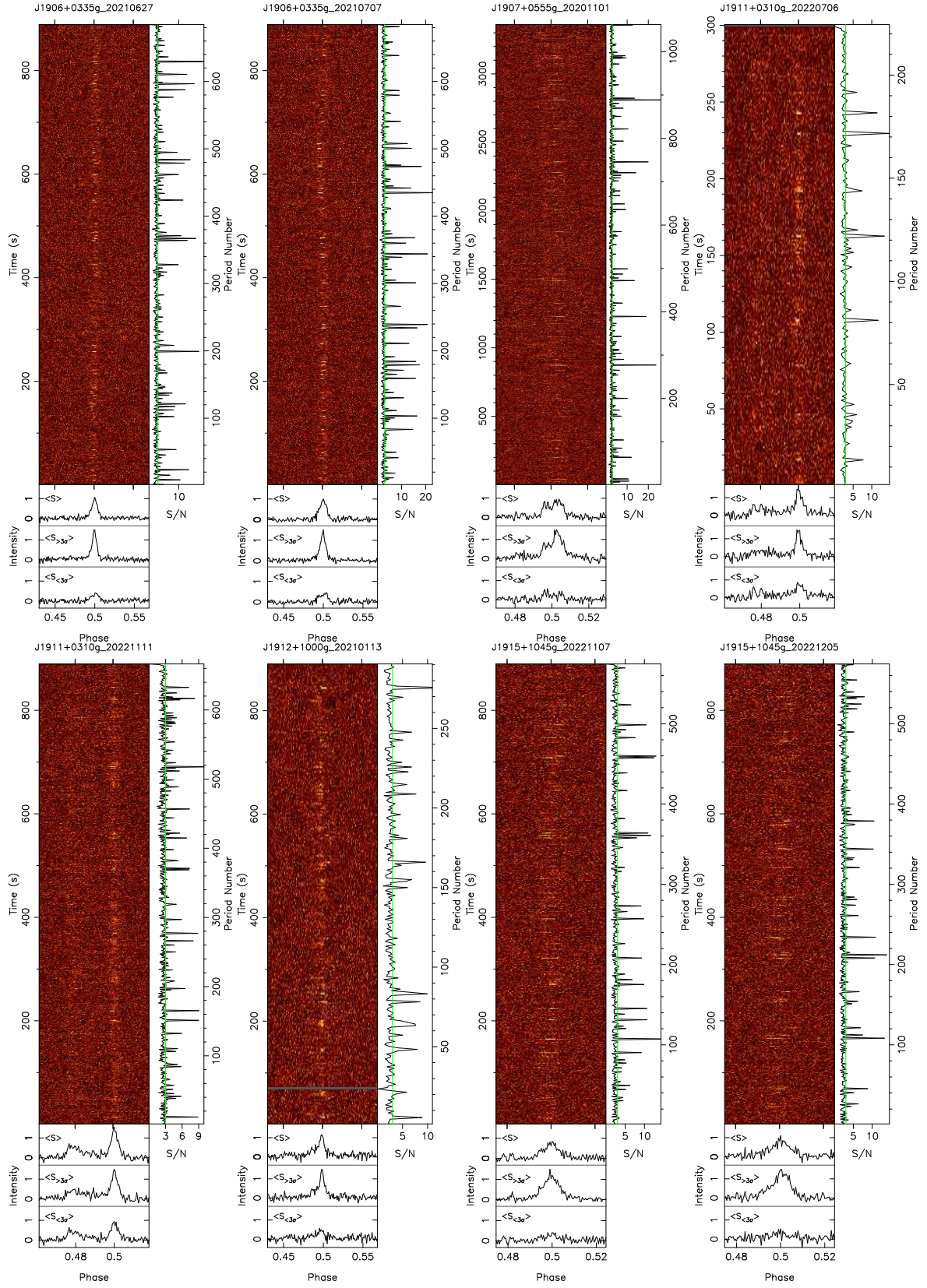


Fig. 26 – continued.

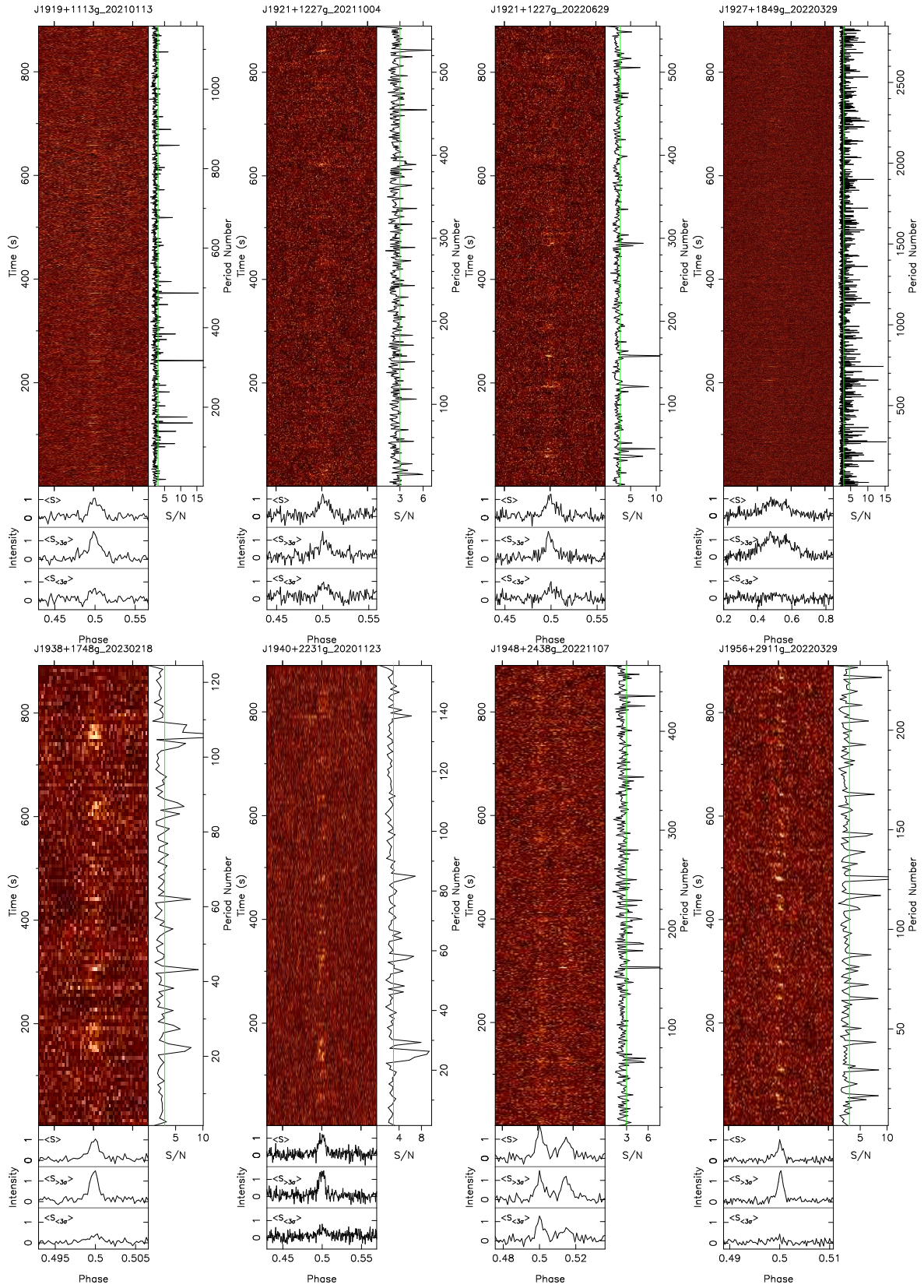


Fig. 26 – continued and ended.

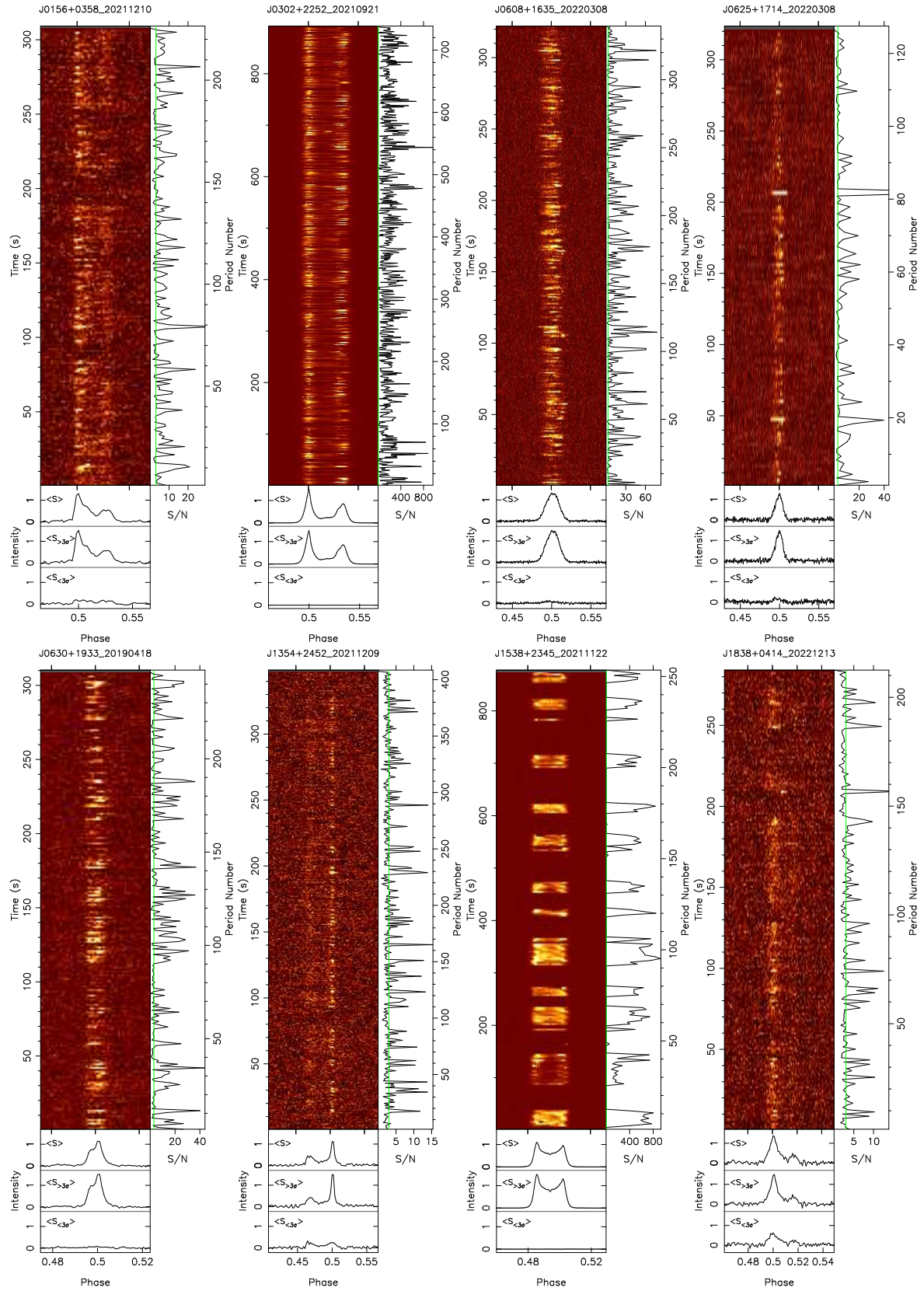


Fig. 27 The known RRATs for just normal pulsars though nulling features occasionally emerges.

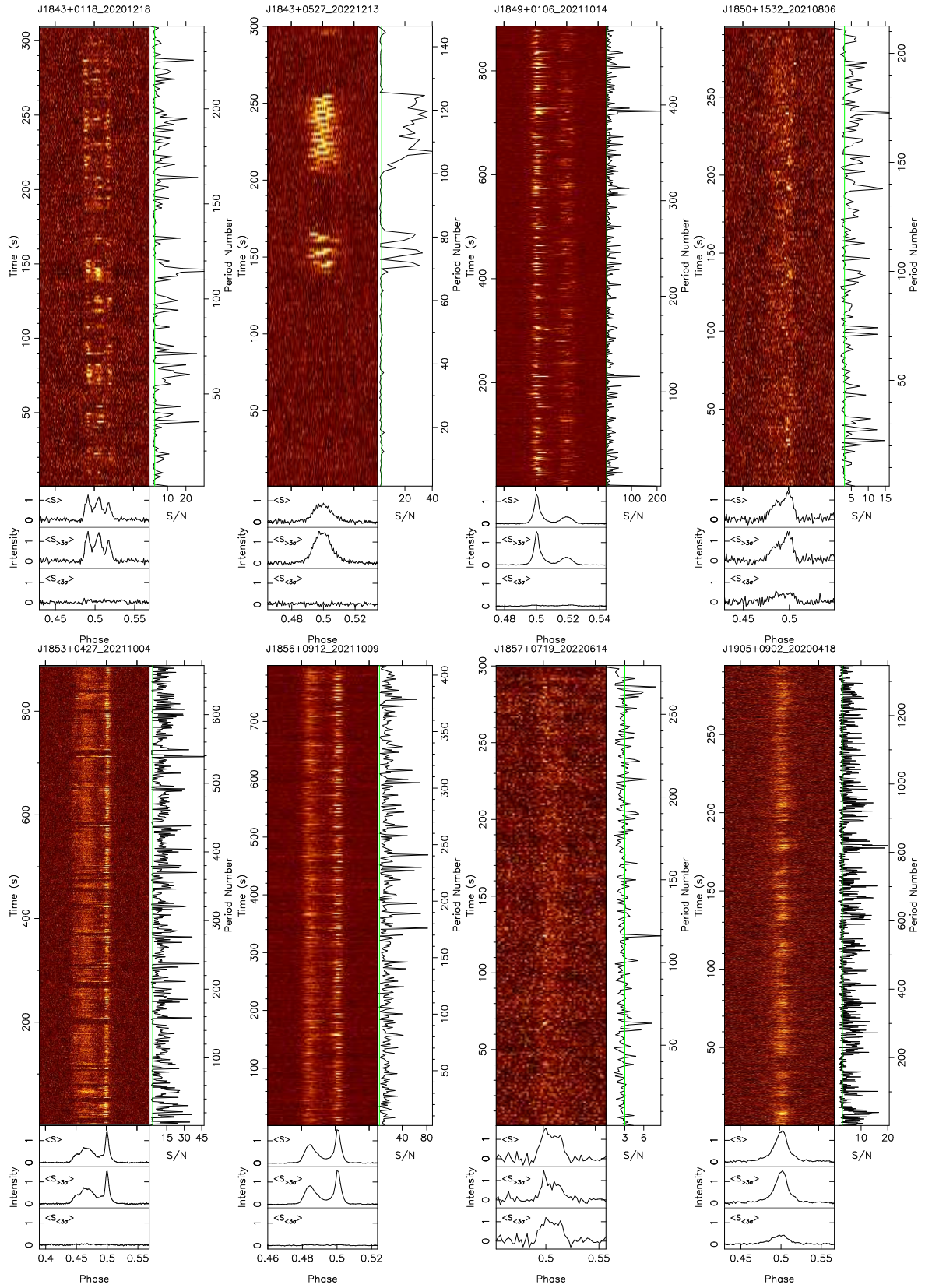


Fig. 27 – continued.

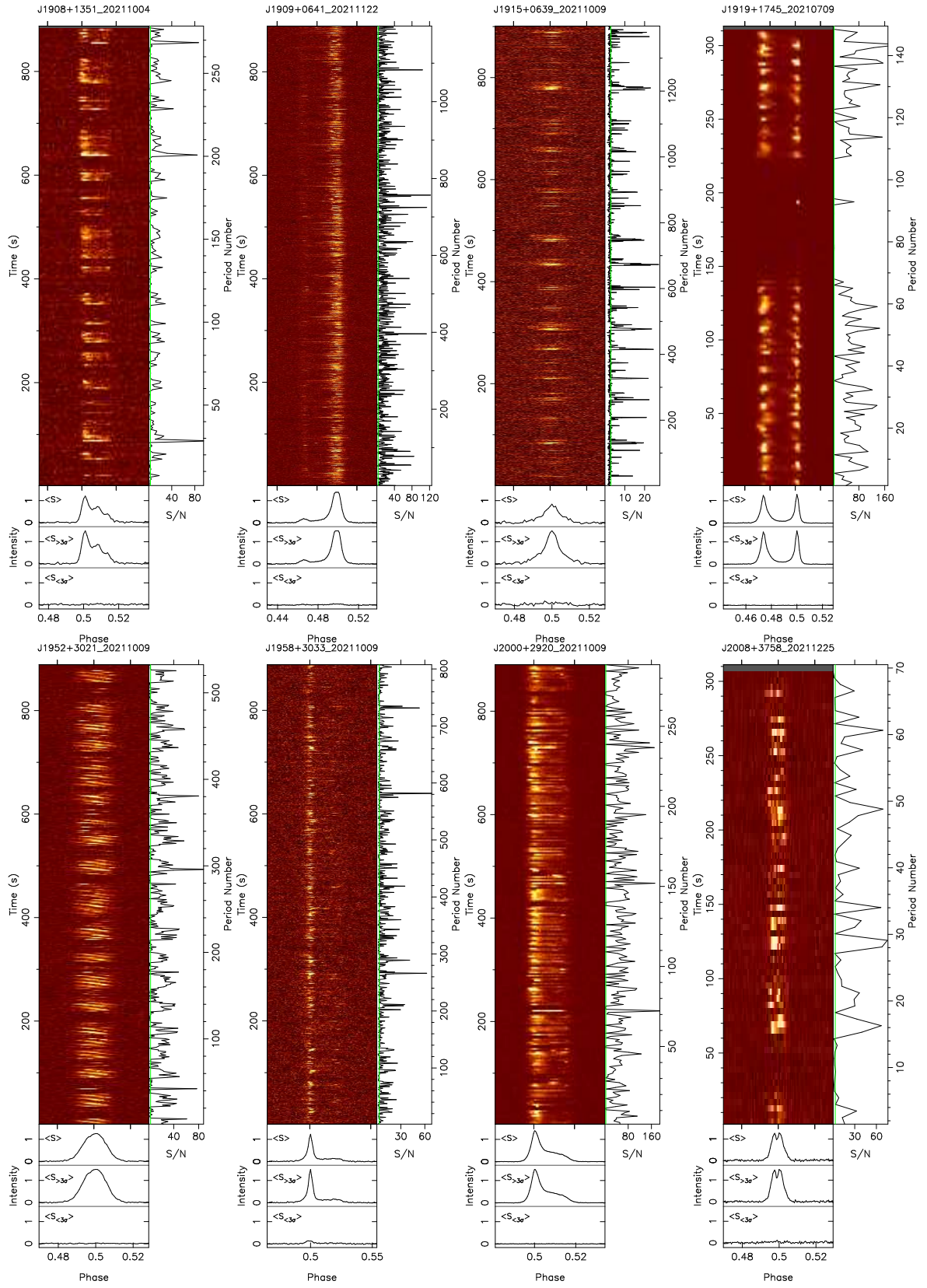


Fig. 27 – continued.

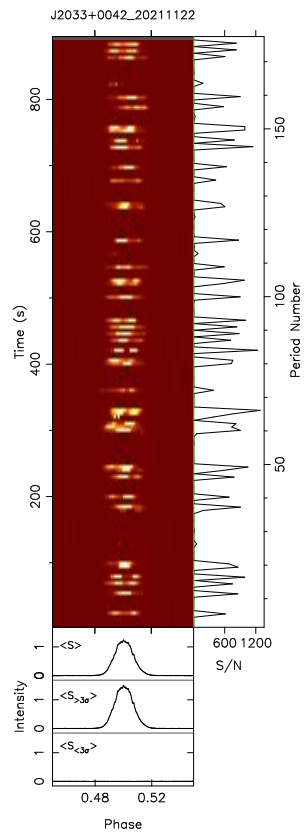


Fig. 27 – *continued and ended.*

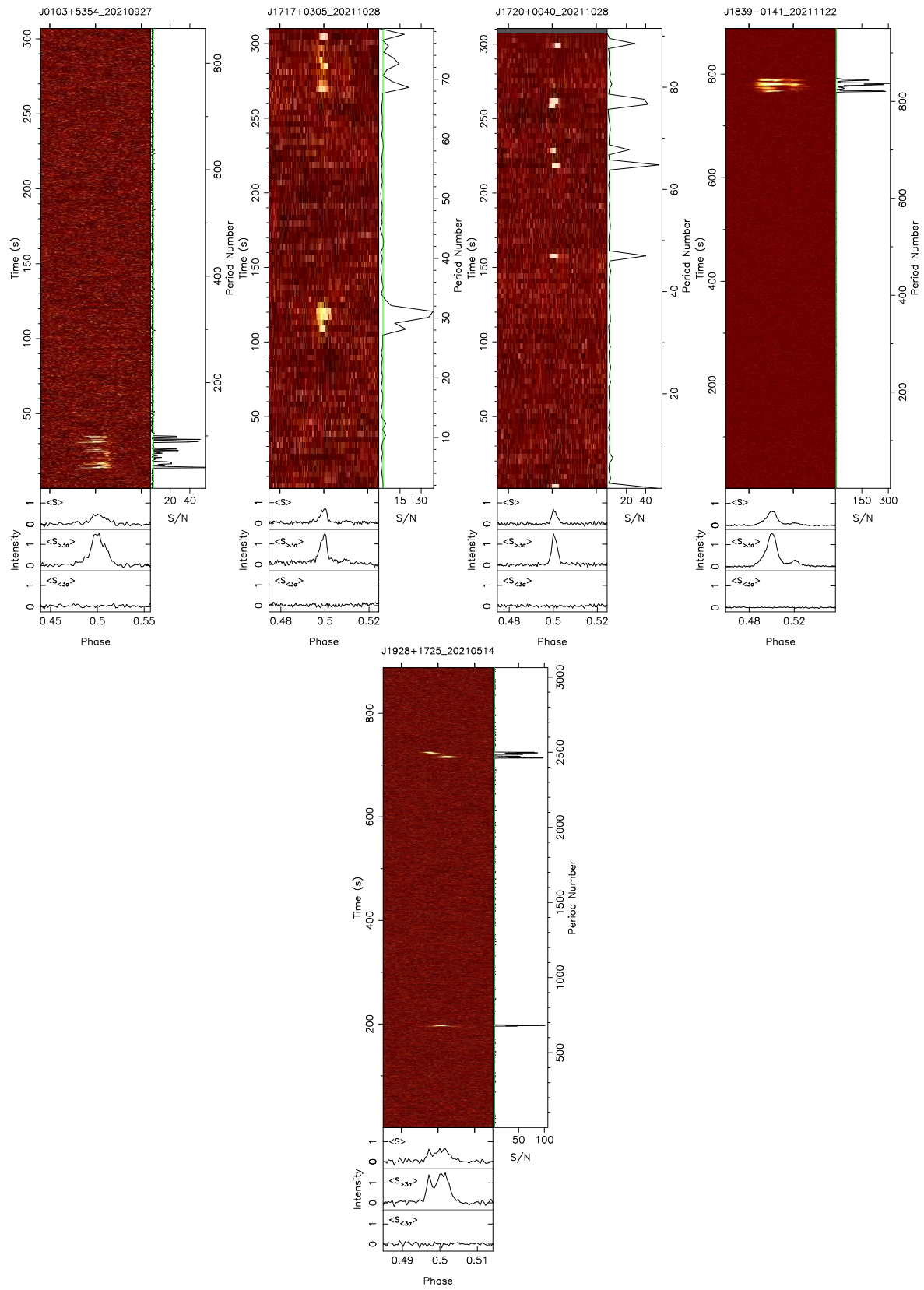


Fig. 28 The known RRATs are shown as group of extremely nulling pulsars.

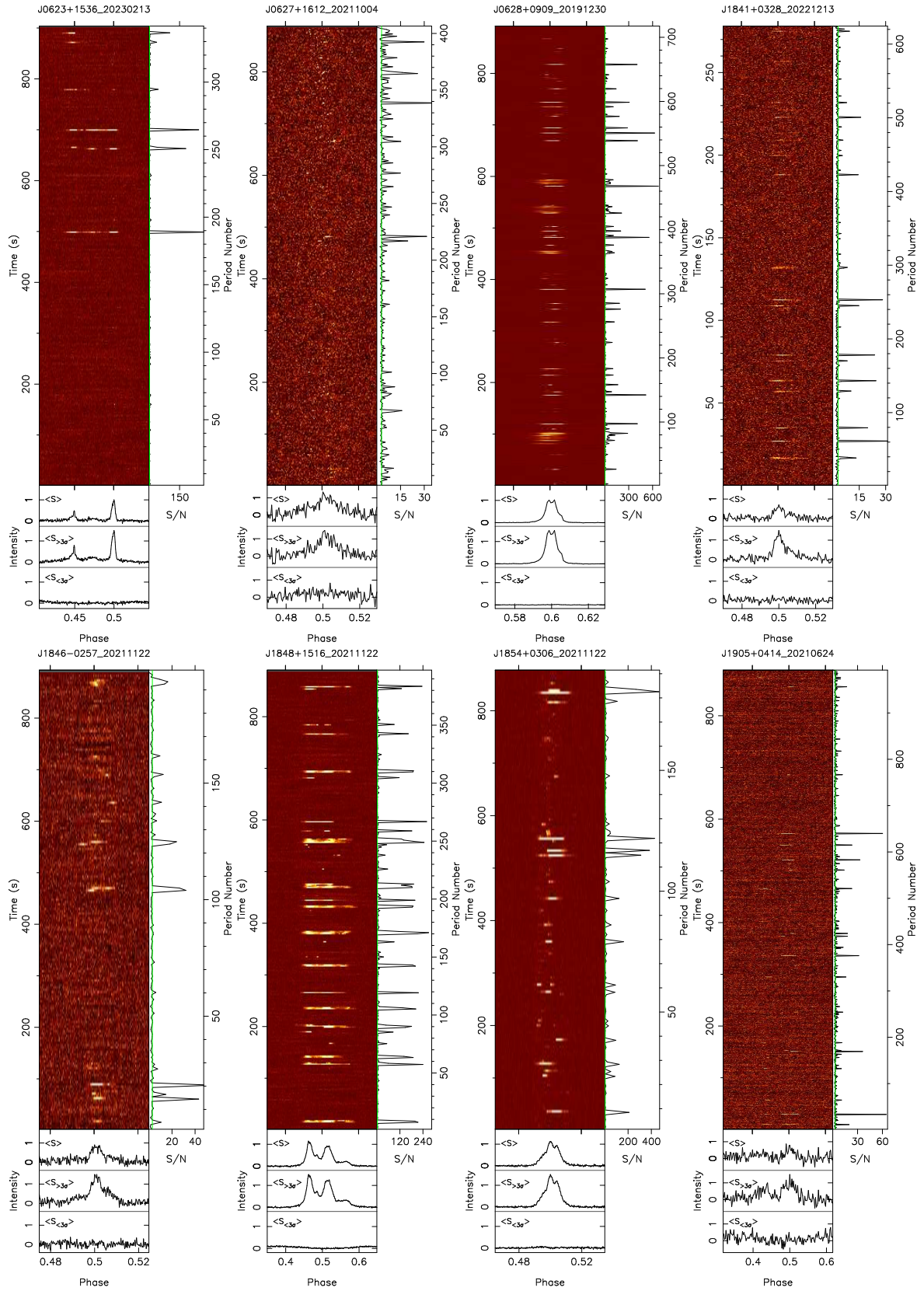


Fig. 29 Pulse-stacks for the Known RRATs of the group for weak pulsars with sparse strong pulses.

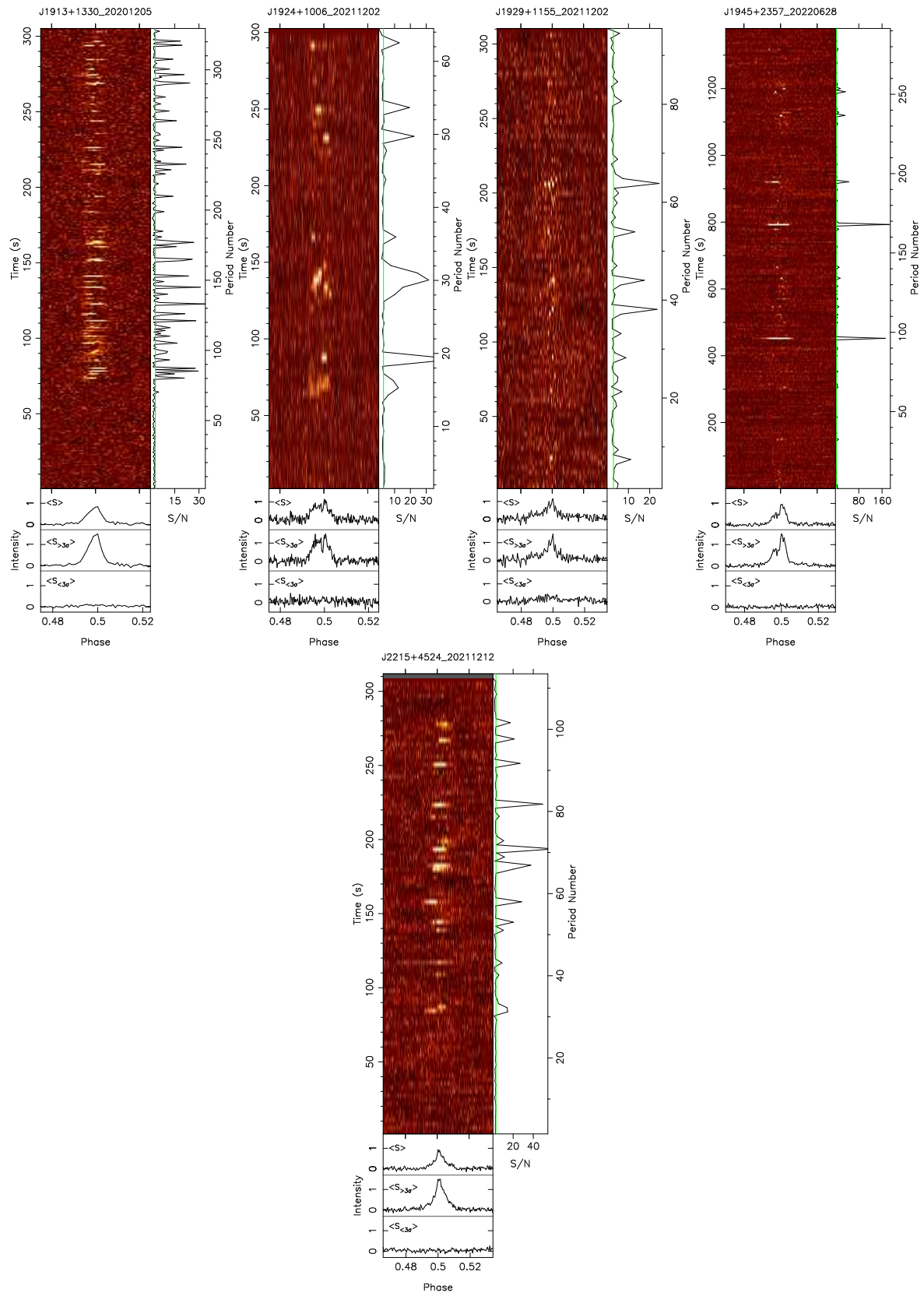


Fig. 29 – continued and ended.

Table 8 – *continued*.

ObsDate (1)	No. (2)	TOA (3)	R (4)	W (5)	F (6)
J1859+0832g = gpps0505					
20220526	1	59724.77170952	50.6	7.7	425.2
20220526	2	59724.77171976	18.5	78.8	239.0
20221107	1	59890.34972011	33.3	8.5	173.6
J1900+0908g = gpps0527					
20220522	1	59720.79041037	41.5	21.5	391.5
	2	59720.79043544	7.3	10.8	32.5
J1902+0557g = gpps0525					
20221018	1	59870.44448379	14.7	3.1	61.6
	2	59870.44530378	12.1	21.0	58.8
20230212	1	59987.12293867	15.1	20.3	73.3
J1916+1142Ag = gpps0287					
20200302	1	58910.09452353	7.2	10.5	14.9
20210128	2	59222.20075862	12.9	3.5	44.7
J1918+0342g = gpps0506					
20211202	1	59550.31150165	33.9	12.0	75.7
20220602	1	59731.85140692	11.9	25.7	88.3
J1918+1514g = gpps0507					
20200531	1	58999.81141189	8.31	12.3	44.1
	2	58999.81210714	10.6	15.2	79.8
J1921+1629g = gpps0288					
20210822	1	59448.63792384	14.3	16.7	80.7
20211004	1	59491.54677614	38.6	5.5	237.6
	2	59491.54955334	49.5	6.63	376.0
J1924+1734g = gpps0289					
20210822	1	59448.65213287	42.5	18.8	578.5
	2	59448.65362293	32.4	33.8	536.2
20211005	1	59492.41449285	36.0	31.7	457.0
	2	59492.41467918	19.2	24.4	189.1
	3	59492.41598276	39.3	20.7	568.4
J1927+1940g = gpps0290					
20190327	1	58569.02255643	10.2	8.7	49.2
20210624	1	59388.71211556	9.0	21.1	71.7
J1932+2126g = gpps0508					
20220323	1	59661.04248301	21.6	13.1	157.1
20220608	1	59737.82493655	24.0	8.0	123.5
20220720	1	59780.62376501	11.8	21.7	80.8
J1933+2401g = gpps0291					
20210301	1	59274.07468225	13.2	33.4	87.1
20210626	1	59390.78088520	9.1	30.4	52.0
J1934+2341g = gpps0292					
20210301	1	59274.07585975	12.5	12.0	89.2
	2	59274.07263818	10.5	8.1	89.2
	3	59274.07382939	19.1	5.0	127.4
20210624	1	59388.81110584	15.1	6.6	88.0
	2	59388.81117695	9.7	16.3	48.7
	3	59388.81247483	16.3	24.5	125.9
	4	59388.81427651	8.5	17.0	34.8
	5	59388.81443653	30.6	5.6	199.7
20221106	1	59889.41136795	10.7	10.6	54.1
	2	59889.43586809	38.2	5.9	229.7
J2001+4209g = gpps0293					
20210802	1	59427.71952664	12.9	11.6	63.3
20211004	1	59491.56354889	17.9	9.0	107.8
	2	59491.56567598	10.1	13.2	40.6
J2005+3154g = gpps0294					
20210804	1	59430.74319212	11.5	8.5	45.5
	2	59430.74537058	14.5	11.8	62.7
20210805	1	59431.65409682	16.8	7.5	98.2
	2	59431.64156848	14.7	15.7	73.4
	3	59431.64187222	8.3	9.8	41.4
20211009	1	59431.64377282	9.5	26.3	52.9
	1	59496.54708948	28.9	7.2	127.2
	2	59496.56473674	11.7	10.1	71.4
	3	59496.56707139	19.5	5.1	113.8

Table 8 – *continued and ended*.

ObsDate (1)	No. (2)	TOA (3)	R (4)	W (5)	F (6)
J2030+3833g = gpps0295					
20210220	1	59265.16695103	9.0	28.7	102.8
	2	59265.16802449	32.8	45.3	185.7
20210317	1	59290.09440744	9.3	38.3	249.1
	2	59290.09889063	10.9	41.5	715.3
20210624	1	59388.82883282	9.5	32.2	32.4
	2	59388.83097994	11.6	40.7	67.1